RESERVOIR ENGINEERING RESEARCH INSTITUTE

Wettability Alteration of Porous Media to Gas-Wetting for Improving Productivity and Injectivity in Gas-Liquid Flows

DE-FG26-00BC15306

Second Annual Report
Period: 9/21/01-9/20/02

Contract Date: 9/21/00-8/31/03

DOE Program Manager: Mr. Chandra Nautiyal

Principal Investigator: Dr. Abbas Firoozabadi

October 21, 2002

385 Sherman Ave., Suite 2B
Palo Alto, CA 94306
(650) 326-9172

Table of Contents

Disclaimer

Acknowledgments

Rajinder Kumar, Erik Santiso, and I were active members of the group working on the US DOE grant DE-FG26-00BC15306 in the second year of the grant. Much progress was made both in theoretical and experimental aspects of the project.

Chapter I and Chapter II from the first year annual report were submitted in the form of two papers. Both papers have been accepted for publication. Once paper will appear in the December issue of *SPE Reservoir Evaluation and Engineering* (Dec. 2002). Another paper will appear in *Transport in Porous Media*.

This report is comprised of three chapters. Chapter I provides the results of our extensive experiments with a new polymer synthesized for the purpose of this project by 3M. The polymer is environmentally sound and is intended for field application. We have shown in the second year of the grant that the polymer is effective 1) with a condensate liquid from a well in Texas, and 2) at temperatures as high as 140^{o}C.

Chapter II provides a theoretical model from interfacial thermodynamics for the effect of curvature on surface tension and surface energy. The approach is new and will lead to the understanding of the energy of the interfaces.

Chapter III provides a theoretical model for the calculation of the composition and surface energy of the interface between phases in multicomponent systems. In this work, we are demonstrating how to compute the interface composition and energy in a gas-liquid system to study the effect of temperature. In the future, we are planning to model the process in fluid-solid (rock) systems.

We expect further progress in the third year of the project. A liquid condensate from a field in Texas and reservoir cores are under intensive laboratory measurements. Advanced theoretical work is also in progress.

Abbas Firoozabadi
Principal Investigator

List of Tables

Chapter I

List of Figures

Chapter I

Chapter II

Chapter III

Chapter I – Experimental Study of the Effect of Wettability Alteration to Intermediate Gas Wetting by a New Polymer

Rajinder Kumar and Abbas Firoozabadi

Summary

We have performed a number of imbibition tests with the treated and untreated cores in nC_{10}, nC_{14}, and nC_{16} and a natural gas condensate liquid. Imbibition testes for nC_{14} and nC_{16} were also carried out at elevated temperatures of 100^0C and 140^0C. An experimental polymer synthesized for the purpose of this project was used in core treatment.

Imbibition results are very promising and imply liquid condensate mobility enhancement in the treated core. We also performed flow tests to quantify the increase in well deliverability and to simulate flow under realistic field conditions.

Introduction

In the past we have performed extensive testing of wettability alteration in intermediate gas wetting for polymer FC759 at temperatures of 24^oC and 90^oC. The results were promising for the purpose of gas well deliverability improvement in gas condensate wells[1,2]. We used FC759 to lower the surface energy of various rocks. The model fluids nC_{10}, and nC_{14} were used to represent condensate liquid, and air was used as the gas phase. A new (L-16349) polymer, which has been recently synthesized for the purpose of the project, was used in the work to be presented here. L-16349 is a water-soluble fluorochemical polymer, with low order, neutral PH and very low volatile organic compound (VOC < 9.1 g/l). It is light yellow in appearance and density in 25% solution is 1.1 g/cc. Polymer L-16349 is very safe from environmental considerations and it is economical for our purpose. In this work, in addition to nC_{10}, and nC_{14}, we used two other liquids nC_{16}, and a liquid condensate in order to study the effect of wettability alteration with a broader range of fluids.

The goal of this work is to perform an extensive set of imbibition tests with the experimental polymer up to a temperature of 140°C. In fact, we have performed treatment of the rock up to 200°C. These temperatures cover almost all potential applications of the polymer. In this report, we present the imbibition results and results for flow tests using a variety of hydrocarbon liquids. We first describe the imbibition results at high temperature for Berea and Chalk cores. Then we present the results of flow tests.

Fluids and Rocks

Fluids – We used normal decane (nC_{10}), normal tetradecane (nC_{14}), and normal hexadecane (nC_{16}), BP condensate, water, air, and nitrogen. The polymer used is an experimental surfactant synthesized for the purpose of this project by 3M. It is dissolved as a solution in water with 25% concentration.

Normal decane (nC_{10}) has a specific gravity of 0.72 at 24°C. Its viscosity and surface tension at the same temperature are 0.92 cp and 24 dyne/cm, respectively.

Normal tetradecane (nC_{14}) has a specific gravity of 0.76 at 24°C and 0.71 at 100°C. Its viscosity and surface tension at 24°C are 3.2 cp and 26 dyne/cm, respectively. The viscosity and surface tension of nC_{14} at 100°C are 0.65 cp and 20 dyne/cm, respectively.

Normal hexadecane (nC_{16}) has a specific gravity of 0.77 at 24°C and 0.68 at 140°C. Its viscosity and surface tension at 24°C are 4.2 cp and 28 dyne/cm, respectively. The viscosity and surface tension at 140°C are 0.6 cp and 21 dyne/cm, respectively.

The condensate liquid is from a well in Texas provided by BP. It is yellow in color and has a specific gravity of 0.785.

Rocks - We used two different rocks in this work: Berea sandstone and Kansas chalk. Later we will discuss these two rocks. We are also using other types of rocks in this project.

Wettability Alteration

Two methods are used to alter rock wettability. The procedure for these two methods is discussed in the following.

Method 1

1. Core was vacuumed in a container (1hr). This step is performed in order to measure the amount of adsorption. It will not be necessary for field conditions.

2. Solution of L-16349 at a known concentration was introduced into the container containing the core (2hr).

3. Container was placed in the oven at a temperature of 105/150 ^{0}C (3-4 hr). In one case, the cores were heated to 200^{o}C.

4. Core was dried and amount of adsorption was determined.

5. Core was prepared for the imbibition test.

Method 2

1. Core was placed in the core-holder.

2. Core was vacuumed for about 1hr. This step is performed in order to measure the amount of adsorption. It will not be necessary for field application.

3. Solution of L-16349 at a known concentration was introduced into the core holder from one end.

4. Two pore volumes of solution were passed from one side and then two pore volumes were introduced from other side.

5. Core holder was closed from both sides and was then placed in an oven for 3 hours at 150^{o}C.

6. Core-holder was cooled to about 100^{o}C. This step was undertaken to avoid vaporization of water. It will not be necessary for field conditions.

7. Chemical was then displaced using water.

8. Core was removed from the core holder and was dried to measure the amount of adsorption.

9. Core was prepared for the imbibition test.

Note that the purpose of vacuuming and drying the core in methods 1 and 2, as was mentioned above, is only necessary for adsorption measurement. Displacement of chemical with water makes method 2 close to field conditions. In the past, some of the steps above were much longer. As an example, the aging step has been cut from days to hours[1,2].

After the treatment process, the air-saturated core was hung under an electronic balance and placed in oil or in water to carry out spontaneous imbibition test and the change in weight of core sample vs. time was recorded (see Fig 1).

Determination of Permeability

Permeability was determined before and after the treatment of the sample. Nitrogen gas was used for the determination of permeability. To determine permeability a core wrapped with heat-shrinkable tubing was placed in a core holder. Overburden pressure of about 500 psi was applied on the core to avoid bypass. Pressure drop, upstream pressure and flow rate were then measured at several rates.

The following expression was used to calculate permeability[3].

$$\frac{(p_1^2 - p_2^2)M}{2\mu zRT(W/A)} = \frac{W}{A}\frac{\beta}{\mu} + \frac{1}{k} \qquad (1)$$

The symbols are defined in the Nomenclature.

Flow Tests

Two types of flow tests were carried out on Berea cores; they are as follows.

Two Parallel Cores

In this test two cores were placed in parallel. Liquid is injected from one end; the other end was kept open to the atmosphere. This test was carried out first for the two parallel-untreated cores of nearly similar permeability and production rate, as a function of time was determined. In the second stage, one of the cores was untreated while other core remained untreated. Production rate as a function of time was determined again. This test establishes the effect of treatment on the mobility of the fluids.

Effect of Pressure Gradient on Saturation

The test was carried out for both treated and untreated Berea. Oil at a flow rate of 4 cc/hr was injected in an air-saturated core and the gas injection rate was varied to provide pressure gradients of 0.1, 0.2 and 0.3 psi/cm. The average oil saturation vs. PV injection of liquid is plotted for each test.

Results

We have carried out a number of tests in studying the imbibition performance of Berea and chalk samples with or without wettability alteration. Several Berea and chalk cores were used in these tests. Table 1 provides the sample dimensions and properties. In the following, we first present results for the Berea samples and then the results for chalk samples.

Berea Imbibition

A number of tests were performed to study the effect of polymer concentration and temperature on the imbibition in Berea.

Effect of Polymer Concentration – Fig. 2a shows imbibition of nC_{10} in untreated and treated Berea. The Berea sample was treated using 3% L-16349 solution. As Fig2a and Fig2b show, the imbibition rate is mainly affected in early time. Note that the duplicate tests show very similar imbibition performance.

Fig. 3 shows nC_{10} imbibition in the untreated and treated Berea with 6% L-16349 solution. As can be seen, there is a significant reduction of imbibition. Note that the results for the duplicate treated samples are close.

Fig. 4a shows nC_{10} imbibition in untreated and treated Berea with 9% L-16349 solution. The figure shows a drastic reduction of imbibition. Note that the duplicate treated samples show a similar imbibition performance. In the remaining tests on Berea, we used the 9% solution for treatment of new Berea cores. We also reused the treated core in a number of tests. Contact angle measurements showed that the contact angle to nC_{10} was about 45-60 degrees (see Fig. 4b).

Fig. 5a shows water and nC_{10} imbibition in the treated Berea. As expected, water imbibition is less than nC_{10}. The measured contact angle for water was about 120-130 degree in the treated Berea (see Fig. 5b)

Condensate Imbibition – Fig. 6 shows the imbibition of nC_{10} and the condensate for the treated core. The figure reveals that both nC_{10} and condensate have similar imbibition performance. This is a very important result.

Effect of Temperature on Imbibition – The above results are all for a room temperature of about 24^{o}C. The reservoir temperatures can be considerably higher. The candidate reservoirs for the treatment application are often in the 90 to 140^{o}C range.

Fig.7 depicts imbibition of untreated Berea in nC_{10}, nC_{14} and nC_{16}. Imbibition of nC_{10} was carried out at room temperature. Imbibition of nC_{14} was carried out at 100 ^{0}C, and imbibition of nC_{16} was carried out both at room temperature and 100 ^{0}C. As can be observed with increase in molecular weight, the imbibition decreases. As can also be observed from this figure, the effect of temperature on imbibition in untreated Berea is substantial. A higher imbibition at higher temperature implies an increase in liquid wettability and may imply a decrease in contact angle.

Fig. 8 portrays the imbibition of nC_{10}, nC_{14}, and nC_{16} in air-saturated Berea at various temperatures. The imbibition of nC_{10} in the untreated Berea is at T=24^{o}C. The imbibition of nC_{14} in the treated Berea is at 100^{o}C. The imbibition of nC_{16} in the treated Berea is at 140^{o}C. There is even significant reduction in imbibition at 140^{o}C in the treated core. The reduction at higher temperatures implies usefulness and hence increasing mobility even at higher temperatures.

Fig. 9a shows imbibition of water in treated and untreated Berea. The Berea sample was treated using 9% L-16349 solution. The imbibition tests were carried out at 24 ^{0}C, 65 ^{0}C and 80 ^{0}C. A sudden jump in the curve may be attributed to the fact that small bubbles cling on the surface at higher temperature. As soon as system is disturbed to take the reading these bubbles get detached causing sudden change in weight. As can be seen from the figure, with increase in temperature imbibition increases but it is significantly lower than imbibition of untreated Berea at room temperature. Fig 9b shows the contact angle with water at room temperature and at 80^{0}C. Contact angle at 24 ^{0}C is about 120-130 degree whereas contact angle at 80 ^{0}C is about 60-70 degree; both for treated core. A higher contact angle at higher temperature implies increased liquid wetting.

In addition to the tests for the Berea, we also performed imbibition in treated and untreated chalk samples.

Chalk Imbibition

In the following, test results for imbibition in untreated and treated chalk samples are presented.

Effect of Polymer Concentration – Fig. 10a shows nC_{10} and water imbibition in untreated and treated chalk with 6% solution. There is a sharp reduction in imbibition for early

time for nC_{10} but later the imbibition is strong. For water, there is substantial reduction in imbibition vs. time for the entire period. Fig. 10b shows the early part of the imbibition performance. The results presented for water imbibition in the treated core imply that water imbibition is drastically reduced with 6% solution treatment.

Fig. 11a depicts the imbibition of nC_{10}, condensate and nC_{16} in the untreated and treated chalk with 9% solution. Note that there is a sharp reduction of imbibition in the treated chalk for both nC_{10} and the condensate. In two different cases even though chalk was treated with 9% L-16349 solution, the amount of adsorption was 8 mg/g of rock in one and 5.07 mg/g of rock in the other. Fig. 11a shows the imbibition of nC_{10} and condensate in these two cases. Note that with the increase in adsorption there is a decrease in imbibition. Also note that imbibition for nC_{16} and condensate are very close. Fig 11b shows the contact angle with $nC_{10,}$ which is about 40 degrees.

Fig. 12 shows the imbibition of nC_{10} in the untreated chalk at room temperature and the imbibition of nC_{16} in the treated chalk at 140^oC, as well as the imbibition of nC_{14} at 100^0C. There is a sizable reduction in imbibition for the treated core at 140^oC, both in the rate and to a lesser extent on final recovery. Note that the imbibition results for the duplicate tests for nC_{16} are very close. Imbibition of nC_{14} at 100^0C is lower than imbibition of nC_{16} at $140\ ^0C$. Imbibition results show that there is reduction of imbibition even at 100^0C and 140^oC.

Fig. 13a shows the imbibition results for untreated chalk in water at $80\ ^0C$ and treated chalk in water at room temperature. As can be observed, imbibition of treated chalk at 80^0C is reduced substantially in comparison to the untreated chalk indicating effectiveness of chemical for reduction of imbibition of water even at an elevated temperature. Fig. 13b shows the contact angles of water at room temperature, which is about 110-115 degrees and at elevated temperature of $80\ ^0C$, which is about 60-65 degrees.

We have also treated a chalk sample with 8% solution of FC759. The imbibition results are presented in Fig. 14. At adsorption of (6.8 mg/g), the imbibition in the treated core very effective, but it is about the same as the one with L-16349.

Permeability Change and Other Aspects

We have measured the permeability before and after treatment for some selected cores. We have also measured adsorption for all the treated cores. Table 1 provides the data. For both the chalk and Berea samples there is a reduction of about 10 to 15 percent in permeability. In the past we have seen an order of magnitude increase in liquid phase mobility after treatment[1,2]. Therefore, a reduction of 10 to 15 percent in absolute permeability may not affect the well deliverability.

A finding in the current work is that the treatment became more effective as the treatment temperature is raised. For a few samples, we have raised the temperature to 200^{o}C (results not shown in Table 1). Contact angle measurements show that the treatment is more effective at 200^{o}C than at 100^{o}C and 140^{o}C. The temperature of the reservoir will dictate the treatment temperature. As long as the temperature is above 90^{o}C, treatment of the Berea and chalk should be effective. We have tested the imbibition at 140^{o}C; the evidence is that at such high temperature there is reduction of imbibition. In case we need better results, we may use higher concentration of the polymer.

The polymer seems very durable based on reusing the treated cores. We are currently performing some atomic force microscopy (AFM) to find the durability of the treatment, especially at high temperatures.

Flow Testing

We have carried out two types of flow testing to examine the effectiveness of chemical treatment in liquid and gas mobilites. In one set of tests, the liquid saturation in the core is measured by liquid and gas injection in which the lower liquid saturation implies higher liquid mobility. In the second type of testing, we carry out injection in two parallel cores of similar permeability one treated, and another untreated to examine the effect of treatment on liquid mobility. The results from these types of tests will be presented in the following.

Liquid Saturation Tests: Three tests were conducted both for treated and untreated cores using the apparatus sketched in Fig 15. Visual core holder was used to see the flow pattern of the liquid. Gas and liquid are mixed in a capillary-tubing mixer and then injected simultaneously into an air-saturated core. Liquid flow rate was maintained at the

rate of 4 cc/hr and a pressure drop of 0.1 psi/cm, 0.2 psi/cm and 0.3 psi/cm were maintained by varying the gas injection rate. In the untreated core, the saturation increased linearly with time before breakthrough of liquid and the movement of liquid front was piston like (see Fig 16). The flow pattern for the treated core was not piston like and it was diffused; no invading oil front was observed for treated core and breakthrough of the oil was earlier than that of the untreated core (see Fig 17).

Accumulated oil saturation for the untreated core was about 0.62 PV for the untreated core whereas for treated core residual oil saturation was about 0.47 PV, for the pressure gradient of 0.1 psi/cm. A lower value of the average saturation in the treated core indicates a high mobility. In the previous work[2] accumulated oil saturation was observed to be about 0.30 when Berea was treated with 2% FC-722.

Oil Injectivity

Parallel core flow test was carried out to study the effect of wettability alteration (see Fig 18). Oil was injected into two parallel cores before and after wettability alteration. Oil was injected at the rate of 240 cc/hr. As may be observed oil injectivity through one of the core (permeability 250 md) is substantially lower than the oil flow through other core (permeability 325 md) indicating mobility of oil in one of the cores is much lower than the other core (see Fig 19). However, after treatment of one of the core trend reverses, (see Fig 20), the core which was with lower production rate, now showed a higher production rate. Treatment of the core increases the oil mobility in the core thereby increasing the production in the treated core.

Conclusions

1. The new polymer, which is environmentally sound, is effective in the alteration of wettability.
2. The 9% solution of polymer in water when used in the treatment, provides effective wettability alteration for both water, nC_{10}, nC_{14}, nC_{16} and the condensate liquid in both Berea and chalk.
3. There is an increase in liquid wetting with temperature but even at a temperature of 140^0C, there is a significant reduction of liquid wetting when treated aand untreated rocks are considered.

4. The new polymer similar to the ones that we have used in the past[1,2] alters wettability permanently. This makes it suitable for field applications.

Because of the above features, the polymer has a promise for field application. We are currently further testing for the field that is being considered for trial.

Nomenclature

W = mass flow rate

p = Pressure

L= Length

A = area

R = gas constant

z = compressibility factor

k = permeability

b = turbulence factor

ρ = density

μ = viscosity

References

1. Tang, G. and Firoozabadi, A.: "Wettability Alteration to Intermediate Gas-Wetting in Porous Media at Elevated Temperature," Transport in Porous Media (to appear)
2. Tang, G. and Firoozabadi, A.: "Relative Permeability Modification in Gas-Liquid Systems Through Wettability Alteration to Intermediate Gas-Wetting," SPE Reservoir Evaluation and Engineering (Dec. 2002)

3. Katz, D.L., Cornell, D., Kobayashi, R., Poettman, F.H., Vary, J.A., Elenbaas, J.R. and Weinaug, C.F.: *Handbook of Natural Gas Engineering*, McGraw-Hill Book Co. Inc., New York City (1959).

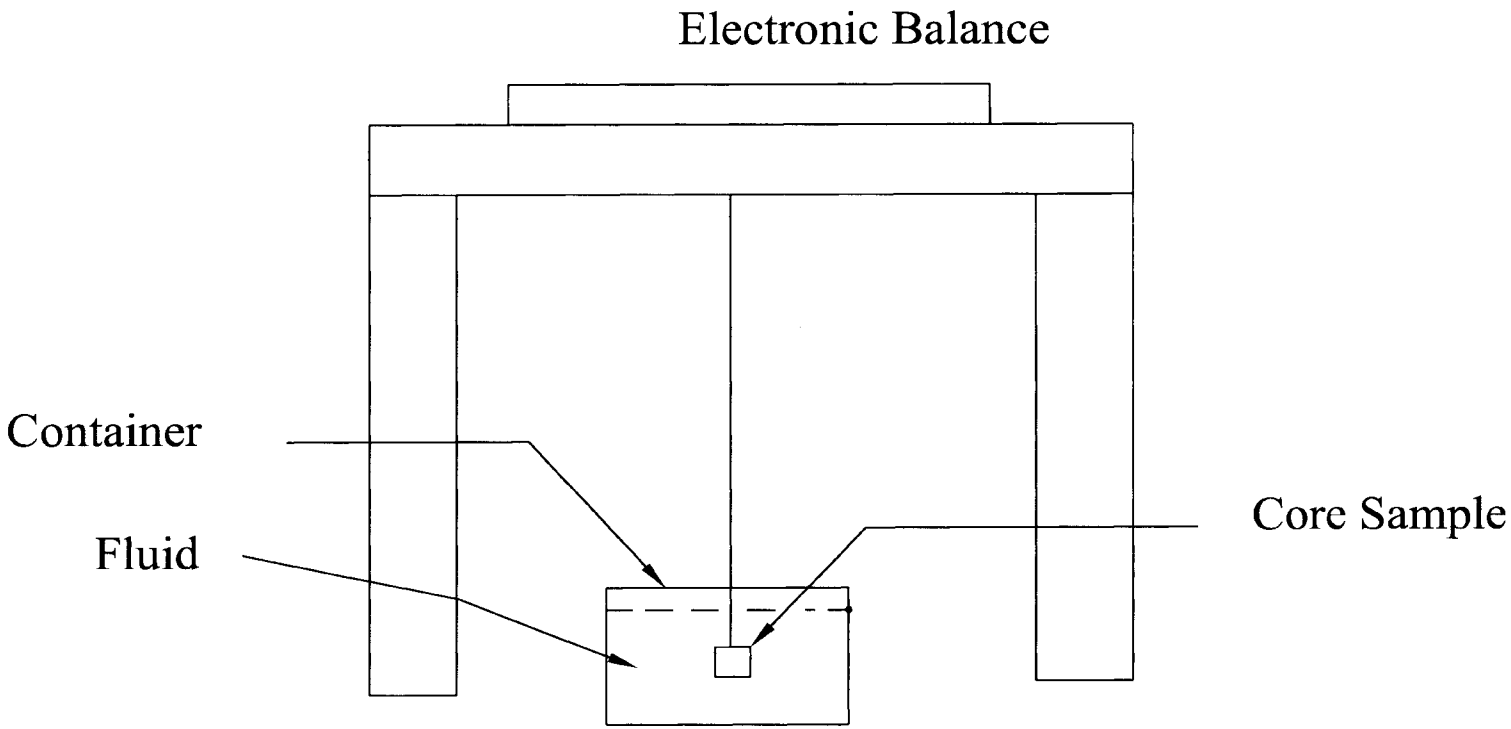

Fig 1. Imbibition Setup

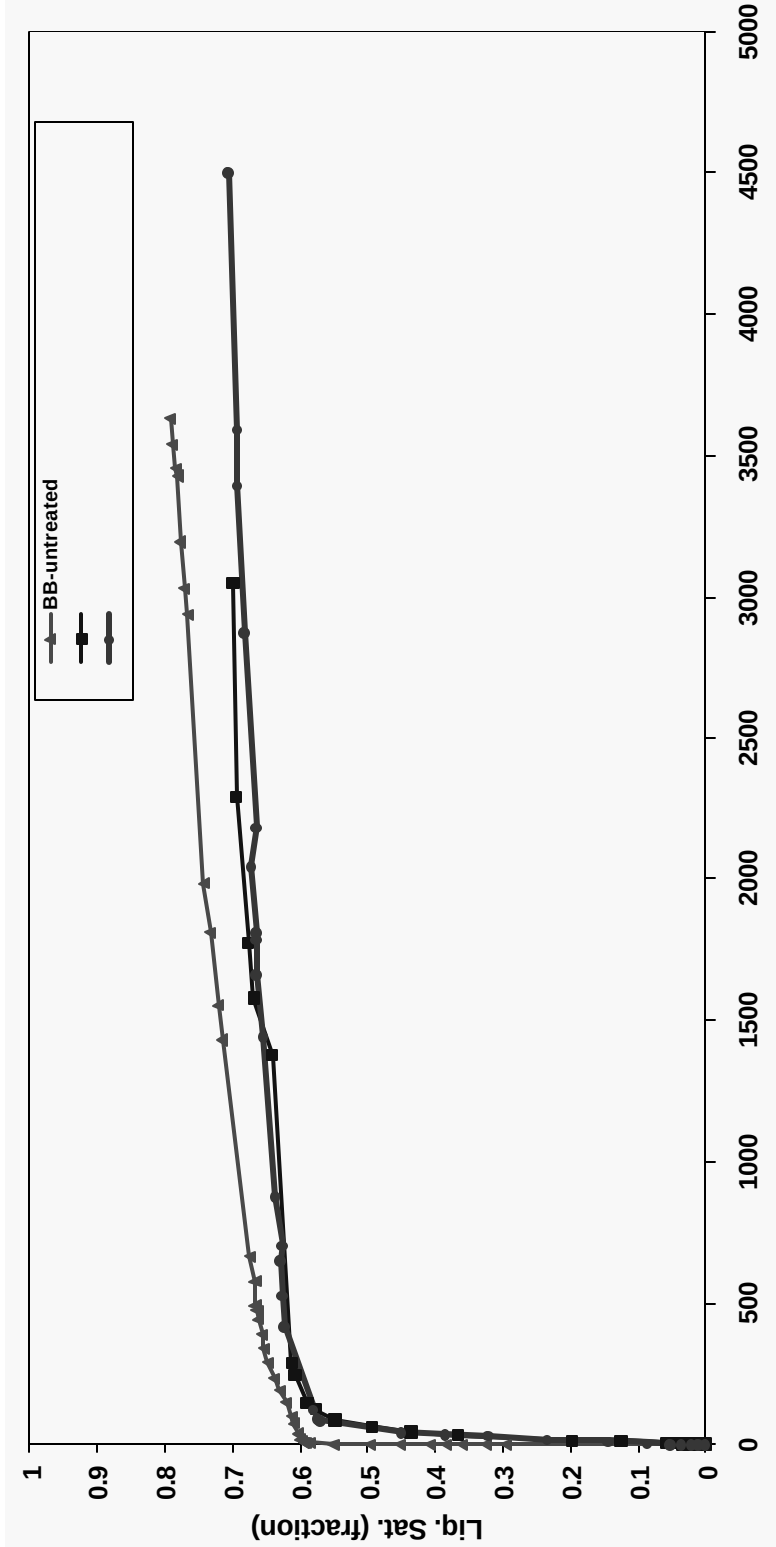

Fig. 2a Imbibition of nC_{10} in air-saturated Berea; untreated, and treated with 3% polymer: *T* ^0C

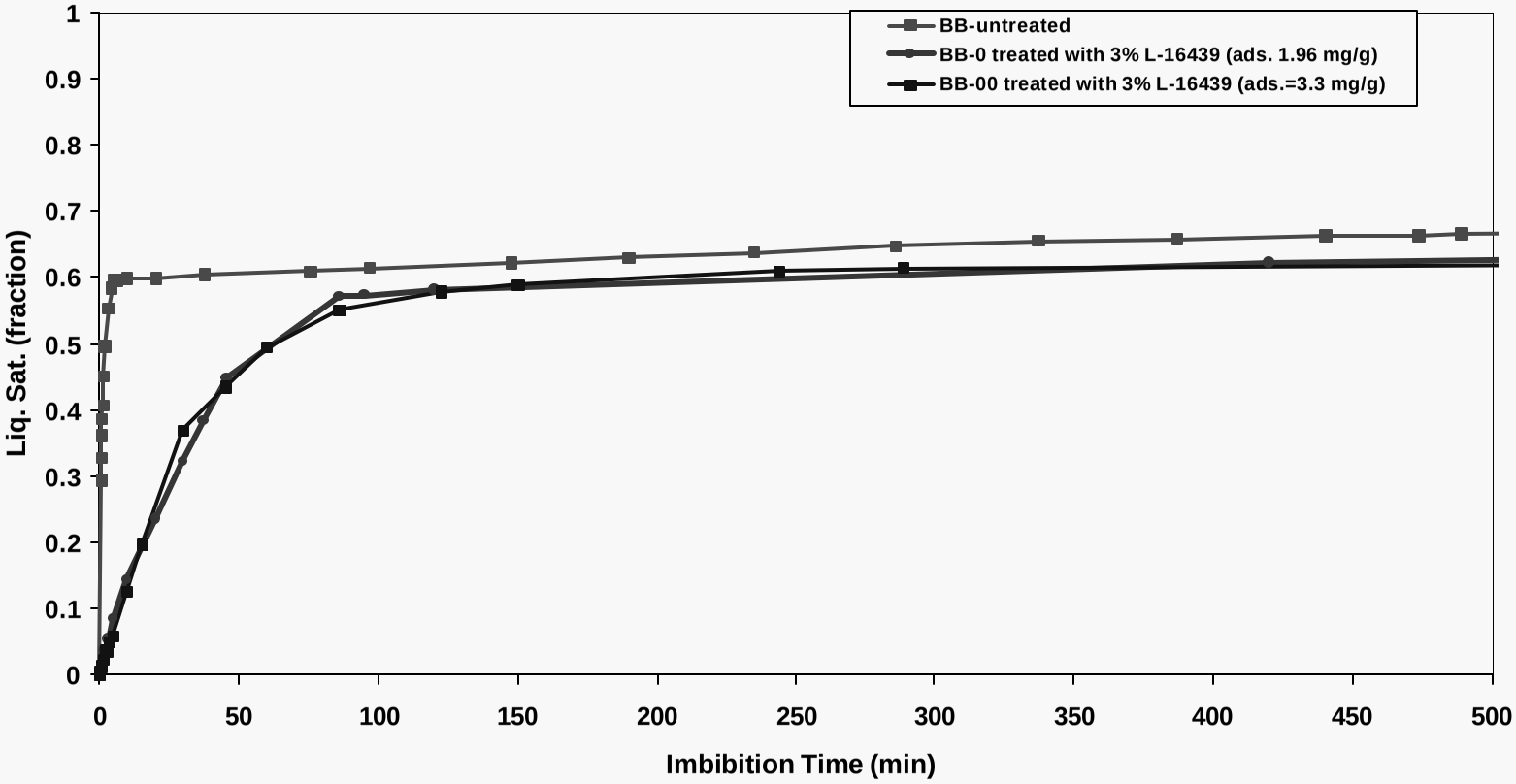

Fig. 2b Imbibition of nC_{10} in air-saturated Berea; untreated, and treated with 3% polymer: T = 24 ^{0}C

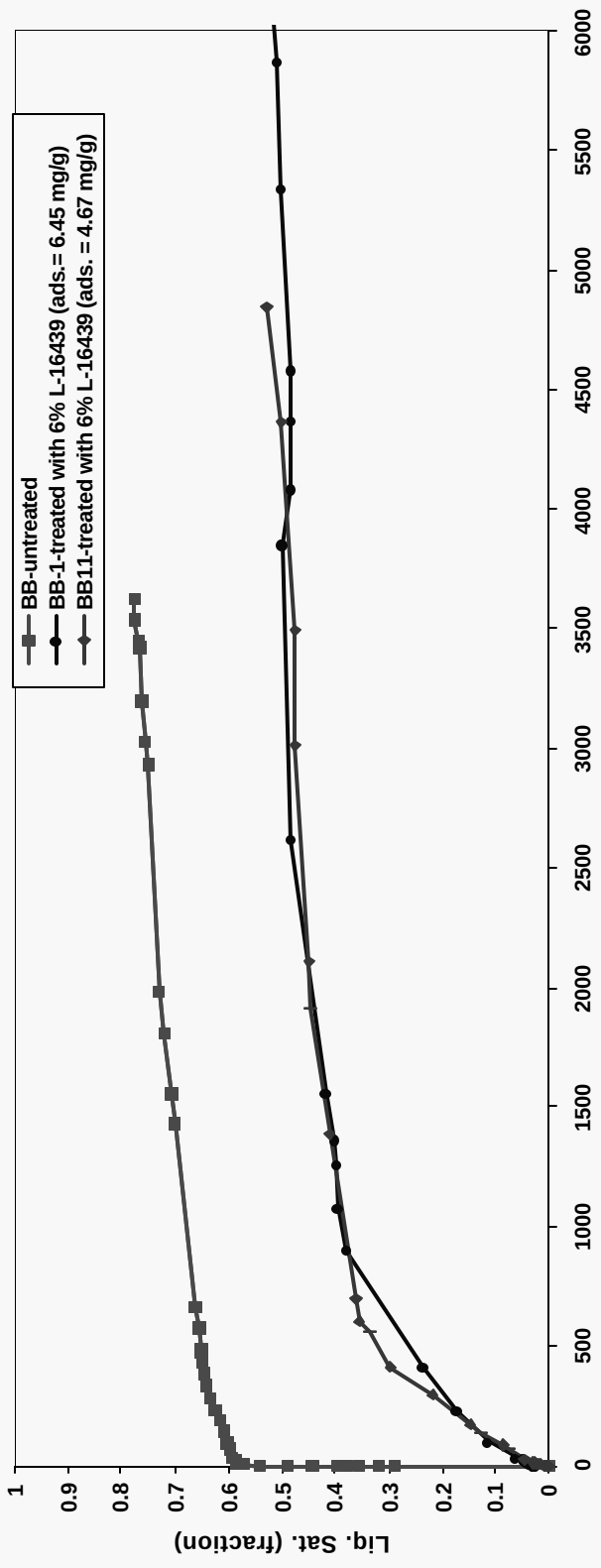

Fig. 3 Imbibition of nC_{10} in air-saturated Berea; untreated, and treated with 6% polymer.: T=24 ^{0}C

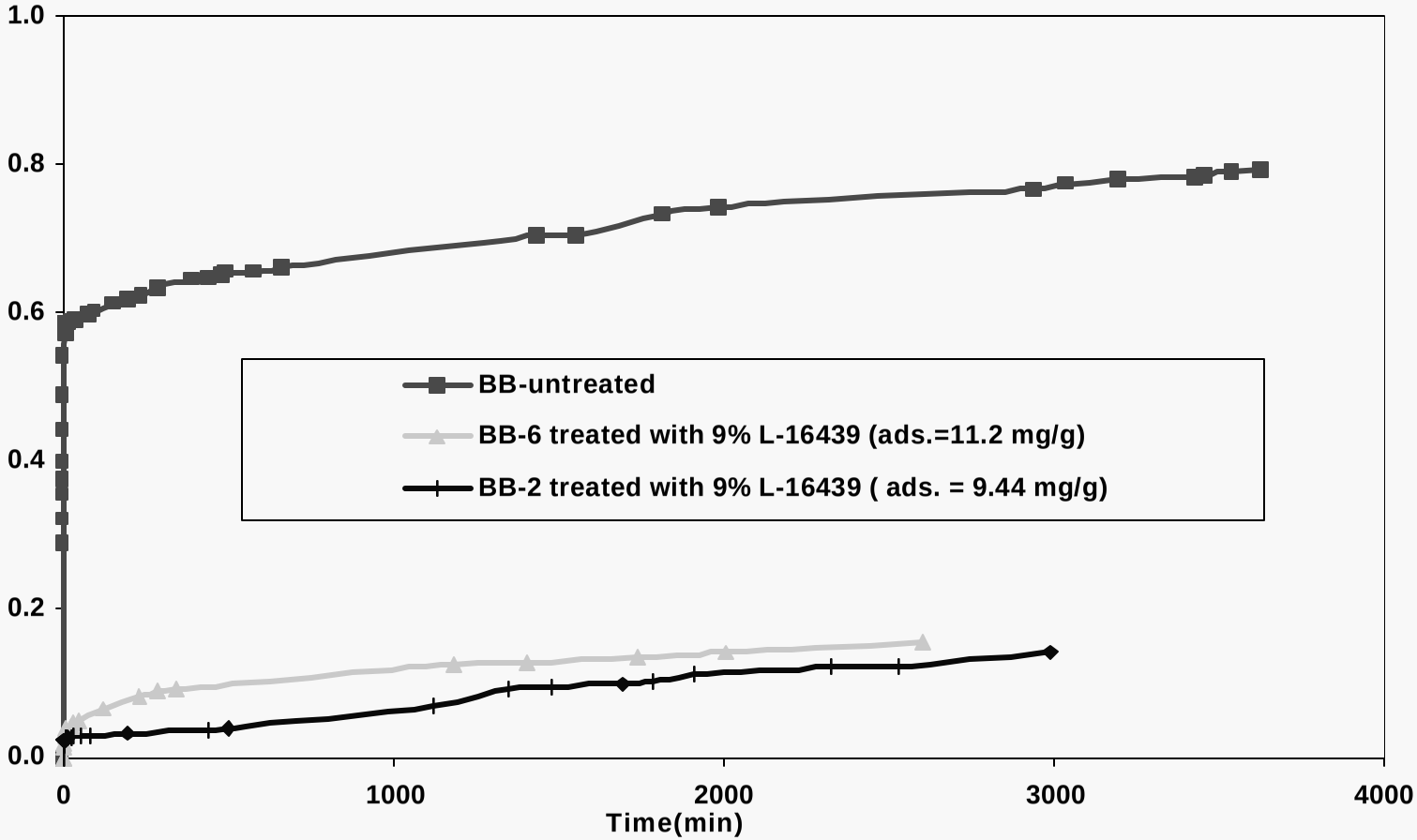

Fig. 4a Imbibition of nC_{10} in air-saturated Berea; untreated and treated with 9% polymer.: $T = 24\ ^0C$

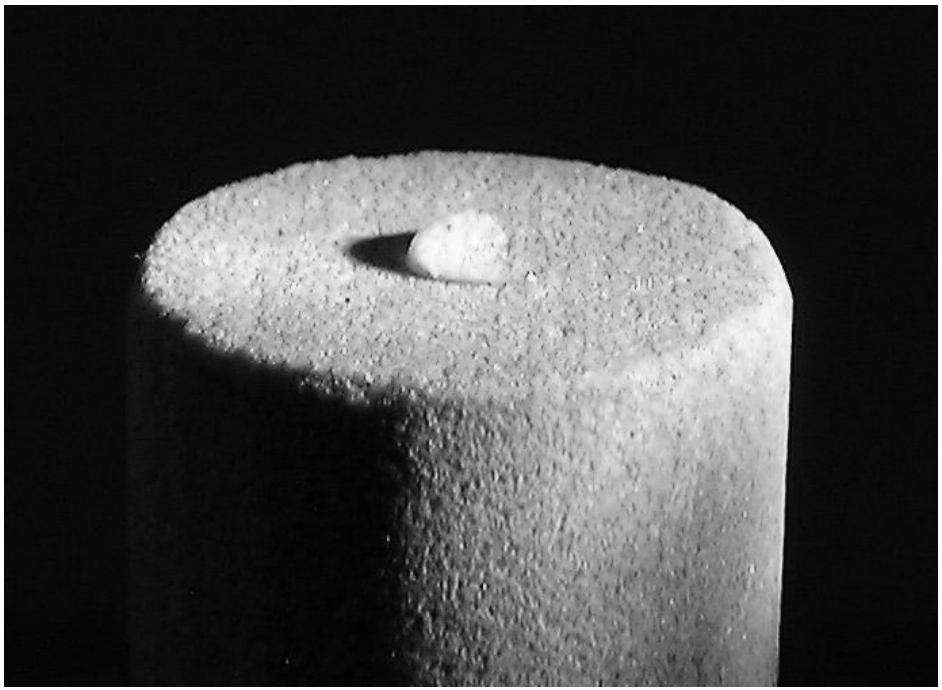

Fig 4b-Contact Angle for Air-nC10-Berea system: treated

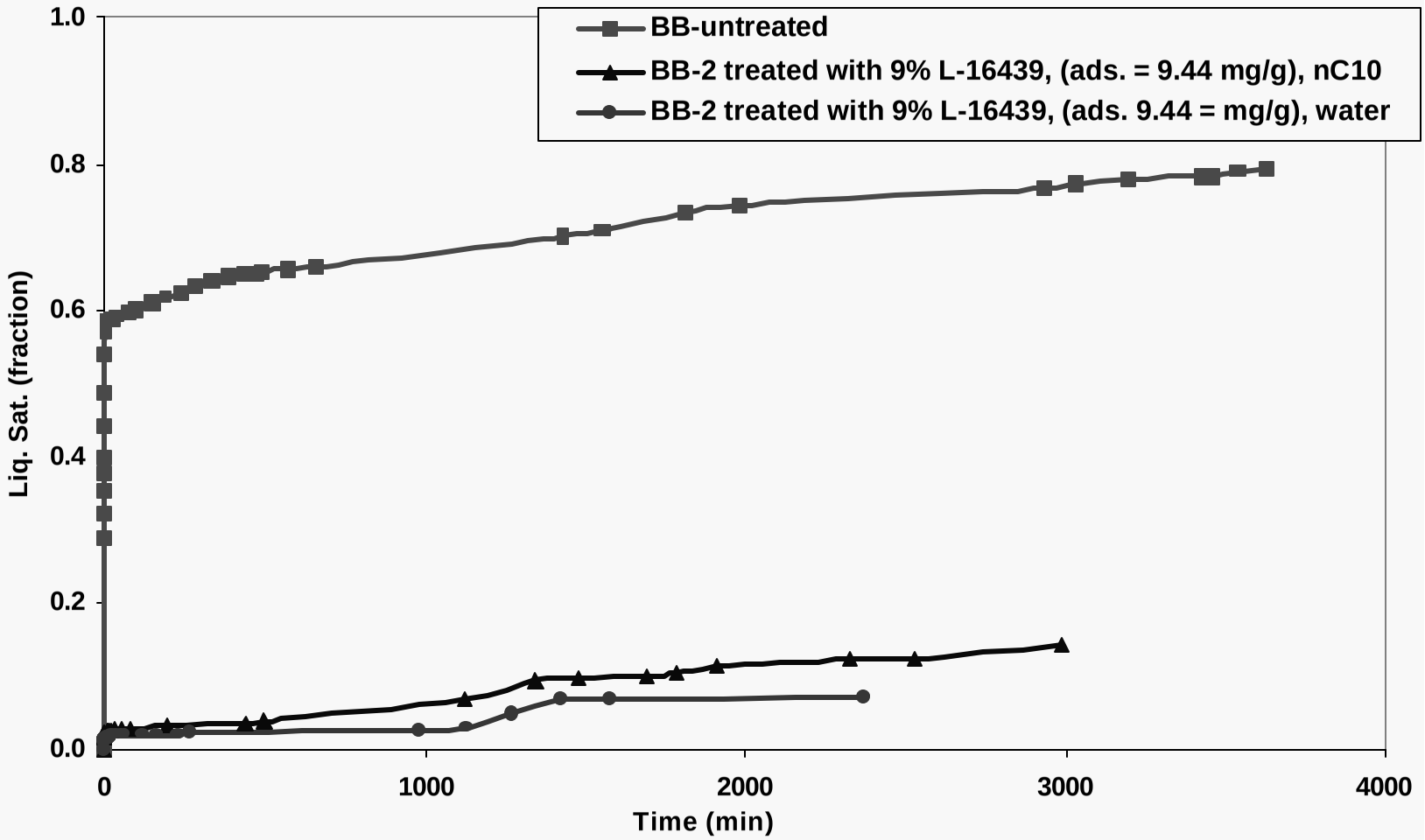

Fig. 5a Imbibition of nC_{10} and water in air-saturated Berea; untreated and treated with 9% polymer.: T =24 ^{0}C

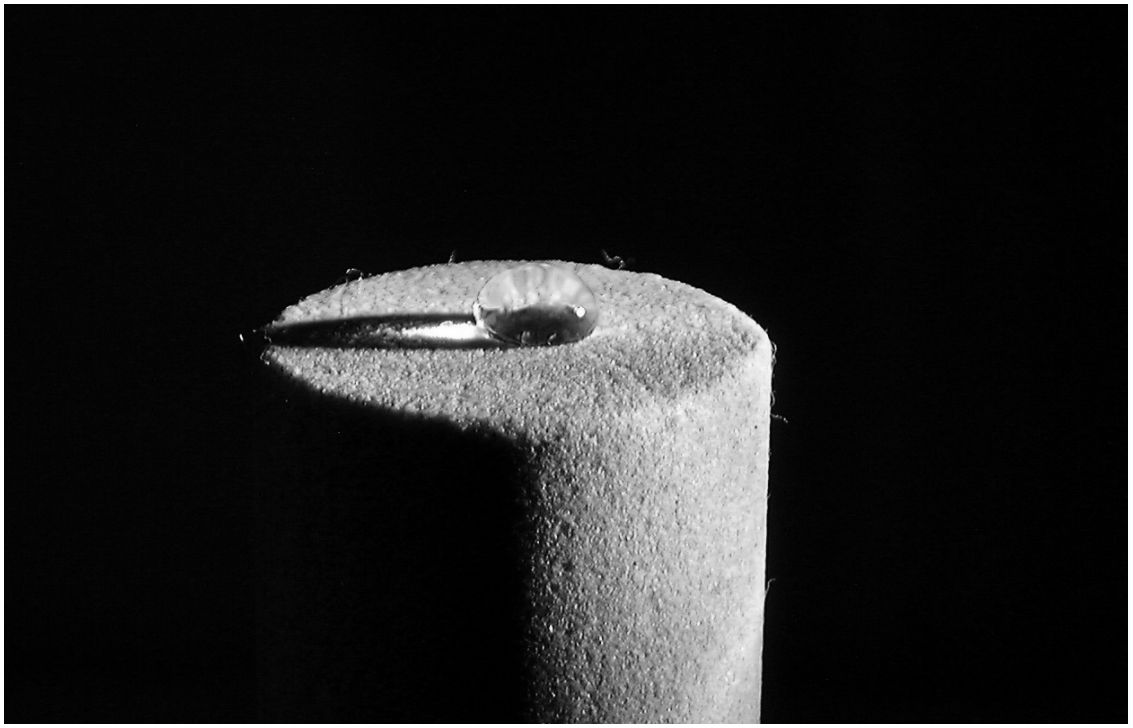

Fig 5b-Contact angle for Air-Water-Berea system: treated core (BB-6)

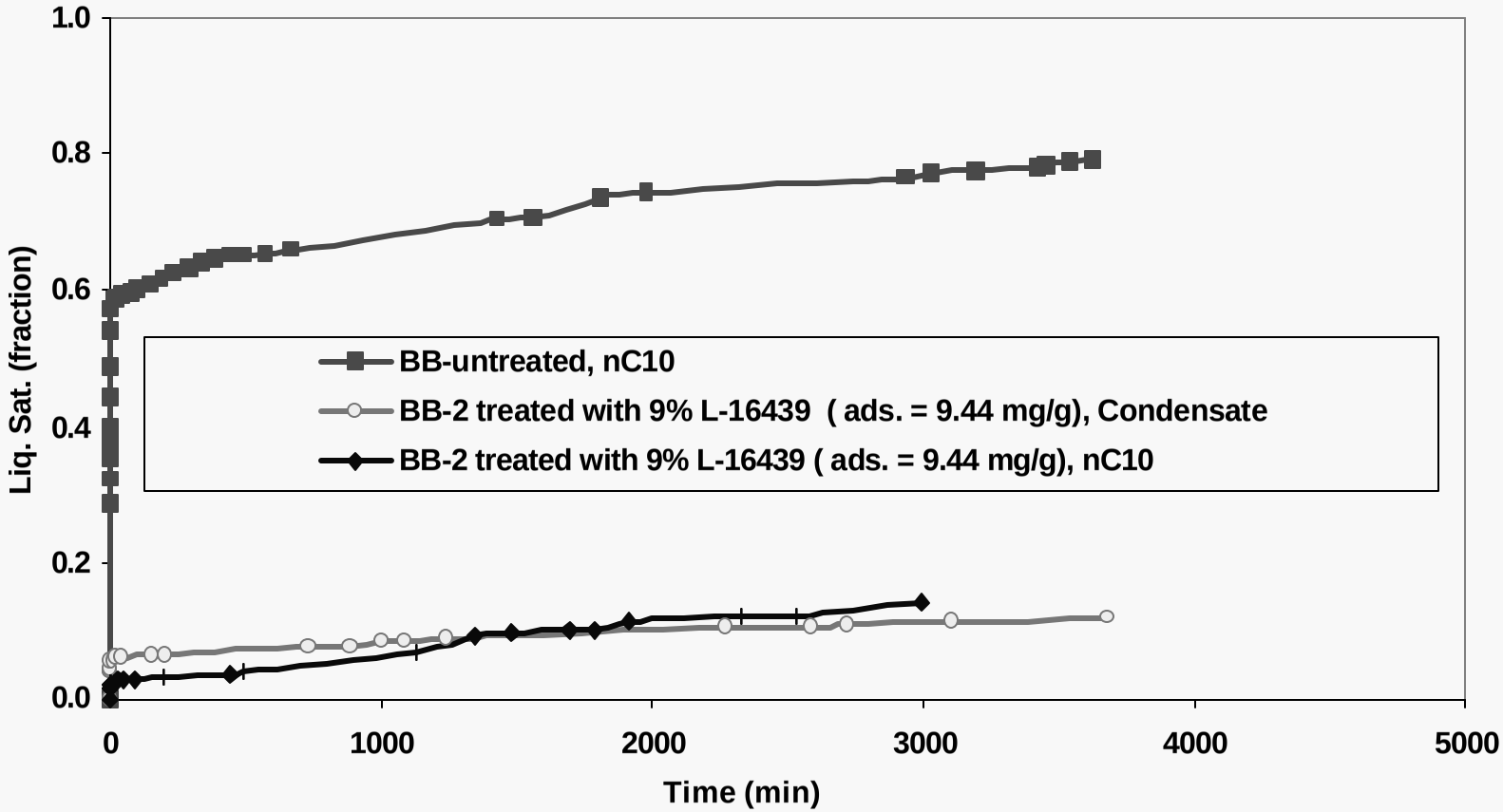

Fig. 6 Imbibition of nC_{10} and condensate in Berea; untreated and treated with 9% polymer.: $T = 24\ ^0C$

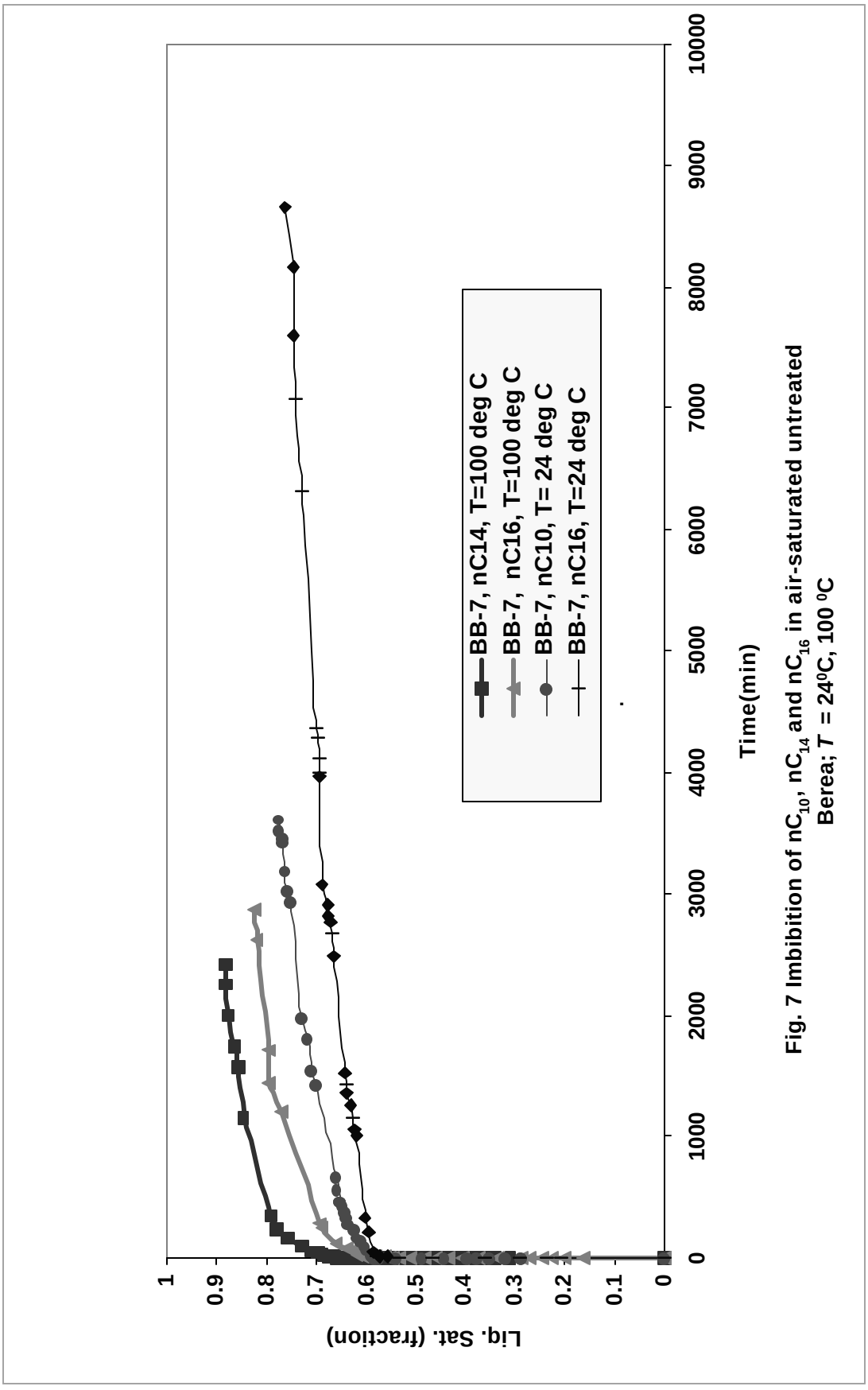

Fig. 7 Imbibition of nC_{10}, nC_{14} and nC_{16} in air-saturated untreated Berea; T = 24^{0}C, 100 ^{0}C

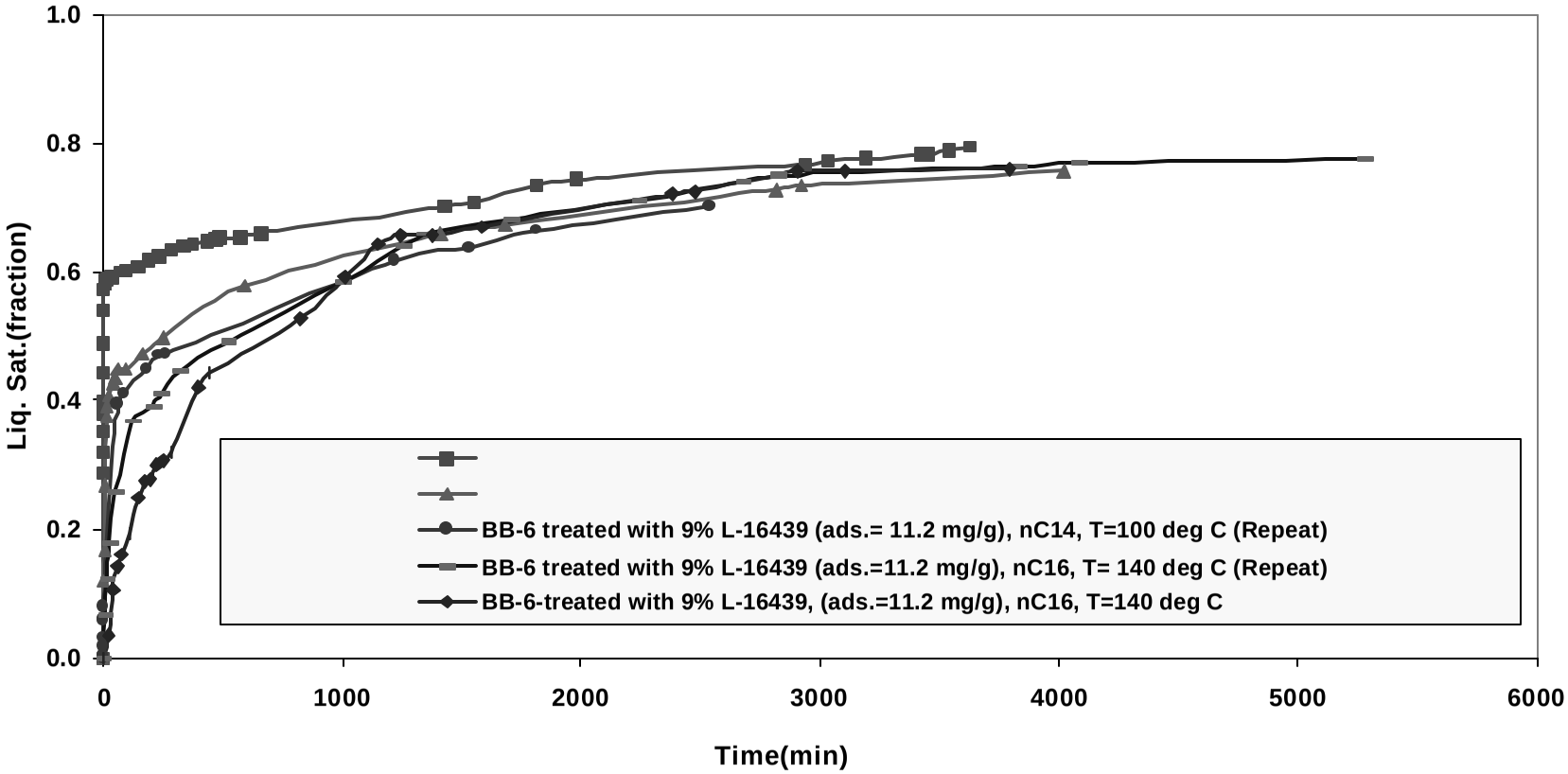

Fig. 8 Imbibition of $nC_{10,}$ nC_{14} and nC_{16} in air-saturated Berea; untreated and treated with 9% polymer.: T = 24 ^{0}C, 100 ^{0}C and 140 ^{0}C

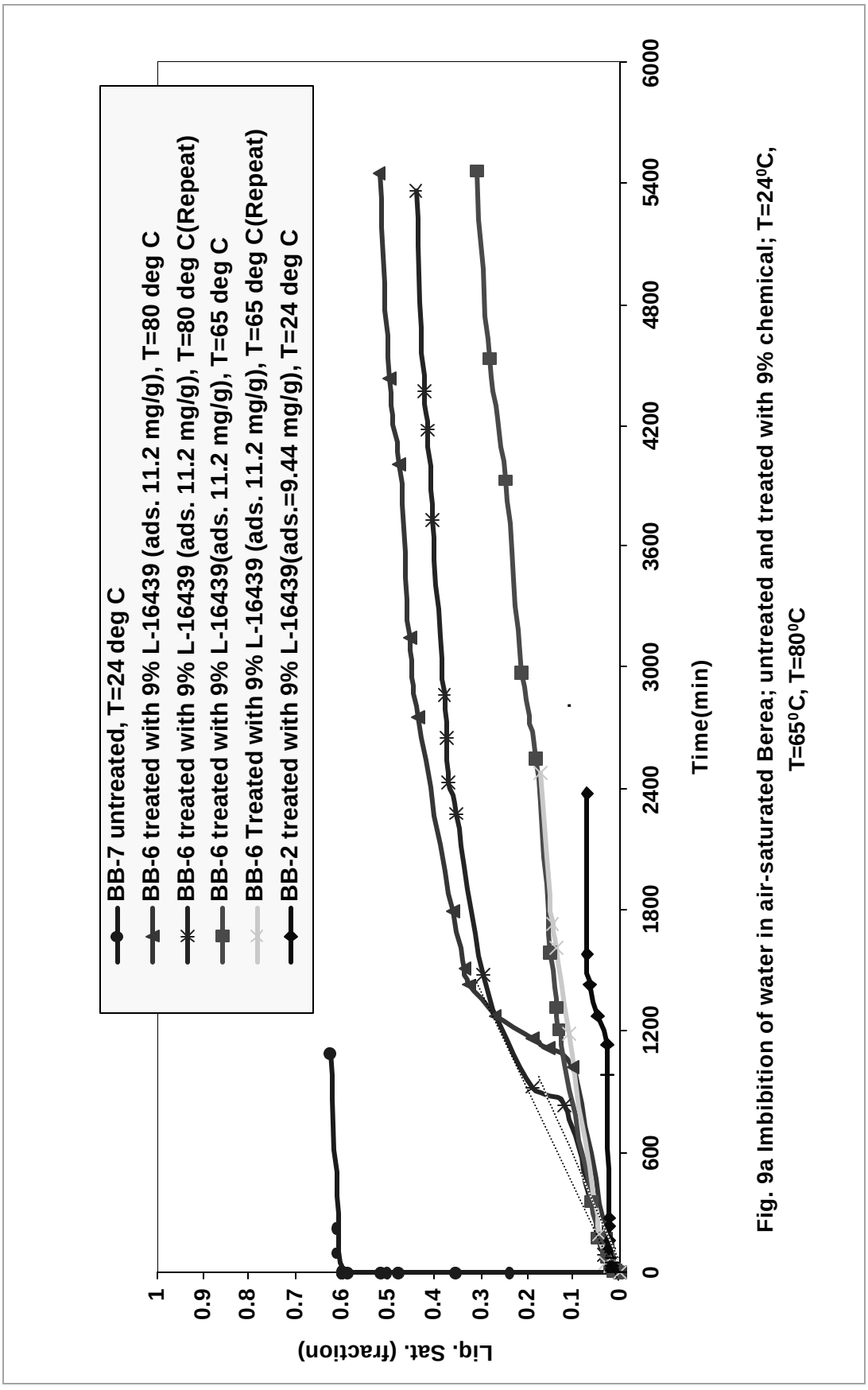

Fig. 9a Imbibition of water in air-saturated Berea; untreated and treated with 9% chemical; T=24^{0}C, T=65^{0}C, T=80^{0}C

Untreated Berea(BB); T=24^{0}C

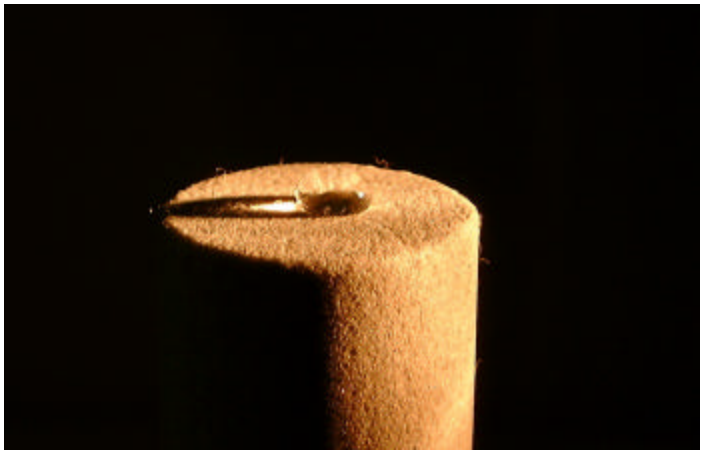

Treated Berea (BB-6); Contact Angle: 120-130 degrees; T=24^{0}C

Treated Berea (BB-6); Contact Angle: 60-70 degrees; T=80^{0}C

Fig 9b Contact angles for Air-Water-Berea system at 24 ^{0}C and at 80 ^{0}C

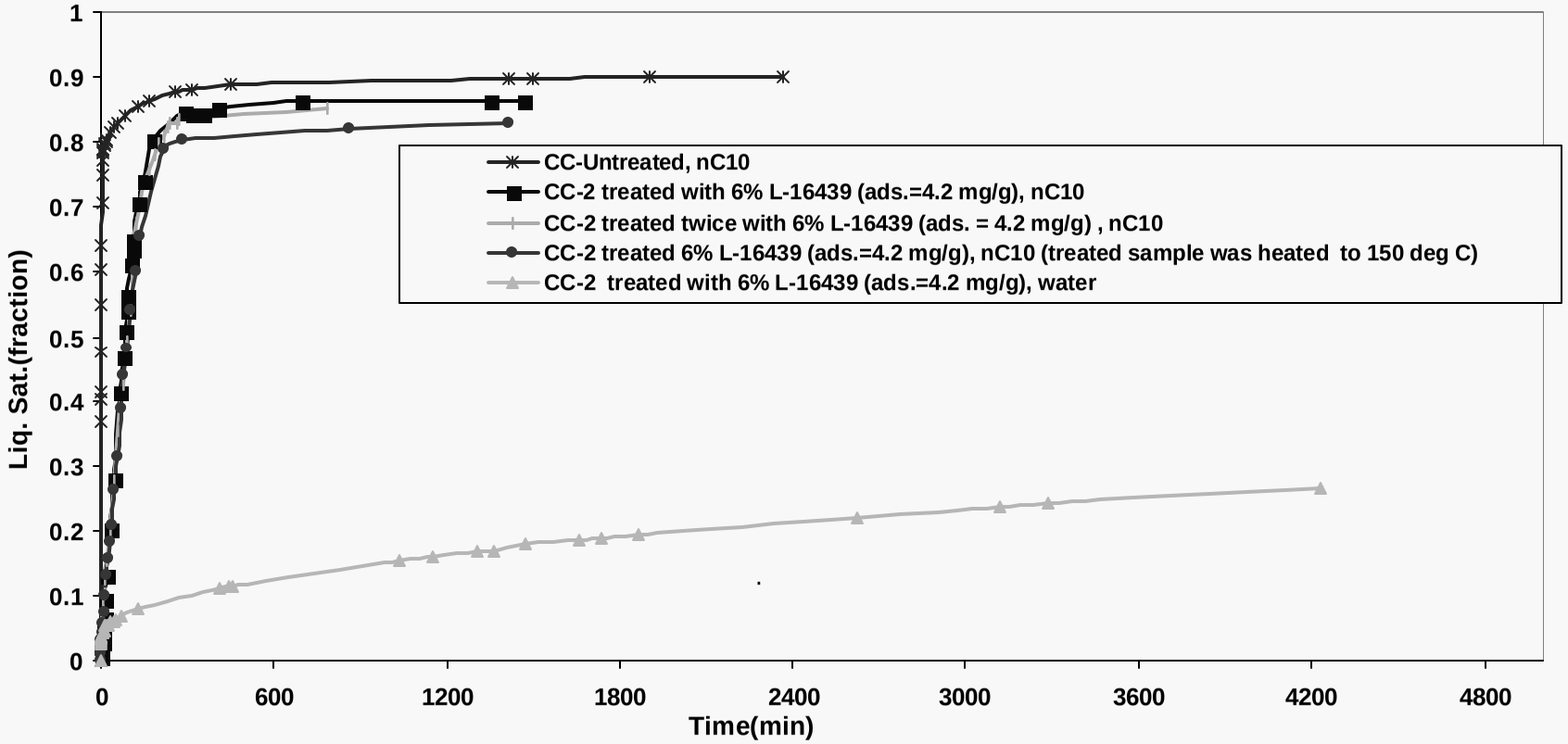

Fig. 10a Imbibition of nC_{10} and water in air-saturated Chalk; unterated and treated with 6% polymer.: T = 24°C

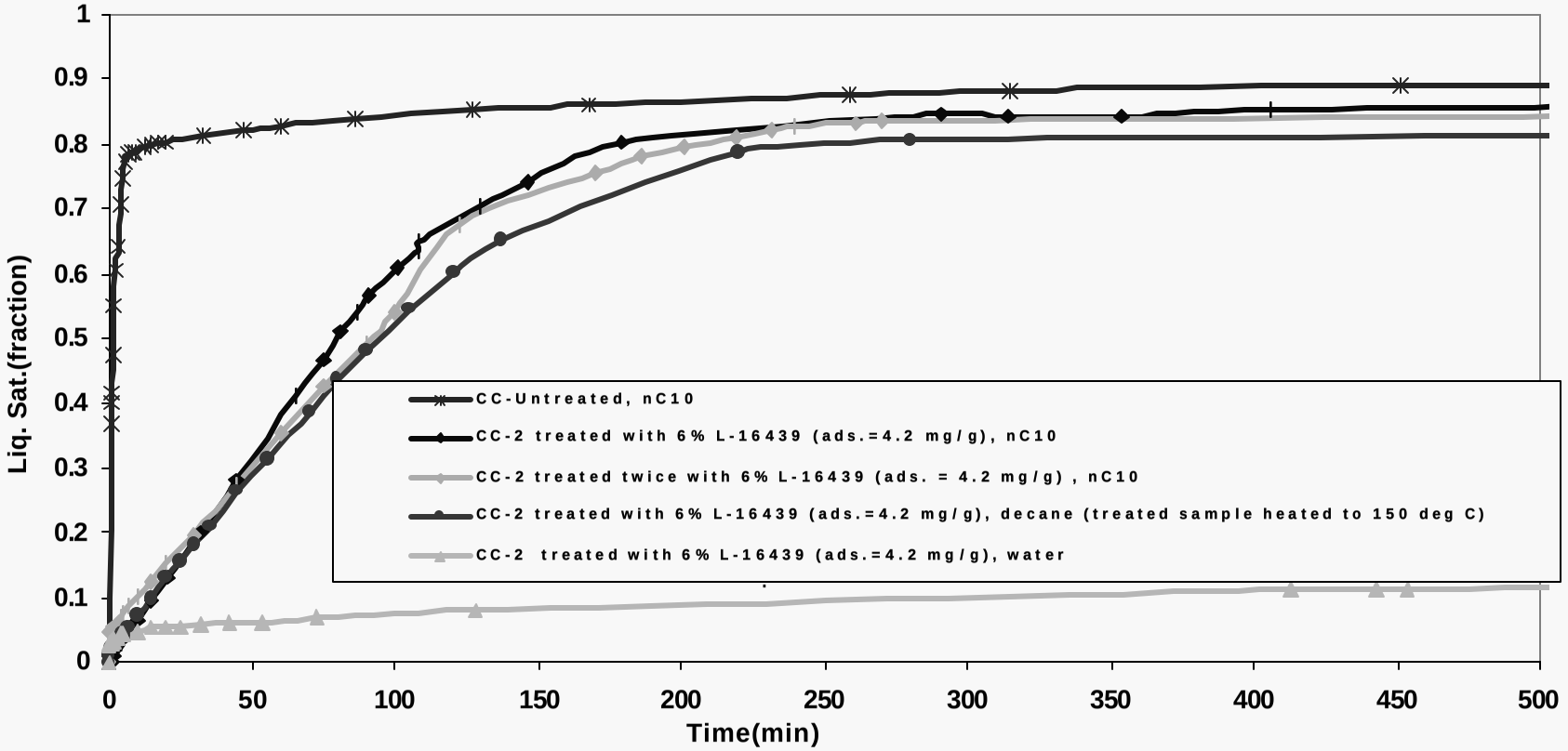

Fig. 10b Imbibition of nC_{10} and water in air-saturated Chalk; untreated and treated with 6% polymer.: $T = 24\ ^0C$

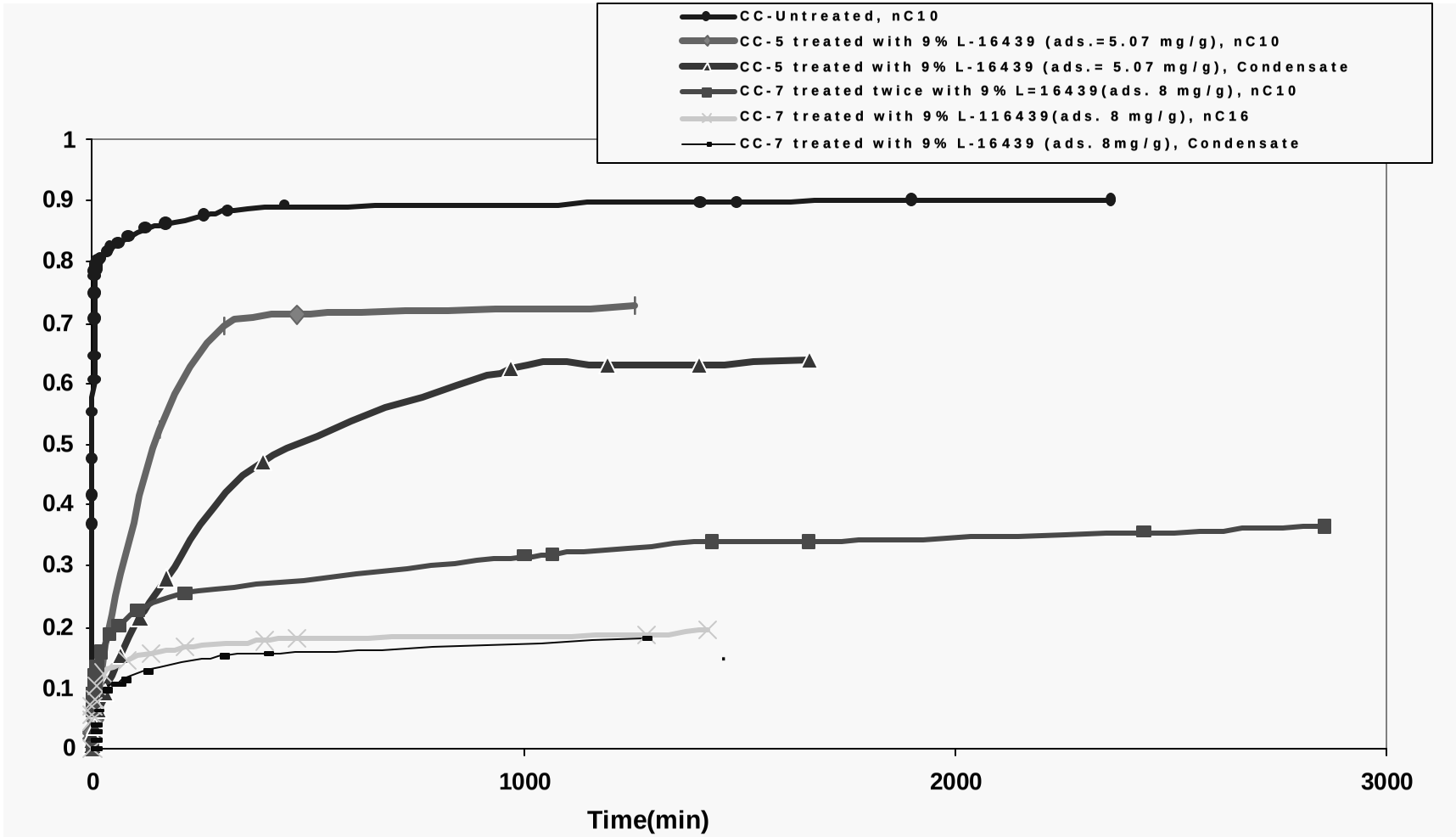

Fig.11a Imbibition of $nC_{10,}$ condensate, and nC_{16} in air-saturated Chalk; untreated and treated with 9% chemical.:*T* = 24 ^{0}C

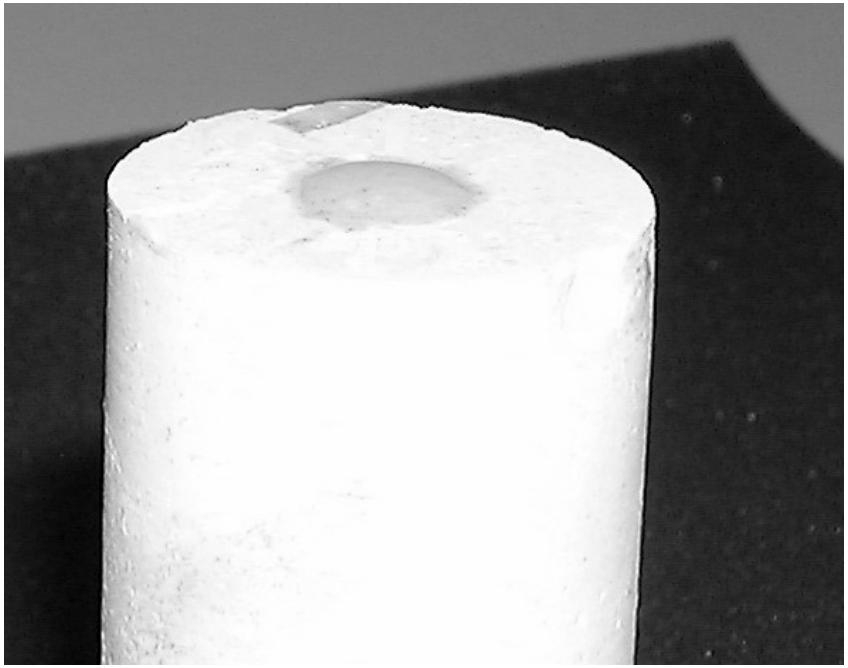

Fig 11b- Contact Angle for Chalk-nC_{10}-Air system; T=24^0C; treated chalk (CC-5)

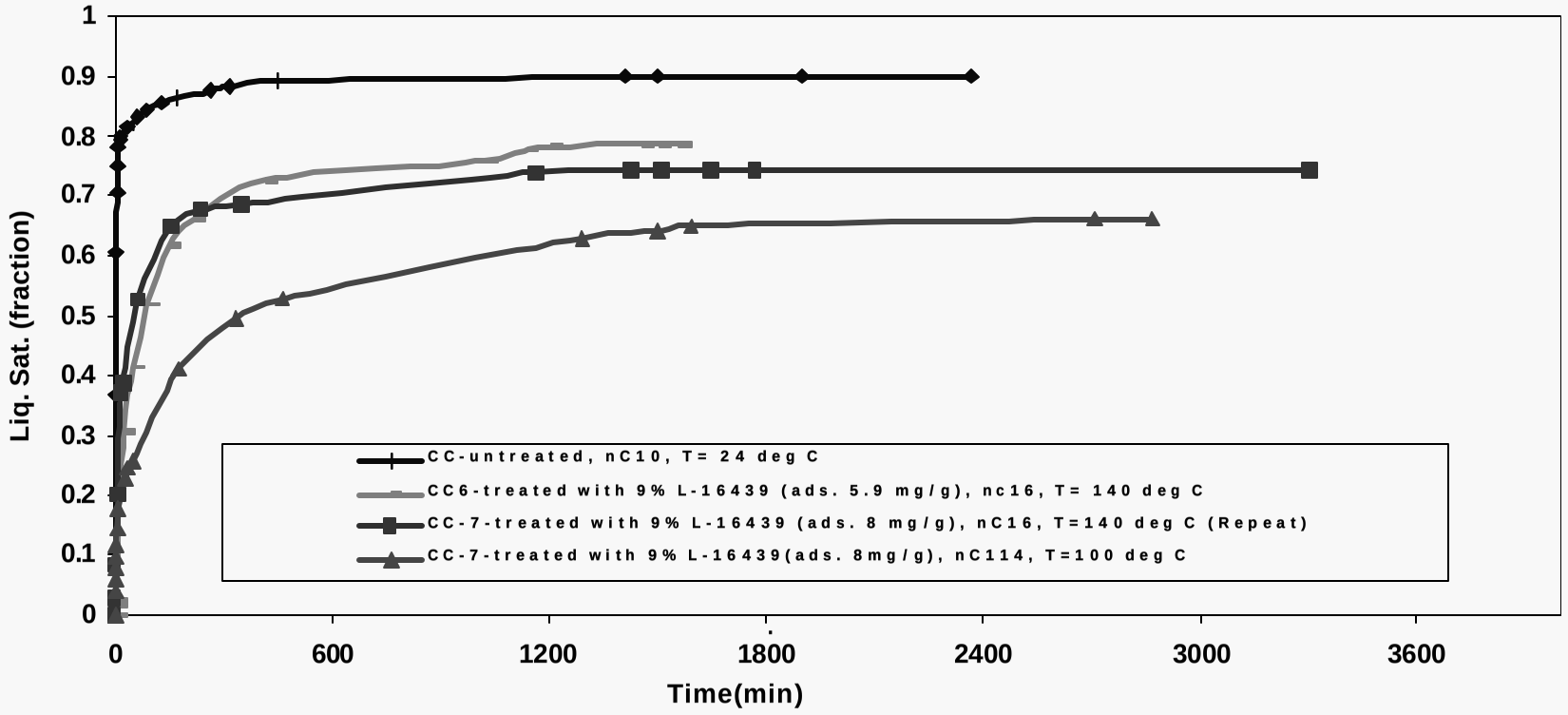

Fig. 12 Imbibition of $nC_{10,}$ nC_{14} and nC_{16} in air-saturated chalk; untreated and treated with 9% chemical :*T* =24 ^{0}C, 100 ^{0}C and 140 ^{0}C

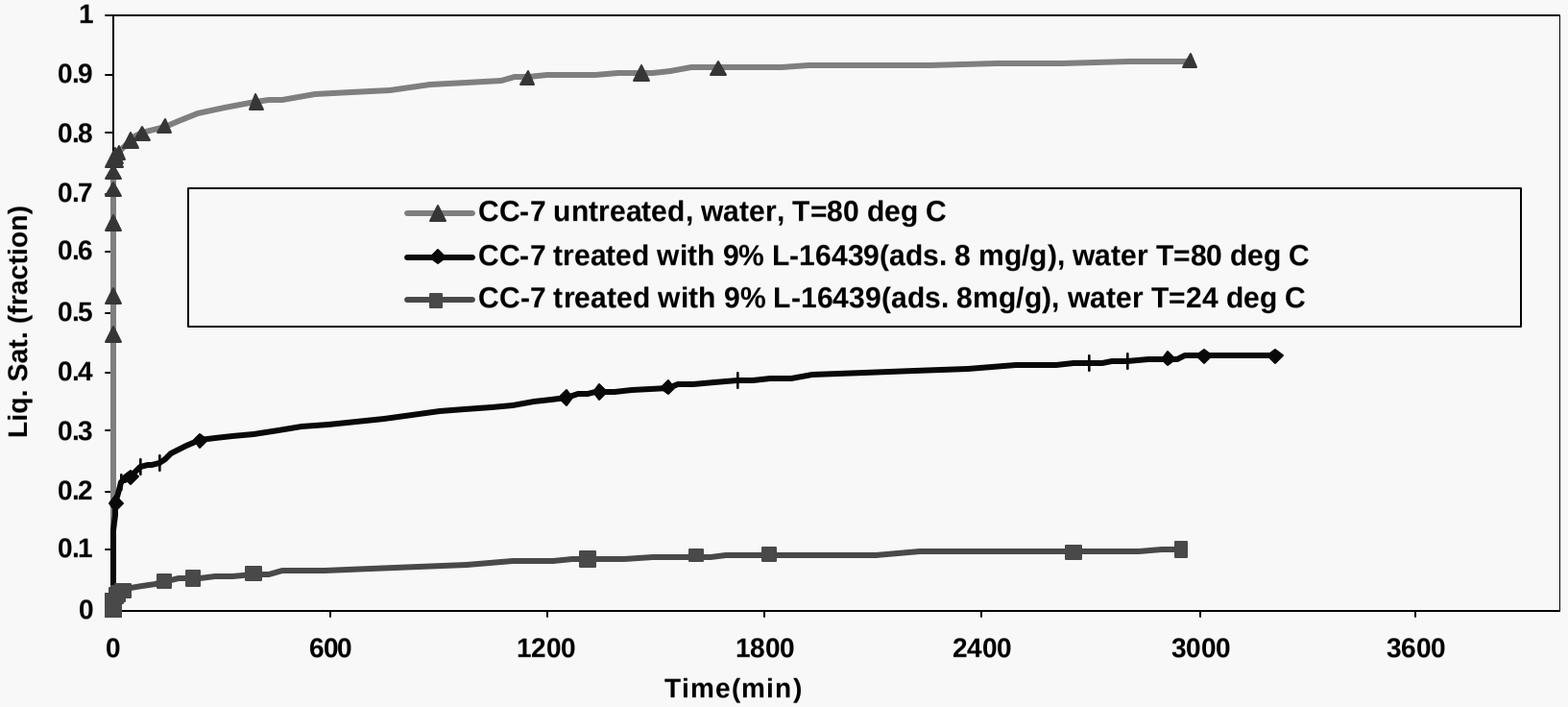

Fig. 13a Imbibition of water in air-saturated Chalk; untreated and treated with 9% chemical : T= 25 ^{0}C, *T* = 80 ^{0}C

Treated chalk (CC-7); Contact Angle: 110-115 degrees; T=24^{0}C

Treated chalk (CC-7) contact angle: 60-65 degrees; T=80^{0}C

Fig 13b-Contact angle for Air-Water-Chalk system at T=24 ^{0}C and at 80 ^{0}C

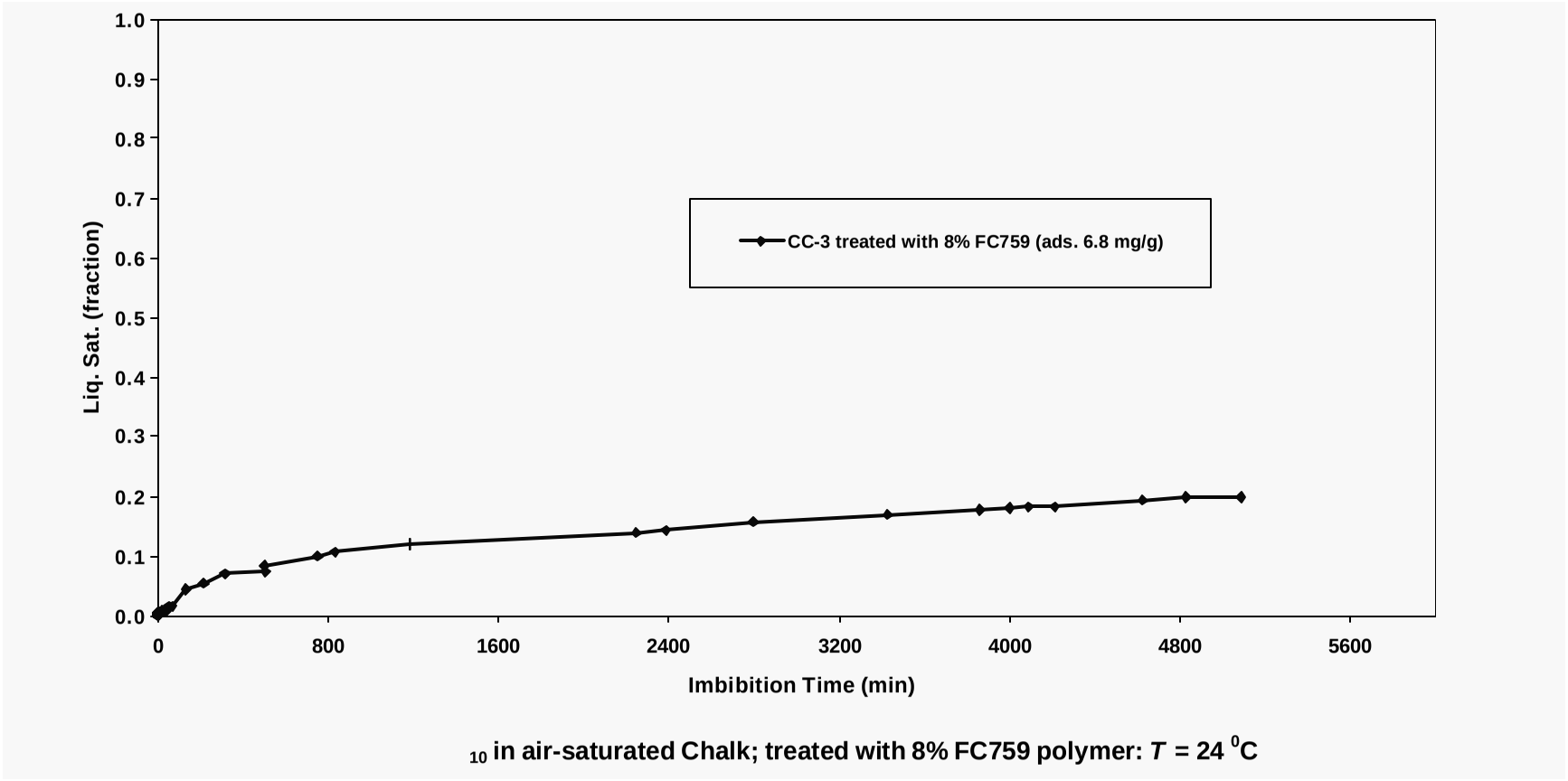

$_{10}$ in air-saturated Chalk; treated with 8% FC759 polymer: T = 24 ^{0}C

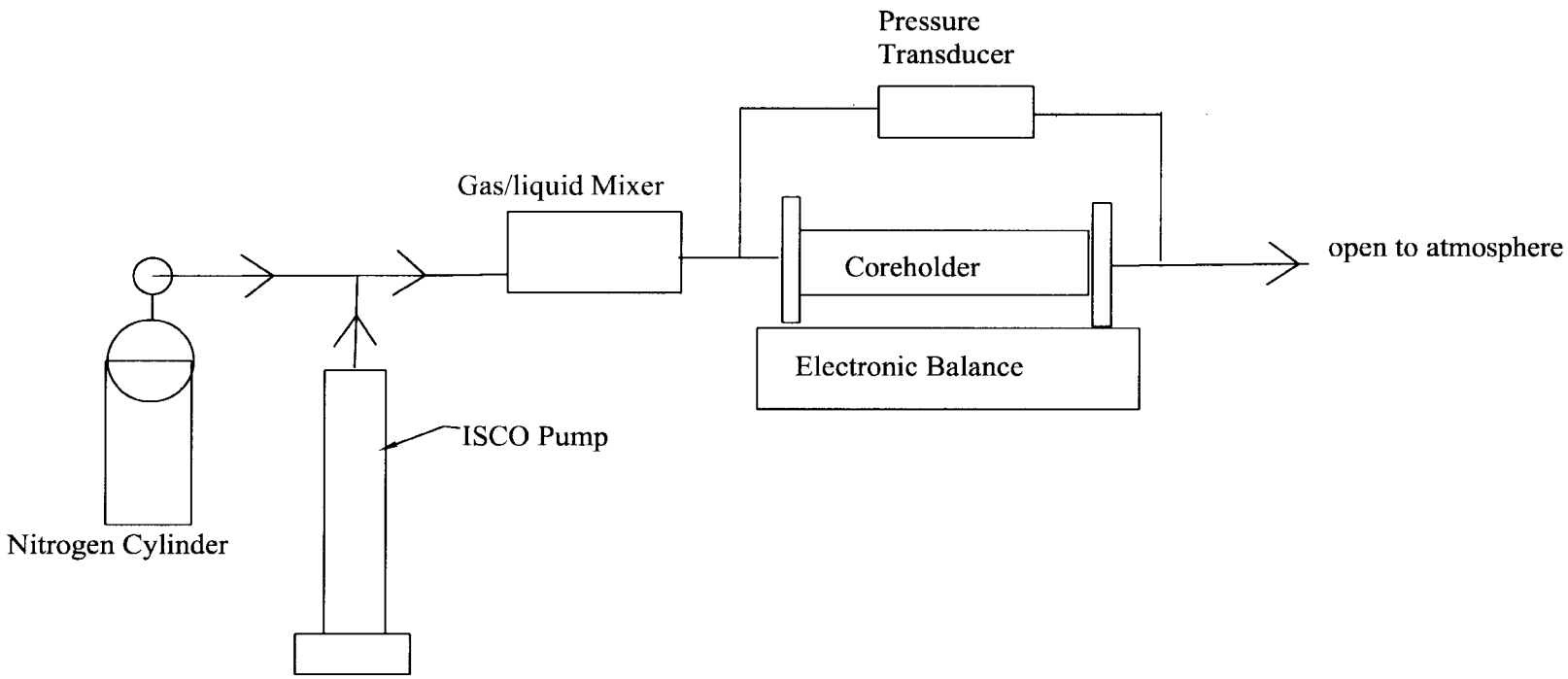

Fig 15- Schematic of Apparatus for Coreflooding

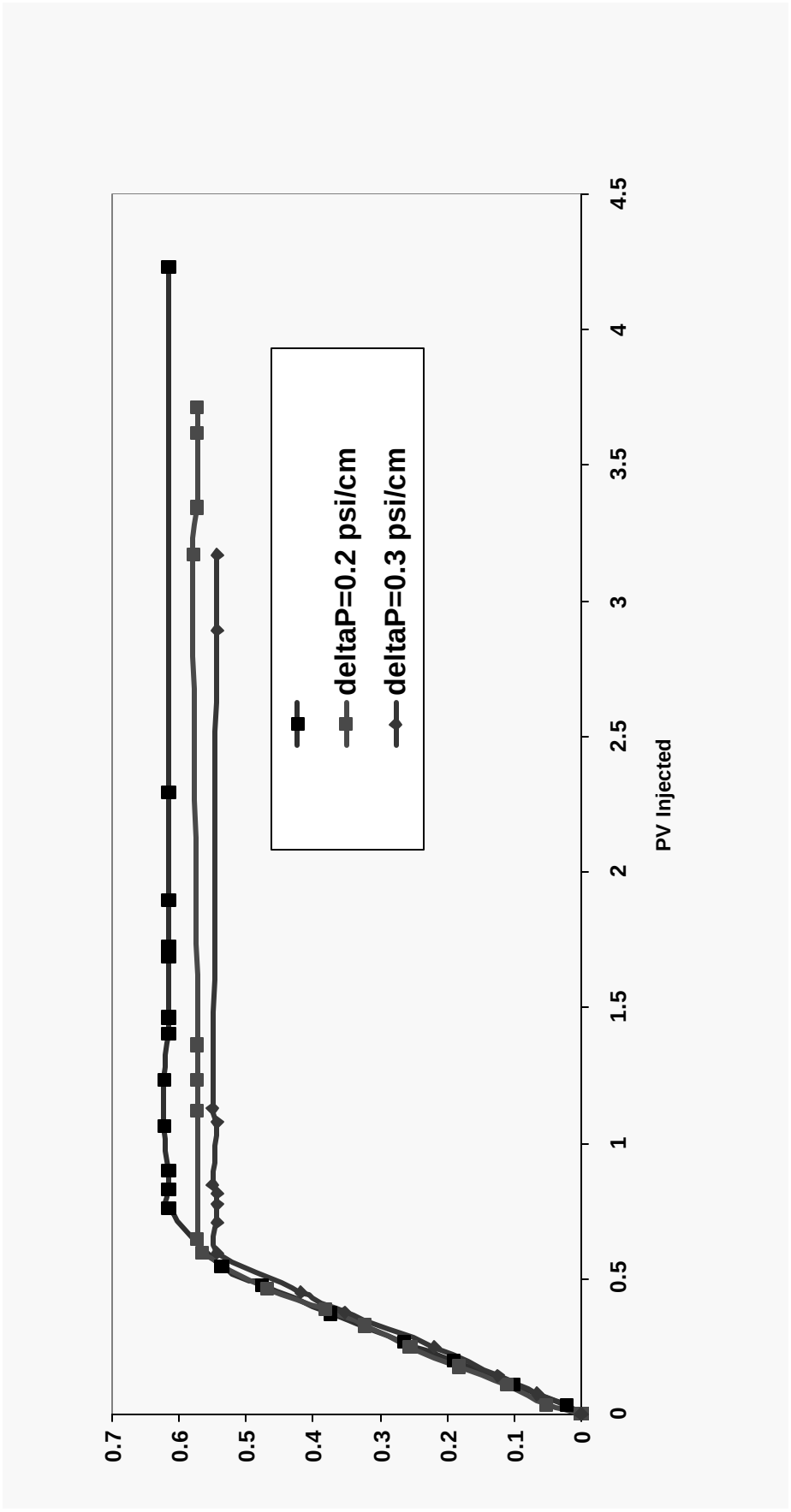
0.7
0.6
0.5
0.4
0.3
0.2
0.1
0
0
0.5
1
1.5
2
2.5
3
3.5
4
4.5
PV Injected
deltaP=0.2 psi/cm
deltaP=0.3 psi/cm

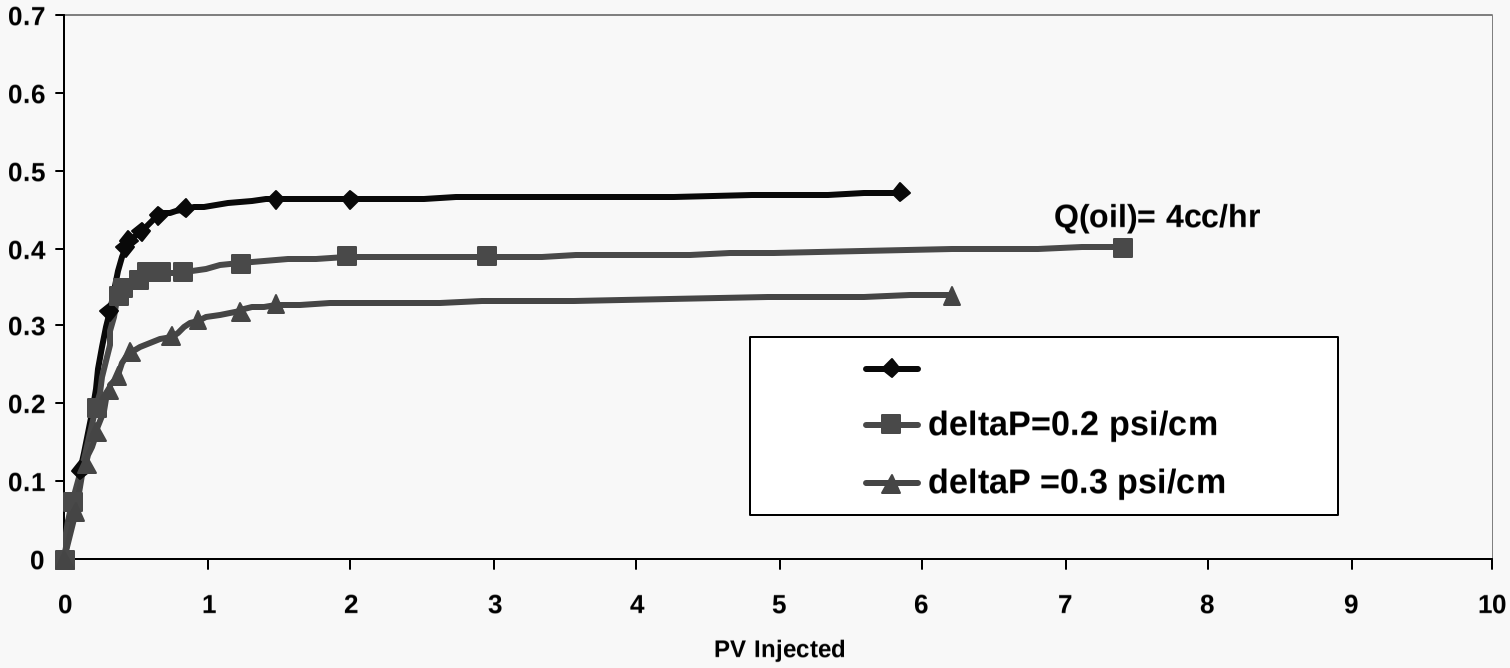

Fig 17: Liquid Saturation for Treated Berea (BB-5)

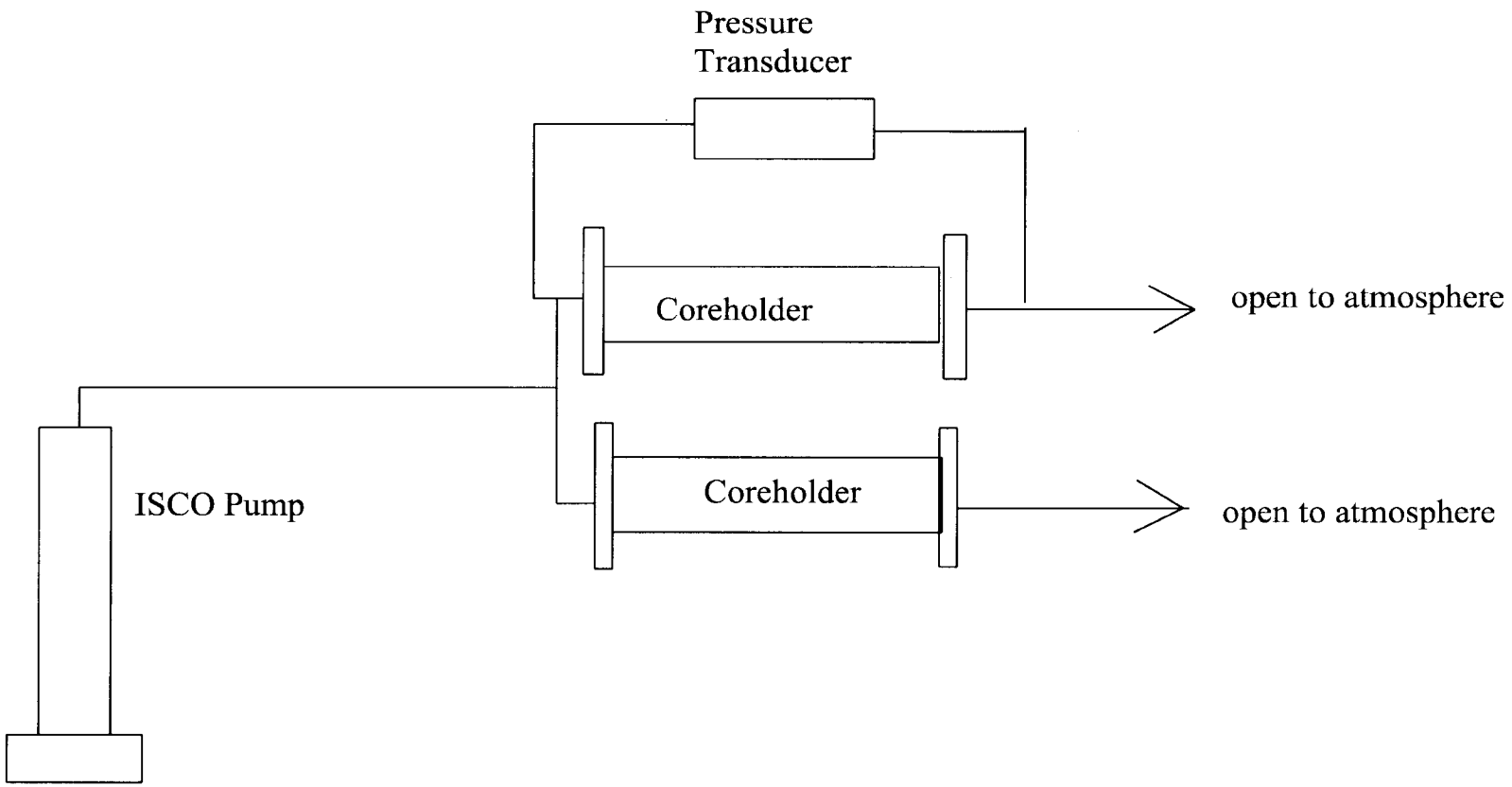

Fig 18-Schematic of Apparatus for Parallel Core Experiment

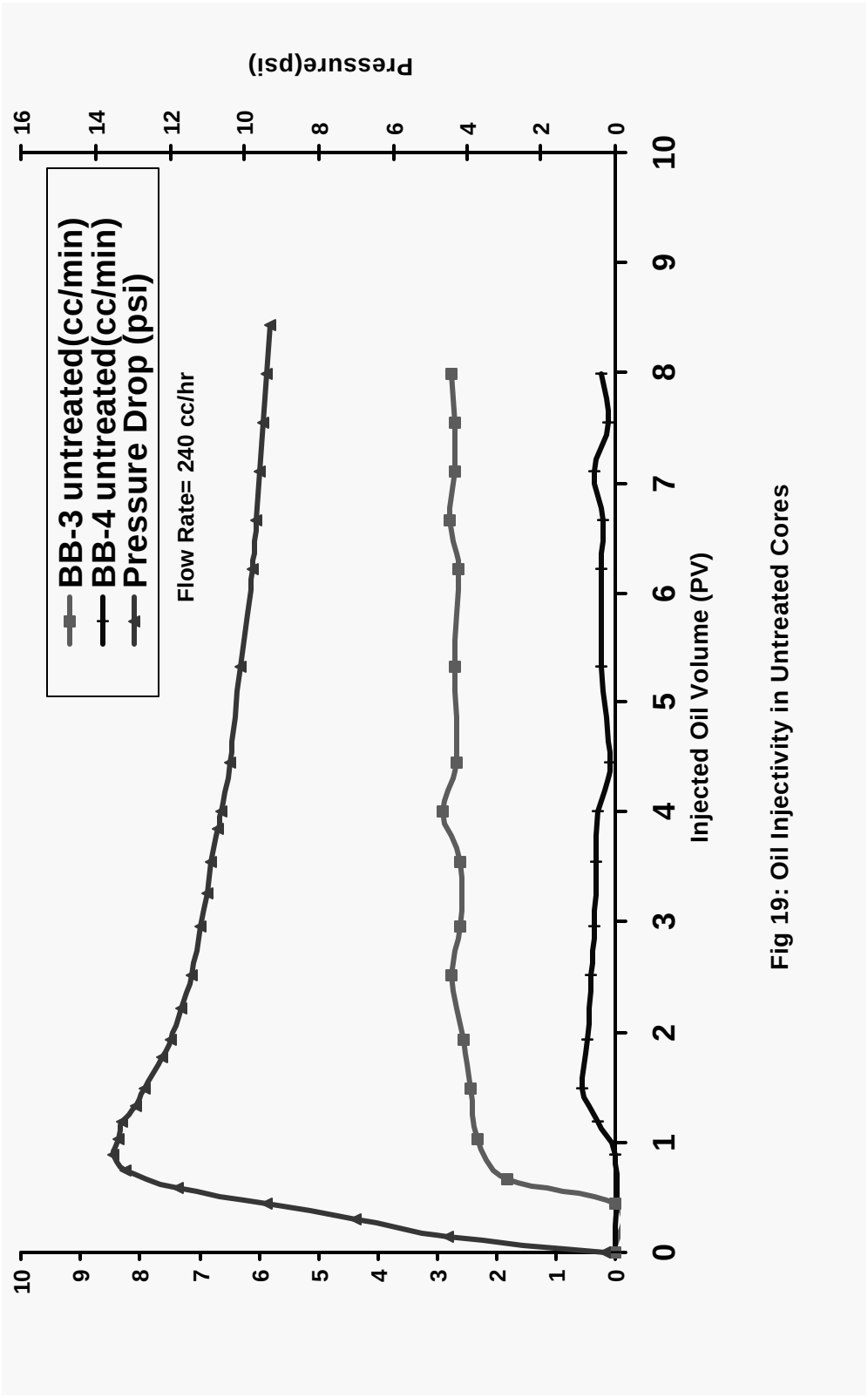

Fig 19: Oil Injectivity in Untreated Cores

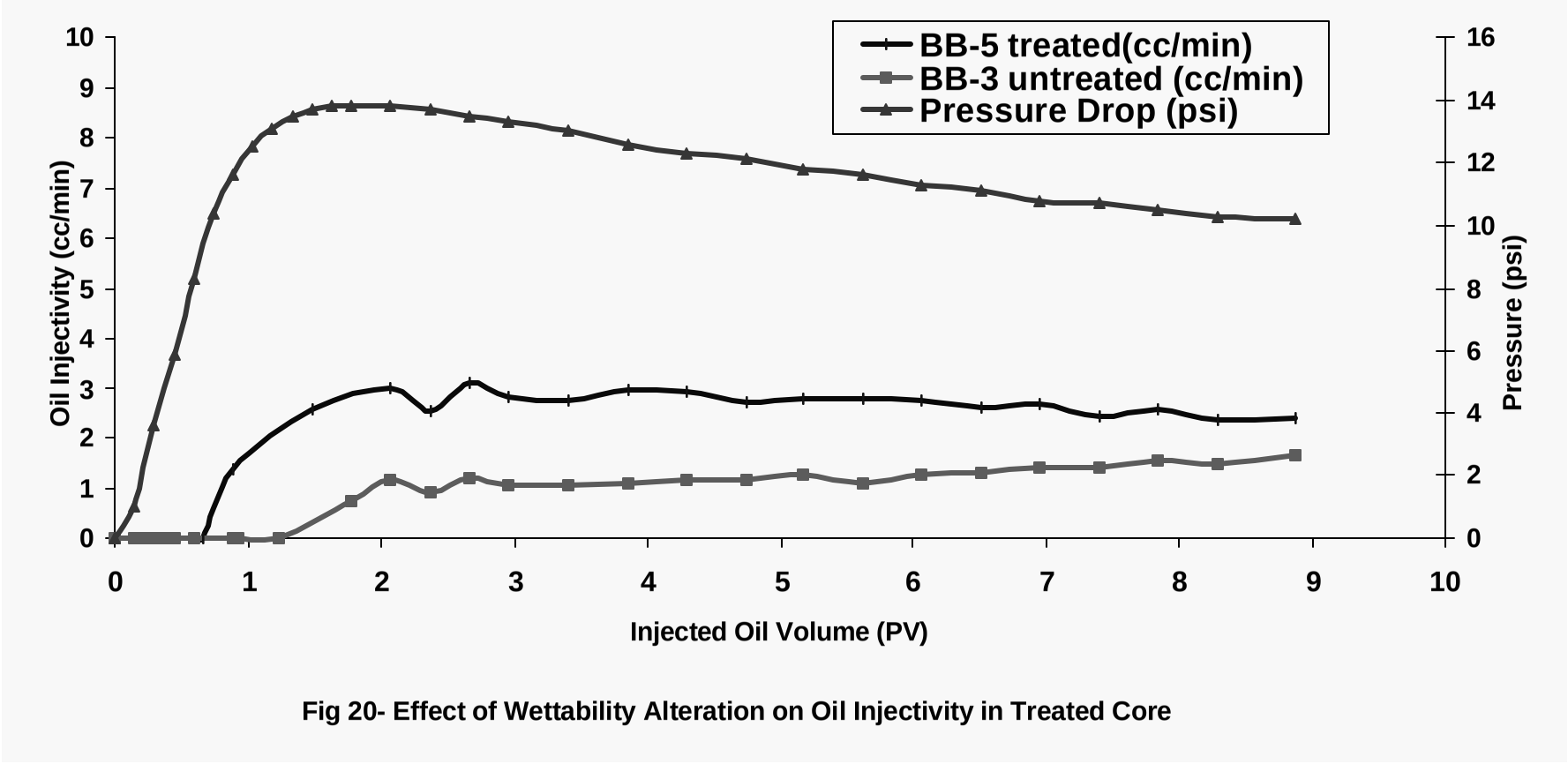

Fig 20- Effect of Wettability Alteration on Oil Injectivity in Treated Core

Table 1 - Summary of properties of (with L16439) treated and untreated cores

Sample	CC	CC-2	CC-2	CC-2	CC-3	CC-4	CC-5	CC-6	CC-7	BB	BB-0	BB-00	BB-1	BB-11	BB-2	BB-3	BB-4	BB-5	BB-6	BB-7
No. of Treatments	1	1	2	2	1	1	1	1	1	0	1	1	1	1	1	0	0	1	1	0
Chemical	-	L16349	L16349	L16349	FC759	L16349	L16349	L16349	L16349	-	L16349	L16349	L16349	L16349	L16349	-	-	L16349	L16349	-
Treatment Temp.(deg C)	-	105	105	150	105	105	150	150	150	-	105	105	105	105	105	-	-	105	105	-
Method of Treatment	-	Method-1	Method-1	Method-1	Method-1	Method-1	Method-2	Method-2	Method-2	-	Method-1	Method-1	Method-1	Method-1	Method-1	-	-	Method-1	Method-1	-
Polymer Conc.	untreated	6%	6%	6%	8%	9%	9%	9%	9%	untreated	3%	3%	6%	6%	9%	untreated	untreated	9%	9%	untreated
k Before Treatment (md)	-	1.84	1.84	1.84	-	-	3.68	4.71	1.92	-	-	-	176	-	410	325	-	250	566	-
k After Treatment (md)	-	1.52	1.52	1.52	-	-		4.51	1.74	-	-	-	137	-	374	-	-	210	451	-
PV (cm3)	13.07	5.50	5.50	5.50	5.59	7.20	17.90	13.07	5.35	7.07	3.51	1.95	3.64	3.76	4.30	13.51	13.51	13.51	6.78	5.97
Length (in)	3.17	1.31	1.31	1.31	1.32	1.73	4.23	3.17	1.26	2.62	1.3	1.47	1.35	1.39	1.59	5	5	5	2.51	2.21
Adsorption (mg./g)	-	4.24	4.24	4.24	6.8	3.07	5.07	5.9	8	-	3.04	1.96	6.45	4.67	9.44	-	-	9.6	11.2	-
Porosity(%)	33	33	33	33	33	33	33	33	33	21	21	21	21	21	21	21	21	21	21	21

Notes
1. Sample BB-1 and CC-2 were heated upto 150^{o}C.
2. Nominal diameter of 1 inch.

Chapter II - Curvature Dependence of Surface Tension in Multicomponent Systems

Erik Santiso and Abbas Firoozabadi

ABSTRACT

The effect of curvature on the surface tension of droplets and bubbles in both single and multicomponent systems is modeled using the basic equations from classical thermodynamics. The three basic expressions used in our work are the Gibbs adsorption equation for multicomponent systems, the relation between the surface tension at the surface of tension and the distance parameter δ and the Macleod-Sugden equation for surface tension and its extension to multicomponent systems. The Peng-Robinson equation of state is used to describe the bulk phases. We also assume that the surface tension expression remains valid in terms of the properties of the bulk phases for both flat and curved interfaces. The results from our model reveal a decrease in surface tension with curvature in bubbles and a non-monotonic behavior in droplets for single-component systems. Our predictions are in good agreement with the literature results when the interface is described using the framework of the density functional theory by three different groups. For multicomponent systems, the results show that the surface tension in a bubble, although monotonic with curvature, can increase or decrease in a large bubble depending on the temperature and composition of the mixture. In a droplet, the surface tension can have a non-monotonic behavior similar to single component systems.

I. INTRODUCTION

Surface tension is a prime parameter in the basic formulation of a large number of processes including nucleation and cluster formation. The work of formation of a critical-size nucleus is proportional to the surface tension to the power three[1]. The solute clustering in supersaturated solutions and concentration gradients in a vertical column of a supersaturated solution may also depend on the surface tension of nano-particles[2]. In addition to applications in nucleation and solute clustering in supersaturated solutions, there is a wide interest in the important role of surface tension in determining the behavior of small droplets and bubbles including oil recovery processes. For a long time it has been recognized that when a cluster of a new phase is small (that is, has a high curvature), the surface tension is size-dependent (that is, curvature dependent).

In an early paper, Tolman derived the expression for the effect of droplet size on surface tension in a single-component system[3,4]. A key parameter in Tolman's work is the parameter δ, the distance between the surface of tension and the equimolecular dividing surface. For a plane surface of separation, Tolman computed δ for a variety of substances, including water[3]. His results show that the distance δ is positive and of the order of 1 to 3.5 Å (of the order of the intermolecular distances in liquids) for pure substances over the range of conditions studied.

Since the early work of Tolman, a large number of investigators have studied the curvature dependence of surface tension and nucleation theory. There is generally consensus that the curvature dependence of surface tension may indeed result in significant variation of the work of formation of the critical nucleus[5] and the nucleation rate[6,7]. However, there is widespread

confusion and controversy in the literature on the effect of curvature on the surface tension of a bubble and a droplet in single component systems. Defay and Prigogine[9] provide results for the effect of curvature on the surface tension of water at 18 ºC for both bubbles and droplets. Their results show an increase of the surface tension with increasing curvature for a bubble whereas there is a decrease of surface tension with increasing curvature for a droplet (see Table 15.7 of Defay and Prigogine[9]). On the other hand, Kashchiev[1] presents results for water bubbles at 583 K and droplets at 293 K, both decreasing with increasing curvature (see Fig. 6.1 of Kashchiev[1]). Kashchiev used a positive value of δ of 1 Å for water droplets and bubbles. Another example is the work of Hadjiagapiou[10], which provides results from density functional theory showing an increase of the surface tension for a droplet with increasing curvature, followed by a decrease at very high curvatures. Guermeur, Biquard and Jacolin[11] have also studied the effect of curvature on the surface tension for nitrogen bubbles and droplets. Their results show that the surface tension in the bubble decreases with increasing curvature. It has a non-monotonic behavior in the droplet. On the other hand, as was stated earlier, many authors predict that the surface tension in, for example, a droplet, should decrease rapidly with the radius (see for example Lee, Gama and Gubbins[12], and the references therein). In a different approach presented in Ref. 13, Schmelzer and Baidakov argue that the Gibbs method for determining the reference states for the description of bulk properties of the critical nucleus does not give a correct description of the bulk properties of the critical clusters at high supersaturation. They postulate that at a non-equilibrium state, the chemical potentials of the interface and the ambient phase (in their terminology, this is, the bulk phase other than the cluster bulk phase) are the same. They also make other postulations and obtain new expressions, including a new expression for the pressure difference between the cluster phase and the other bulk phase given by

$p_\alpha - p_\beta = 2\sigma / R_+ + \rho_\alpha(\mu_\alpha - \mu_\beta)$ where p is the pressure, ρ is the density, μ is the chemical potential, σ is the surface of tension, and R_+ is the radius of the critical cluster (or critical nucleus); α is the cluster phase, and β is the ambient phase. All pertain to a critical cluster. (We are using nomenclature from Ref. 13; later, we will use our own.) Obviously, the expression for $(p_\alpha - p_\beta)$ from Ref. 13 is different from the Laplace equation given by $p_\alpha - p_\beta = (2\sigma / R_+)$. When the work from Ref. 13 is used, the surface tension both for a bubble and for a droplet decrease with curvature and approach zero at the spinodal. For a droplet, first there is a slight increase (not noticable) followed by a decrease with curvature. The work of critical cluster also approaches zero at the spinodal. We will get back to this point later.

Most of the work on curvature dependence of the surface tension is limited to single components. Schmelzer et al.[5] have developed an empirical relation for δ in multicomponent systems for a droplet. In a more recent work, Baidakov, Boltashev, and Schmelzer[14], use an approach based on Ref. 13 to study the effect of curvature on surface tension in mixtures. The results show that similar to a single component system, the surface tension vanishes at the spinodal for a two-component mixture. In this work, we present results to show that there are differences in surface tension curvature dependency of pure components and multicomponent systems.

The purpose of this work is to derive the expressions for the curvature dependence of the surface tension for bubbles and droplets in both single and multicomponent systems. The derivations are based on the general expressions from classical thermodynamics using the work of Gibbs. We use an equation of state to describe the bulk gas and liquid phase properties. Therefore, there is no need to make assumptions regarding compressibility and compositional effects.

In the following, we first derive basic thermodynamic relations for the curvature dependence of the surface tension using a new simple approach. Then we apply the derived expressions coupled with a surface tension model to obtain the basic expressions for bubbles and droplets in single-component systems. Next, the basic expressions in multicomponent systems, also for both bubbles and droplets, are obtained. In the above two sections we provide numerical examples. At the end we make several concluding remarks.

II. THERMODYNAMIC RELATIONS FOR THE CURVATURE DEPENDENCE OF SURFACE TENSION

The two fundamental equations that form the basis of this work can be directly obtained from the basic postulates of thermodynamics and have been derived in Ref. 15. The first equation is the *Gibbs adsorption equation* that, for a multicomponent system with a spherical interface can be written as[15]:

$$d\sigma = -s^{\sigma} dT - \sum_{i=1}^{c} \Gamma_i d\mu_i^{\sigma} + \left[\frac{\partial \sigma}{\partial a}\right] da \tag{1}$$

In this expression, σ is the surface tension, s^{σ} is the entropy per unit area of the interface (the superscript σ denotes a surface property) Γ_i and μ_i^{σ} are, respectively, the number of moles per unit area and chemical potential of component *i* in the interface, *c* is the number of components, *a* is the radius of the interface and $[\partial\sigma/\partial a]$ represents the change in the surface tension when the

mathematical diving surface between the two phases is displaced. The particular dividing surface for which $[\partial\sigma/\partial a]=0$ is called the *surface of tension*. Throughout this work, all properties referred to the surface of tension are identified with the subscript *s*. The second key equation mentioned above relates the surface tension to the radius of the interface and can be written as[15]:

$$\left(\frac{\partial \ln \sigma_s}{\partial \ln a_s}\right)=2\left(\frac{\delta}{a_s}\right)\frac{1+(\delta/a_s)+(1/3)(\delta/a_s)^2}{1+2(\delta/a_s)[1+(\delta/a_s)+(1/3)(\delta/a_s)^2]} \tag{2}$$

Note that in the above equation, the derivative is taken along a path where the temperature and composition of the continuous bulk phase are held constant (we refer to the small bulk phase as the cluster phase in the work). The parameter δ is the distance between two dividing surfaces: one is the surface of tension and the other is the dividing surface defined by:

$$\sum_{i=1}^{c}\Gamma_i\tilde{v}_i^{\alpha}=0 \tag{3}$$

where $\tilde{v}_i^{\alpha}$ is the partial molar volume of component *i* in the continuous bulk phase (denoted by the superscript α). Parameters and properties referred to the dividing surface defined by (3) will be identified by the subscript *v*. The parameter δ is given by:

$$\delta = a_v - a_s \tag{4}$$

One of the most challenging tasks in the past has been the estimation of δ. Some authors have made calculations to show that δ for a flat interface is positive, some others suggest that it is negative, and there is a third group who estimate δ to be zero for a flat interface. The implication for δ being zero for a flat interface is that there is no adsorption at the interface. The δ parameter for a flat interface may also have different signs in a bubble and in a droplet (see Ref. 16 and references therein). Our goal in this work is to find a suitable approach in predicting this parameter. To achieve this goal, we need to find a clearer relation between δ and other properties of the system.

The total volume of the two-phase system based on the dividing surface defined by (3) can be expressed as:

$$V = V_v^{\alpha} + V_v^{\beta} = \sum_{i=1}^{c} N_{i,v}^{\alpha} \tilde{v}_i^{\alpha} + \sum_{i=1}^{c} N_{i,v}^{\beta} \tilde{v}_i^{\beta} \tag{5}$$

where N_i is the number of moles of component *i*. We have introduced the superscript β to identify the cluster phase. Using the mass balance of component *i* to eliminate $N_{i,v}^{\alpha}$ from (5) we obtain:

$$V = \sum_{i=1}^{c} N_i \tilde{v}_i^{\alpha} + \sum_{i=1}^{c} N_{i,v}^{\beta} \left(\tilde{v}_i^{\beta} - \tilde{v}_i^{\alpha} \right) \tag{6}$$

In (6) we have used (3) to eliminate the amounts of adsorption at the interface. The total volume of the two-phase system based on the surface of tension leads to:

$$V = \sum_{i=1}^{c} N_i \tilde{v}_i^{\alpha} + \sum_{i=1}^{c} N_{i,s}^{\beta} \left(\tilde{v}_i^{\beta} - \tilde{v}_i^{\alpha} \right) - A_s \sum_{i=1}^{c} \Gamma_{i,s} \tilde{v}_i^{\alpha} \tag{7}$$

In (7) A_s is the surface area of the interface. Equating the right-hand sides of (6) and (7) and simplifying we obtain:

$$V_v^{\beta} - \sum_{i=1}^{c} N_{i,v}^{\beta} \tilde{v}_i^{\alpha} = V_s^{\beta} - \sum_{i=1}^{c} N_{i,s}^{\beta} \tilde{v}_i^{\alpha} - A_s \sum_{i=1}^{c} \Gamma_{i,s} \tilde{v}_i^{\alpha} \tag{8}$$

Introducing the molar concentrations c_i and rearranging we obtain:

$$V_v^{\beta} = V_s^{\beta} - \frac{A_s \sum_{i=1}^{c} \Gamma_{i,s} \tilde{v}_i^{\alpha}}{1 - \sum_{i=1}^{c} c_i^{\beta} \tilde{v}_i^{\alpha}} \tag{9}$$

The equation above provides a relationship between the sizes of the cluster calculated for the two dividing surfaces. It can be written in terms of the radii as:

$$a_v = a_s^{2/3}\left(a_s - \frac{3\sum_{i=1}^{c} \Gamma_{i,s}\tilde{v}_i^{\alpha}}{1-\sum_{i=1}^{c} c_i^{\beta}\tilde{v}_i^{\alpha}} \right)^{1/3} \tag{10}$$

Combining (4) and (10) we obtain:

$$\frac{\delta}{\mathrm{a_s}} = \left(1 - \frac{3}{a_s}\frac{\sum_{i=1}^{c} \Gamma_{i,s}\tilde{v}_i^{\alpha}}{1-\sum_{i=1}^{c} c_i^{\beta}\tilde{v}_i^{\alpha}} \right)^{1/3} - 1 \tag{11}$$

which provides δ. For studying the curvature dependence of the surface tension, one may rearrange (11) to:

$$\delta\left[\frac{1}{3}\left(\frac{\delta}{\mathrm{a_s}} \right)^2 + \frac{\delta}{a_s} + 1 \right] = \frac{-\sum_{i=1}^{c} \Gamma_{i,s}\tilde{v}_i^{\alpha}}{1-\sum_{i=1}^{c} c_i^{\beta}\tilde{v}_i^{\alpha}} \tag{12}$$

Equation (12) relates δ to the properties of the two-bulk phases and the interface for a multicomponent system. For a single-component system, (12) simplifies to:

$$\delta\left[\frac{1}{3}\left(\frac{\delta}{\mathrm{a_s}} \right)^2 + \frac{\delta}{a_s} + 1 \right] = \frac{\Gamma_s}{\rho^{\beta} - \rho^{\alpha}} \tag{13}$$

where ρ is the molar density. Tolman[4] derived (13) using an integral approach; we use the relationships from classical thermodynamics in our derivation. Note that one may not use (13) to generalize it to multicomponent mixtures without certain assumptions[5]. Substituting (12) into (2) we find an equation for the curvature dependence of the surface tension that does not include δ:

$$\left(\frac{\partial \ln \sigma_s}{\partial \ln a_s}\right) = \frac{2\sum_{i=1}^{c} \Gamma_{i,s} \tilde{v}_i^{\alpha}}{2\sum_{i=1}^{c} \Gamma_{i,s} \tilde{v}_i^{\alpha} - a_s\left(1 - \sum_{i=1}^{c} c_i^{\beta} \tilde{v}_i^{\alpha}\right)} \tag{14}$$

Note that in the above equation the problem has shifted from obtaining the parameter δ to obtaining the amounts of adsorption of the components at the interface. To proceed further, we relate the surface tension to the properties of both phases to obtain the sum that includes the amounts of adsorption.

The sum in (14) that contains the amounts of adsorption can be related to the surface tension by combining Gibbs adsorption equation and the chemical equilibrium conditions. Writing (1) for the surface of tension and replacing the surface chemical potentials by the chemical potentials in the bulk continuous phase we obtain:

$$d\sigma_s = -s_s^{\sigma} dT - \sum_{i=1}^{c} \Gamma_{s,i} d\mu_i^{\alpha} \tag{15}$$

The differential of the chemical potentials of the continuous bulk phase can be expressed as:

$$d\mu_i^\alpha = -\tilde{s}_i^\alpha dT + \tilde{v}_i^\alpha dP^\alpha + \sum_{j=1}^{c-1}\left(\frac{\partial \mu_i^\alpha}{\partial x_j^\alpha}\right)_{T,P^\alpha,x_{k\neq j,c}^\alpha} dx_j^\alpha \qquad i = 1,..,c \tag{16}$$

where x represents the mole fraction. Substituting (16) into (15) we find:

$$d\sigma_s = \left(-s_s^\sigma + \sum_{i=1}^{c}\Gamma_{i,s}\tilde{s}_i^\alpha\right)dT - \left(\sum_{i=1}^{c}\Gamma_{i,s}\tilde{v}_i^\alpha\right)dP^\alpha - \sum_{j=1}^{c-1}\left[\sum_{i=1}^{c}\Gamma_{i,s}\left(\frac{\partial \mu_i^\alpha}{\partial x_j^\alpha}\right)_{T,P^\alpha,x_{k\neq j,c}^\alpha}\right]dx_j^\alpha \tag{17}$$

Which leads to:

$$\left(\frac{\partial \sigma_s}{\partial P^\alpha}\right)_{T,x_i^\alpha} = -\sum_{i=1}^{c}\Gamma_{i,s}\tilde{v}_i^\alpha \tag{18}$$

Equation (18) is the sought relationship. Providing a model for the surface tension as a function of the properties of both phases, (14) and (18) can be combined to evaluate the curvature dependence of the surface tension. In the following two sections we will present the methodology first for single-component and then for multicomponent systems.

III. SINGLE-COMPONENT SYSTEMS

For a single-component system (14) simplifies to:

$$\left(\frac{\partial \ln \sigma_s}{\partial \ln a_s}\right) = \frac{2\Gamma_s}{2\Gamma_s - a_s\left(\rho^{\alpha} - \rho^{\beta}\right)} \tag{19}$$

Also, (18) becomes:

$$\left(\frac{\partial \sigma_s}{\partial P^{\alpha}}\right)_T = \frac{-\Gamma_s}{\rho_s} \tag{20}$$

To proceed further we desire an equation for the equilibrium surface tension. For a single-component system, the well-known Macleod-Sugden equation for the surface tension of a flat interface[17-19] can be used:

$$\sigma_{\infty}^{1/4} = \Pi\left(\rho^{L} - \rho^{V}\right) \tag{21}$$

In (21), σ_{∞} is the surface tension of the flat interface, Π is the parachor and the superscripts L and V denote liquid and vapor, respectively. Equation (21) provides the surface tension of non-polar fluids with a remarkable accuracy over a wide range of temperature conditions[20] and although it was introduced empirically[17,18], it was later derived theoretically[19]. In what follows we will use two different approaches: we assume that (21), 1) is valid for large values of the interface radius and obtain the limiting dependence of δ for a flat interface (that is, δ_{∞}); then assume that δ is constant to obtain the curvature dependence of the surface tension, and 2) applies to a surface with a curved interface, which implies that δ can change with curvature.

The assumptions have to be examined for their validity. Let us use the terms "δ_∞ model" and "Π model" to refer to the two methods.

It turns out that in either approach it will be necessary to obtain δ as a function of curvature assuming that (21) is valid for a curved interface. For the δ_∞ model we will take the limit as the interface radius tends to infinity. Thus, we will replace σ_∞ by σ_s in (21). Let us first consider a bubble in a continuous bulk liquid phase and replace *L* and *V* in (21) by α and β, respectively. The expression for surface tension will take the form:

$$\sigma_s^{1/4} = \Pi\left(\rho^\alpha - \rho^\beta\right) \tag{22}$$

The droplet in a continuous bulk vapor phase will be considered later. Substituting (22) into (20) we obtain:

$$\Gamma_s = 4\Pi\rho^\alpha\sigma_s^{3/4}\left[\left(\frac{\partial\rho^\beta}{\partial P^\alpha}\right)_T - \left(\frac{\partial\rho^\alpha}{\partial P^\alpha}\right)_T\right] \tag{23}$$

The second derivative in the square bracket in (23) is given by:

$$\left(\frac{\partial\rho^\alpha}{\partial P^\alpha}\right)_T = \rho^\alpha C_T^\alpha \tag{24}$$

where C_T^{α} is the isothermal compressibility of phase α, which can be readily obtained from an equation of state. Next we find an expression for the first derivative in (23). From the chain rule we write:

$$\left(\frac{\partial \rho^{\beta}}{\partial P^{\alpha}}\right)_T = \left(\frac{\partial \rho^{\beta}}{\partial P^{\beta}}\right)_T \left(\frac{\partial P^{\beta}}{\partial P^{\alpha}}\right)_T = \rho^{\beta} C_T^{\beta} \left(\frac{\partial P^{\beta}}{\partial P^{\alpha}}\right)_T \tag{25}$$

The derivatives in (25) are taken along an equilibrium path. Therefore we can write:

$$\left(\frac{\partial \mu^{\alpha}}{\partial P^{\alpha}}\right)_T = \left(\frac{\partial \mu^{\beta}}{\partial P^{\alpha}}\right)_T = \left(\frac{\partial \mu^{\beta}}{\partial P^{\beta}}\right)_T \left(\frac{\partial P^{\beta}}{\partial P^{\alpha}}\right)_T \tag{26}$$

Replacing the derivatives of the chemical potentials with respect to the pressure of their respective phases by the inverse of the molar densities, we obtain:

$$\left(\frac{\partial P^{\beta}}{\partial P^{\alpha}}\right)_T = \left(\frac{\rho^{\beta}}{\rho^{\alpha}}\right) \tag{27}$$

Combining (23), (24), (25) and (27) we get:

$$\Gamma_s = 4\Pi\sigma_s^{3/4}\left[(\rho^{\beta})^2 C_T^{\beta} - (\rho^{\alpha})^2 C_T^{\alpha}\right] \tag{28}$$

Equations (22) and (28), together with an equation of state, allow the calculation of the amount of adsorption at the surface of tension. For the δ_∞ model, we will use (28) to obtain the limiting value of δ as the radius of the interface goes to infinity. Substituting (28) into (13) and taking the limit as $a_s \to \infty$ we obtain:

$$\delta_\infty = 4\Pi\sigma_\infty^{3/4} \frac{\left(\rho^\beta\right)^2 C_T^\beta - \left(\rho^\alpha\right)^2 C_T^\alpha}{\rho^\beta - \rho^\alpha} \tag{29}$$

Using δ_∞ as the constant value of δ we numerically integrate (2) and calculate the variation of σ_s with curvature. For the Π model, we will substitute (28) into (19) to get:

$$\left(\frac{\partial \ln \sigma_s}{\partial \ln a_s}\right) = \frac{8\Pi\sigma_s^{3/4}\left[\left(\rho^\beta\right)^2 C_T^\beta - \left(\rho^\alpha\right)^2 C_T^\alpha\right]}{8\Pi\sigma_s^{3/4}\left[\left(\rho^\beta\right)^2 C_T^\beta - \left(\rho^\alpha\right)^2 C_T^\alpha\right] - a_s\left(\rho^\alpha - \rho^\beta\right)} \tag{30}$$

Equation (30) can be integrated numerically to compute the curvature dependence of the surface tension. In Figure 1 we show the surface tension σ_s as a function of the radius of the surface of tension for a bubble of n-pentane at 310.9 K using the two models. The Peng-Robinson equation of state[21] and the standard 4-th order Runge-Kutta method were employed for calculations in Figure 1 and similar calculations to be presented later. The parachor of n-pentane was taken as 230. From this graph we note that: 1) the surface tension is constant down to $a_s \approx 100\,\text{nm}$, and 2) the Π model predicts a sharper variation of the surface tension with curvature for $a_s < 10\,\text{nm}$; the difference between the two models increases as the radius decreases. Figure 2

shows the variation of δ with curvature as predicted by the Π model. In this figure, it is clear too that there is almost no difference between the two models for sizes down to $a_s \approx 10\,\text{nm}$, but as the radius decreases further, δ grows sharply, which accounts for the steeper variation of the surface tension predicted by this model at larger curvatures. This change in δ can be explained by the fact that the pressure, and thus the densities, starts changing much faster at these large curvatures. Ref. 22 provides results similar to Figure 2 based on the semi-empirical van der Waals/Cahn-Hilliard theory. Note that δ vs. the radius is positive in Figure 2.

For a droplet in a continuous vapor phase, it is necessary to exchange the superscripts α and β in (22). Repeating the procedure we used for a bubble we obtain, for the limiting value of δ for a flat interface:

$$\delta_\infty = 4\Pi\sigma_\infty^{3/4}\frac{\left(\rho^\alpha\right)^2 C_T^\alpha - \left(\rho^\beta\right)^2 C_T^\beta}{\rho^\beta - \rho^\alpha} \tag{31}$$

Note that the above expression for δ_∞ in a droplet is different from the expression derived in Ref. 16. There is no need to assume that density or volume can be expanded linearly with pressure. There is also no need for other assumptions except a need for a general expression for σ_∞. According to Eq. 31, even when $C_T^\alpha = 0$, δ_∞ may not be zero. Substituting δ_∞ from (31) into (2) and integrating we obtain the variation of σ_s with curvature for the δ_∞ model. For the constant-Π model, we obtain:

$$\left(\frac{\partial \ln \sigma_s}{\partial \ln a_s}\right) = \frac{8\Pi\sigma_s^{3/4}\left[\left(\rho^{\alpha}\right)^2 C_T^{\alpha} - \left(\rho^{\beta}\right)^2 C_T^{\beta}\right]}{8\Pi\sigma_s^{3/4}\left[\left(\rho^{\alpha}\right)^2 C_T^{\alpha} - \left(\rho^{\beta}\right)^2 C_T^{\beta}\right] - a_s\left(\rho^{\alpha} - \rho^{\beta}\right)} \tag{32}$$

Figure 3 shows the variation of the surface tension with the radius of the surface of tension using the two models for a droplet of n-pentane at 310.9 K. For a droplet the difference between the δ_∞ model and the Π model is more pronounced: for the δ_∞ model, the surface tension increases monotonically with decreasing radius whereas the Π model predicts that the surface tension will go through a maximum at an approximate radius of 1.1 nm and then decreases rapidly with decreasing radius. Hadjiagapiou[10] and Guermeur et al.[11] have predicted a similar non-monotonic behavior. Figure 4 shows the variation of δ with curvature as predicted by the Π model, where the variation of δ with curvature is similar to that of the bubble, being almost constant at small curvatures and then growing fast as the radius decreases. However, δ_∞ is negative for the droplet and δ changes sign and causes the surface tension to go through a maximum. A negative value for δ_∞ in a droplet has been presented in Refs. 16 and 22 using different approaches. In Ref. 16, δ_∞ is approximated by $-C_T^{\alpha}\sigma_\infty/3$ based on a number of assumptions. Based on another set of assumptions[6] $\delta_\infty \approx -C_T^{\alpha}\sigma_\infty$. Ref. 22 also discusses the difference between the density function (DF) approach in predicting a negative δ_∞ and the molecular dynamics (MD) simulations which predicts a position δ_∞ for a droplet.

Note that, for a single-component system, the dividing surface defined by (3) is the same regardless of which phase is selected to be phase α. Thus, the absolute value of δ_∞ obtained as the limit for the bubble will be the same as that obtained for the droplet, only with opposite sign.

The change in sign is due to the fact that in the bubble the distances are measured from the gas side and in a droplet they are measured from the liquid side (see (29)). However, for a multicomponent system, this is not the case because the dividing surface defined by (3) is different for different choices of the phase α since the two phases have different partial molar volumes (to be shown later). Thus, the limiting value δ_∞ obtained using the equations for a bubble may be different from that obtained with the equations for a droplet not only in sign, but also in magnitude. To avoid ambiguity, in the discussion for multicomponent systems we will use the symbols δ_∞^b for the former and δ_∞^d for the latter.

The results shown above for the curvature dependency of surface tension in bubbles and droplets have similar trends to those of Guermeur et al.[11] and Hadjiagapiou[10]. Figure 5 shows a comparison between the results of Guermeur et al. for bubbles of nitrogen at 77.3 K and the results for the same system obtained with our Π model (nitrogen parachor of 52 was used in our calculations based on surface tension data for nitrogen). Figure 6 shows the same comparison for a droplet of nitrogen at the same temperature. In both figures we observe that the trends predicted by our model and the work of Guermeur et al. are the same, although the two models are very different. Guermeur et al. describe the inhomogeneous fluid in the interface using a stress tensor in the frame of gradient theory, and predict a sharper variation of the surface tension with curvature for the bubbles and a smaller variation for the droplets. Although they also obtain a maximum in the surface tension plot for the droplet, the maximum is at a smaller curvature and the corresponding surface tension is also smaller. The results for our δ_∞ model (not shown) are farther from their results in both cases.

In order to compare with Hadjiagapiou's results, we computed the surface tension as a function of curvature for a droplet of Argon at a reduced temperature of 0.8 (argon parachor of 52 was used in our calculations). Argon was chosen for comparison because it is a substance well suited for Hadjiagapiou's treatment of thermodynamic properties. The results, in terms of the reduced variables defined in his work, are shown in Figure 7. In this case, our Π model predicts a smaller variation of the surface tension with curvature than Hadjiagapiou's model, however our Π model predicts a smaller droplet radius for the maximum surface tension. In view of the simplicity of our model, it is interesting to note that its predictions are close to those of Hadjiagapiou, which is based on density functional theory.

Before proceeding to multicomponent system, we would like to point out a deficiency in regard to the work of critical cluster formation at the spinodal (that is, at the limit of stability). The work of critical cluster formation is expected to vanish as we approach the spinodal. In the classical theory of nucleation, the barrier height approaches a finite value at the spinodal, which is not correct[23]. When one accounts for the effect of curvature on the surface tension, the work of critical cluster formation at the spinodal reduces, but may not vanish. This is to be expected because of extremely small size of the clusters, comprised of say some 40 atoms, at the spinodal. Instead of using classical thermodynamics, one may use statistical or molecular thermodynamics for very small clusters (that is, at very high supersaturation) to account for non-classical effects[23]. In our approach, similar to Guermeur et al.[11], the surface tension for a droplet is greater than the flat interface for large droplets but becomes smaller for smaller droplets. For bubbles, the surface tension remains less than σ_∞. These results are consistent with work of Ref. 23, that

classical and non-classical barrier heights cross from droplet formation but do not for bubble formation.

Schmelzer and coworkers, in a different approach, as we stated earlier, use certain postulations which lead to a vanishing of the critical cluster formation at the spinodal, as well as the vanishing of the surface tension (Ref. 13 and references within).

Figure 8 shows the plot for the work of critical cluster formation (in dimensionless units) vs. a_s in a bubble of n-pentane at 310.9 K. Note that as the spinodal is approached, W/kT decreases. Despite a small W of about 1.5 kT, it does not vanish at the spinodal. The droplet has also a similar behavior. The work of critical cluster formation for the Argone bubble at the spinodal (for $T_r = 0.8$) is about 2.5 kT, which is not far from kT.

IV. MULTICOMPONENT SYSTEMS

For multicomponent systems we follow an approach similar to that of single-component systems. Weinaugh and Katz have extended (21) to multicomponent systems[24,25]:

$$\sigma_{\infty}^{1/4} = \sum_{i=1}^{c} \Pi_i \left(c_i^L - c_i^V \right) \tag{33}$$

The above equation provides good predictions in non-polar multicomponent hydrocarbon mixtures[18,20,21]. In order to apply (33) to obtain the curvature dependence of the surface tension,

we will follow an approach similar to the one used in the previous section. Again, we will explore two options: 1) assume that (33) is valid for curved interfaces with a very large radius, use it to obtain the limiting value δ_∞ for the flat interface and then use δ_∞ to integrate (2), and 2) assume that (33) is valid for a curved interface, thus allowing for δ to vary with curvature. To keep the terminology used in section III, we will call the first approach the "δ_∞ model" and the second the "Π model".

Similar to a single-component system, we need to find an expression for δ as a function of curvature assuming that (33) is valid for a curved interface. For the δ_∞ model we will take the flat interface limit in the resulting expression. Thus, we will replace σ_∞ by σ_s in (33). First we will consider a bubble in a continuous bulk liquid phase and replace L and V in (21) by α and β, respectively. With the altered notation, (33) takes the form:

$$\sigma_s^{1/4} = \sum_{i=1}^{c} \Pi_i \left(c_i^\alpha - c_i^\beta \right) \tag{34}$$

Substituting (34) into (18) leads to:

$$\sum_{i=1}^{c} \Gamma_{i,s} \tilde{v}_i^\alpha = 4\sigma_s^{3/4} \sum_{i=1}^{c} \Pi_i \left[\left(\frac{\partial c_i^\beta}{\partial P^\alpha} \right)_{T,x_j^\alpha} - \left(\frac{\partial c_i^\alpha}{\partial P^\alpha} \right)_{T,x_j^\alpha} \right] \tag{35}$$

As in (23), the second derivative inside the square bracket in (35) can be readily obtained from an equation of state:

$$\left(\frac{\partial c_i^{\alpha}}{\partial P^{\alpha}}\right)_{T,x_j^{\alpha}} = C_T^{\beta} c_i^{\alpha} \quad i = 1, \cdots, c \tag{36}$$

The first derivative, however, is more complicated to evaluate. Let us first write the differential of the variable c_i^{β} in two different ways: first as a function of the variables of phase β and then as a function of the variables of phase α:

$$dc_i^{\beta} = \left(\frac{\partial c_i^{\beta}}{\partial T}\right)_{P^{\beta},x_j^{\beta}} dT + \left(\frac{\partial c_i^{\beta}}{\partial P^{\beta}}\right)_{T,x_j^{\beta}} dP^{\beta} + \sum_{j=1}^{c-1}\left(\frac{\partial c_i^{\beta}}{\partial x_j^{\beta}}\right)_{T,P^{\beta},x_{k\neq j,c}^{\beta}} dx_j^{\beta} \quad i = 1, \cdots, c \tag{37}$$

$$dc_i^{\beta} = \left(\frac{\partial c_i^{\beta}}{\partial T}\right)_{P^{\alpha},x_j^{\alpha}} dT + \left(\frac{\partial c_i^{\alpha}}{\partial P^{\alpha}}\right)_{T,x_j^{\alpha}} dP^{\alpha} + \sum_{j=1}^{c-1}\left(\frac{\partial c_i^{\beta}}{\partial x_j^{\alpha}}\right)_{T,P^{\alpha},x_{k\neq j,c}^{\alpha}} dx_j^{\alpha} \quad i = 1, \cdots, c \tag{38}$$

Considering a process at constant temperature and composition of the phase α, which are the conditions for which (2) holds, and equating (37) and (38) we obtain:

$$\left(\frac{\partial c_i^{\beta}}{\partial P^{\alpha}}\right)_{T,x_j^{\alpha}} dP^{\alpha} = \left(\frac{\partial c_i^{\beta}}{\partial P^{\beta}}\right)_{T,x_j^{\beta}} dP^{\beta} + \sum_{j=1}^{c-1}\left(\frac{\partial c_i^{\beta}}{\partial x_j^{\beta}}\right)_{T,P^{\beta},x_{k\neq j,c}^{\beta}} dx_j^{\beta} \quad i = 1, \cdots, c \tag{39}$$

Or, in terms of derivatives with respect to P^{α}:

$$\left(\frac{\partial c_i^\beta}{\partial P^\alpha}\right)_{T,x_j^\alpha} = \left(\frac{\partial c_i^\beta}{\partial P^\beta}\right)_{T,x_j^\beta}\left(\frac{\partial P^\beta}{\partial P^\alpha}\right)_{T,x_j^\alpha} + \sum_{j=1}^{c-1}\left(\frac{\partial x_j^\beta}{\partial P^\alpha}\right)_{T,x_j^\alpha}\left(\frac{\partial c_i^\beta}{\partial x_j^\beta}\right)_{T,P^\beta,x_{k\neq j,c}^\beta} \qquad i=1,\cdots,c \tag{40}$$

Half of the derivatives in the right-hand side of (40) can be directly obtained from an equation of state:

$$\left(\frac{\partial c_i^\beta}{\partial P^\beta}\right)_{T,x_j^\beta} = C_T^\beta c_i^\beta \quad i=1,\cdots,c \tag{41}$$

$$\left(\frac{\partial c_i^\beta}{\partial x_j^\beta}\right)_{T,P^\beta,x_{k\neq j,c}^\beta} = \rho^\beta\left[\delta_{ij} - \delta_{ic} + c_i^\beta\left(\tilde{v}_j^\beta - \tilde{v}_c^\beta\right)\right] \qquad i=1\cdots,c; \quad j=1,\cdots,c-1 \tag{42}$$

Equation (42) is obtained from the definition of $c_i^\beta = x_i^\beta \rho^\beta$ and the Gibbs-Duhem equation in terms of partial molar volumes (see problem 1.5 of Chapter I in Ref. 26). The symbol δ in (42) is the Kronecker delta. Substituting (41) and (42) into (40) we obtain:

$$\left(\frac{\partial c_i^\beta}{\partial P^\alpha}\right)_{T,x_j^\alpha} = \left(C_T\right)^\beta c_i^\beta\left(\frac{\partial P^\beta}{\partial P^\alpha}\right)_{T,x_j^\alpha} + \rho^\beta\left(\frac{\partial x_i^\beta}{\partial P^\alpha}\right)_{T,x_i^\alpha} + \rho^\beta c_i^\beta\sum_{j=1}^{c-1}\left(\tilde{v}_c^\beta - \tilde{v}_j^\beta\right)\left(\frac{\partial x_j^\beta}{\partial P^\alpha}\right)_{T,x_j^\alpha} \tag{43}$$

$$i=1,\cdots,c-1$$

And, for $i=c$:

$$\left(\frac{\partial c_i^\beta}{\partial P^\alpha}\right)_{T,x_j^\alpha} = \beta^\beta c_i^\beta \left(\frac{\partial P^\beta}{\partial P^\alpha}\right)_{T,x_j^\alpha} - \rho^\beta \sum_{j=1}^{c-1}\left(\frac{\partial x_j^\beta}{\partial P^\alpha}\right)_{T,x_j^\alpha} + \rho^\beta c_i^\beta \sum_{j=1}^{c-1}\left(\tilde{v}_c^\beta - \tilde{v}_j^\beta\right)\left(\frac{\partial x_j^\beta}{\partial P^\alpha}\right)_{T,x_j^\alpha} \tag{44}$$

However, from the sum condition of phase β:

$$\sum_{j=1}^{c-1}\left(\frac{\partial x_j^\beta}{\partial P^\alpha}\right)_{T,x_j^\alpha} = -\left(\frac{\partial x_c^\beta}{\partial P^\alpha}\right)_{T,x_j^\alpha} \tag{45}$$

Substituting (45) into (44) we obtain (43) with $i = c$. Thus, we can regard (43) as valid for all $i = 1, \cdots, c$. In order to use (43) we need to find the derivatives of the pressure and composition of phase β with respect to the pressure of phase α. We use an approach similar to the one used for the single-component system. Since the derivatives appearing in (43) are taken in an equilibrium path, we use:

$$\mu_i^\alpha = \mu_i^\beta \quad i = 1, \cdots, c \tag{46}$$

Differentiating (46) with respect to the pressure of phase α at constant temperature and composition of phase α we obtain:

$$\left(\frac{\partial \mu_i^\alpha}{\partial P^\alpha}\right)_{T,x_j^\alpha} = \left(\frac{\partial \mu_i^\beta}{\partial P^\alpha}\right)_{T,x_j^\alpha} \quad i = 1, \cdots, c \tag{47}$$

The derivative on the left-hand side of (47) is the partial molar volume of component *i* in phase α. For the derivative in the right hand-side, one can write:

$$\left(\frac{\partial \bar{v}_i^{\alpha}}{\partial P^{\alpha}}\right)_{T,x_j^{\alpha}} = \left(\frac{\partial \bar{v}_i^{\beta}}{\partial P^{\beta}}\right)_{T,x_j^{\beta}} \left(\frac{\partial P^{\beta}}{\partial P^{\alpha}}\right)_{T,x_j^{\alpha}} + \sum_{j=1}^{c-1} \left(\frac{\partial x_j^{\beta}}{\partial P^{\alpha}}\right)_{T,x_j^{\alpha}} \left(\frac{\partial \bar{v}_i^{\beta}}{\partial x_j^{\beta}}\right)_{T,P^{\beta},x_{k\neq j,c}^{\beta}} \qquad i = 1,\cdots,c \tag{48}$$

The first derivative on the right-hand side is the partial molar volume of component *i* in phase β. Substituting (48) into (47) we obtain:

$$\tilde{v}_i^{\alpha} = \tilde{v}_i^{\beta} \left(\frac{\partial P^{\beta}}{\partial P^{\alpha}}\right)_{T,x_j^{\alpha}} + \sum_{j=1}^{c-1} \left(\frac{\partial x_j^{\beta}}{\partial P^{\alpha}}\right)_{T,x_j^{\alpha}} \left(\frac{\partial \mu_i^{\beta}}{\partial x_j^{\beta}}\right)_{T,P^{\beta},x_{k\neq j,c}^{\beta}} \qquad i = 1,\cdots,c \tag{49}$$

Multiplying (49) by x_j^{β} and taking the sum we find:

$$\sum_{j=1}^{c} x_j^{\beta} \tilde{v}_j^{\alpha} = v^{\beta} \left(\frac{\partial P^{\beta}}{\partial P^{\alpha}}\right)_{T,x_l^{\alpha}} + \sum_{k=1}^{c-1} \left(\frac{\partial x_k^{\beta}}{\partial P^{\alpha}}\right)_{T,x_l^{\alpha}} \sum_{j=1}^{c} x_j^{\beta} \left(\frac{\partial \mu_j^{\beta}}{\partial x_k^{\beta}}\right)_{T,P^{\beta},x_{l\neq k,c}^{\beta}} \tag{50}$$

where *v* is the molar volume. From the Gibbs-Duhem equation for phase β:

$$\sum_{j=1}^{c} x_j^{\beta} \left(\frac{\partial \mu_j^{\beta}}{\partial x_k^{\beta}}\right)_{T,P^{\beta},x_{l\neq k,c}^{\beta}} = 0 \tag{51}$$

Combining (50) and (51) provides:

$$\left(\frac{\partial P^{\beta}}{\partial P^{\alpha}}\right)_{T,x_j^{\alpha}} = \rho^{\beta}\sum_{i=1}^{c} x_i^{\beta}\tilde{v}_i^{\alpha} = \sum_{i=1}^{c} c_i^{\beta}\tilde{v}_i^{\alpha} \tag{52}$$

Substituting (52) into (49) leads to:

$$\sum_{j=1}^{c-1}\left(\frac{\partial x_j^{\beta}}{\partial P^{\alpha}}\right)_{T,x_j^{\alpha}}\left(\frac{\partial \mu_i^{\beta}}{\partial x_j^{\beta}}\right)_{T,P^{\beta},x_{k\neq j,c}^{\beta}} = \tilde{v}_i^{\alpha} - \tilde{v}_i^{\beta}\sum_{j=1}^{c} c_j^{\beta}\tilde{v}_j^{\alpha} \quad i=1,\cdots,c \tag{53}$$

Note that, although (53) is valid for $i=1,\cdots,c$, only (c-1) of the equations are independent because we already used their sum to obtain (52). The first (c-1) equations in (53) can be used to obtain the derivatives of the compositions of phase β with respect to the pressure of phase α, provided we use an equation of state to obtain the derivatives of the chemical potentials with respect to the compositions in phase β.

Substituting (36), (43) and (52) into (35):

$$\begin{aligned}\sum_{i=1}^{c}\Gamma_{i,s}\tilde{v}_i^{\alpha} = -4\sigma_s^{3/4}\sum_{i=1}^{c}\Pi_i\Bigg[& C_T^{\alpha}c_i^{\alpha} - C_T^{\beta}c_i^{\beta}\sum_{j=1}^{c}c_j^{\beta}\tilde{v}_j^{\alpha} - \rho^{\beta}\left(\frac{\partial x_i^{\beta}}{\partial P^{\alpha}}\right)_{T,x_i^{\alpha}} \\ & + \rho^{\beta}c_i^{\beta}\sum_{j=1}^{c}\tilde{v}_j^{\beta}\left(\frac{\partial x_j^{\beta}}{\partial P^{\alpha}}\right)_{T,x_j^{\alpha}}\end{aligned} \tag{54}$$

where the derivatives of the composition of phase β are obtained by solving the system of equations (53). For the δ_∞ model we will substitute (54) into (12) and take the limit as $a_s \to \infty$ to obtain:

$$\delta_\infty^b = \frac{-4\sigma_\infty^{3/4} \sum_{i=1}^{c} \Pi_i \left[C_T^\beta c_i^\beta \sum_{j=1}^{c} c_j^\beta \tilde{v}_j^\alpha + \rho^\beta \left(\frac{\partial x_i^\beta}{\partial P^\alpha} \right)_{T,x_i^\alpha} - \rho^\beta c_i^\beta \sum_{j=1}^{c} \tilde{v}_j^\beta \left(\frac{\partial x_j^\beta}{\partial P^\alpha} \right)_{T,x_j^\alpha} - C_T^\alpha c_i^\alpha \right]}{1 - \sum_{i=1}^{c} c_i^\beta \tilde{v}_i^\alpha} \tag{55}$$

Note that the superscript *b* indicates the limiting value for the bubble, as explained at the end of the previous section. For this model, δ_∞ will be regarded as independent of curvature. Substituting (55) into (2) and integrating we can calculate the curvature dependence of the surface tension. For the Π model, (54) is substituted into (14) and the resulting equation is integrated numerically.

Figure 9 shows the variation of surface tension with the radius of the bubble in an equimolar liquid mixture of propane and n-octane at 300 K, using the δ_∞ and the Π models. The parachors in the surface tension model are: C_3, 150; nC_4, 200; nC_6; 300; nC_8, 400. The binary interaction parameters in the Peng-Robinson equation of state were taken as zero. The behavior shown is similar to that obtained for the single-component system. The variation in surface tension is only important for bubble sizes of less than 10 nm. The overall change in surface tension in the two-component system considered is smaller than in the single-component system.

The variation of δ with curvature for the Π model is shown in Figure 10, which is consistent with the variation of the surface tension.

The equations for a droplet in a continuous bulk vapor phase can be obtained by exchanging the α and β superscripts in (34) and repeating the above procedure. In the following equations α will refer to the vapor phase and β to the liquid phase:

$$\sum_{i=1}^{c} \Gamma_{i,s} \tilde{v}_i^{\alpha} = 4\sigma_s^{3/4} \sum_{i=1}^{c} \Pi_i \left[\beta^{\alpha} c_i^{\alpha} - \beta^{\beta} c_i^{\beta} \sum_{j=1}^{c} c_j^{\beta} \tilde{v}_j^{\alpha} - \rho^{\beta} \left(\frac{\partial x_i^{\beta}}{\partial P^{\alpha}} \right)_{T,x_i^{\alpha}} + \rho^{\beta} c_i^{\beta} \sum_{j=1}^{c} \tilde{v}_j^{\beta} \left(\frac{\partial x_j^{\beta}}{\partial P^{\alpha}} \right)_{T,x_j^{\alpha}} \right] \qquad (56)$$

The derivatives of the composition in (56) will be found by solving the system of equations (53). For the limiting value of δ in a droplet:

$$\delta_{\infty}^{d} = \frac{4\sigma_{\infty}^{3/4} \sum_{i=1}^{c} \Pi_i \left[C_T^{\beta} c_i^{\beta} \sum_{j=1}^{c} c_j^{\beta} \tilde{v}_j^{\alpha} + \rho^{\beta} \left(\frac{\partial x_i^{\beta}}{\partial P^{\alpha}} \right)_{T,x_i^{\alpha}} - \rho^{\beta} c_i^{\beta} \sum_{j=1}^{c} \tilde{v}_j^{\beta} \left(\frac{\partial x_j^{\beta}}{\partial P^{\alpha}} \right)_{T,x_j^{\alpha}} - C_T^{\alpha} c_i^{\alpha} \right]}{1 - \sum_{i=1}^{c} c_i^{\beta} \tilde{v}_i^{\alpha}} \qquad (57)$$

Comparison of (55) and (57) reveals the sign difference as well as the phase identity differences. For the δ_{∞} model, we will substitute (57) into (2) and integrate to calculate the curvature dependence of the surface tension. For the Π model, (56) is substituted into (14) and the result is integrated numerically.

Figure 11 shows the variation of the surface tension with the radius of the droplet in an equimolar gaseous mixture of propane and n-octane at 400 K. The same model as that of the bubble example was used. The behavior of the droplet in the multicomponent system is similar to that of the single-component droplet. Figure 12, showing the variation of δ as a function of curvature, indicates a stronger increase of δ towards the high curvature region.

Figure 14 shows the behavior of the parameter δ_{∞}^{b} (taking the liquid as the continuous bulk phase) as a function of temperature for an equimolar liquid mixture of propane and n-octane. The behavior is somewhat different from that observed in the single-component system; δ_{∞}^{b} becomes negative at temperatures closer to the critical point. This is an important new result, showing that the surface tension for the bubble can either increase or decrease with curvature depending on the temperature; this may be the case for a large bubble. In Figure 13 we show the effect of composition at different temperatures on the parameter δ_{∞}^{b}. At low temperatures and pressures, where the system can be regarded as ideal, δ_{∞}^{b} increases monotonically with composition of propane, growing from the value for pure n-octane to the value for pure propane. At higher temperatures, the curve first decreases and then increases with composition. As the temperature increases towards the critical point, the curve becomes monotonically decreasing and δ_{∞}^{b} for higher compositions of propane becomes negative. This shows that the surface tension increase or decrease with curvature depends not only on the temperature but also on the composition of the mixture – the increase for a large bubble. As the system approaches the limit of stability (that is, the spinodal), the behavior changes.

We have carried out some calculations for ternary systems; the behavior found is similar to that shown in figures 9-14. Since the features are similar to what we obtained for the binaries, we have not included the results for the sake of brevity.

V. CONCLUDING REMARKS

A rigorous thermodynamic model is presented for the effect of curvature on the surface tension in bubbles and droplets for both single and multicomponent systems. The results for the nonpolar hydrocarbon systems that we have studied reveal that:

(1) There is generally a decrease of surface tension in bubbles with increasing curvatures in single component systems. The distance parameter δ for these systems is positive.

(2) For a droplet, if the distance parameter δ is assumed constant and equal to the value for the flat interface, there is an increase in the surface tension with increasing curvature in single component systems. The distance parameter of the flat interface is generally negative. With a variable distance parameter model, the behavior of the surface tension is non-monotonic; the surface tension increases with curvature first and then decreases. The predicted results from our thermodynamic model with a variable distance parameter are in qualitative agreement with the work of Guermeur et al.[11] and the work of Hadjiagapiou[10] based on density functional theory. It is also in line with the work of Oxtoby and Evans[23].

(3) In multicomponent systems the distance parameter of the flat interface for a bubble may be either positive or negative depending on the temperature and composition. The surface tension may thus increase or decrease with curvature at different conditions for a large bubble.

(4) In both a bubble and in a droplet the surface of tension decreases for a small cluster from the Π model presented in the work. This is another evidence in support of the validity of the results from our Π model.

Acknowledgments

The work was supported by DOE DE-FC26-00BC15306, and member companies of Reservoir Engineering Research Institute. Some of the work was done while Abbas Firoozabadi was on sabbatical at Yale University.

VI. REFERENCES

(1) D. Kashchiev, *Nucleation*: *Basic Theory with Applications* (Butterworth Heinemann, Oxford, 2000).

(2) M.A. Larson and J. Garside, J. of Crystal Growth **76**, 88 (1986).

(3) R.C. Tolman, J. Chem. Phys. **17**, No. 2, 118 (1949a).

(4) R.C. Tolman, J. Chem. Phys. 333 (1949b).

(5) J.W.P. Schmelzer, I. Gutzow, and J. Schmelzer Jr., J. of Colloid and Interface Science **178**, 657 (1996).

(6) A. Laaksonen and R. McGraw, Europhys Letters **35**, No. 5, 367 (1996).

(7) R. McGraw and A. Laaksonen, J. Chem. Phys. **106**, No. 12, 5284 (March 1997).

(8) V. Baidakov, A. Kaverin, and G. Boltachev, J. Phys. Chem. B. **106**, No. 1, 167 (2002).

(9) R. Defay and J. Prigogine, *Surface Tension and Adsorption* (Longman, London, 1966).

(10) I. Hadjiagapiou, J. Physics: Condens. Matter, **6**, 5303 (1994).

(11) R. Guermeur, F. Biquard, and C. Jacolin, J. of Chem. Phys. **82**, No. 4, 2040 (Feb. 1985).

(12) D.J. Lee, M.M. Telo da Gama, and K.E. Gubbins, J. Chem. Phys. **85**, No. 1, 490 (July 1986).

(13) J.W.P. Schmelzer and V.G. Baidakov, J. Phys. Chem. B., 105, 11595 (2001).

(14) V.G. Baidakov, G. Sh. Boltashev, and J.W.P. Schmelzer, J. Coll. Int. Sciences, **231**, 312 (2000).

(15) Ono and Kondo, Encyclopedia of Physics, edited by S. Flugge **10**, 134 (Springer, Berlin, 1960).

(16) L.S. Bartell, J. Phys. Chem. B, 105, 11615 (2001).

(17) D.B. Macleod, Trans Faraday Soc. **19**, 38 (1923).

(18) S. Sugden, Ind. & Eng. Chem. **35**, 239 (Feb. 1943).

(19) R.H. Fowler, Proc. Royal Soc. of London, Series A, 229 (1937).

(20) B.E. Poling, J.M. Prausnitz, and J.P. O'Connell, *The Properties of Gases and Liquids* (McGraw-Hill, 5th Ed., New York, 2001).

(21) D.Y. Peng and Robinson, Ind. Eng. Chem. Found. **15**, 59 (1976).

(22) L. Granasy, J. Chem. Phys., **109**, 22, 9660 (1998).

(23) D.W. Oxtoby and R. Evans, J. Chem Phys., **89**, 12, 7521 (Dec. 1988).

(24) C.F. Weinaugh and D.L. Katz, Ind. & Eng. Chem. **35**, 239 (Feb. 1943).

(25) A. Firoozabadi, D.L. Katz, H. Soroosh, and V.A. Sajjadian, SPE Reservoir Engineering, 265 (Feb. 1988).

(26) A. Firoozabadi, *Thermodynamics of Hydrocarbon Reservoirs* (McGraw-Hill, New York, 1999).

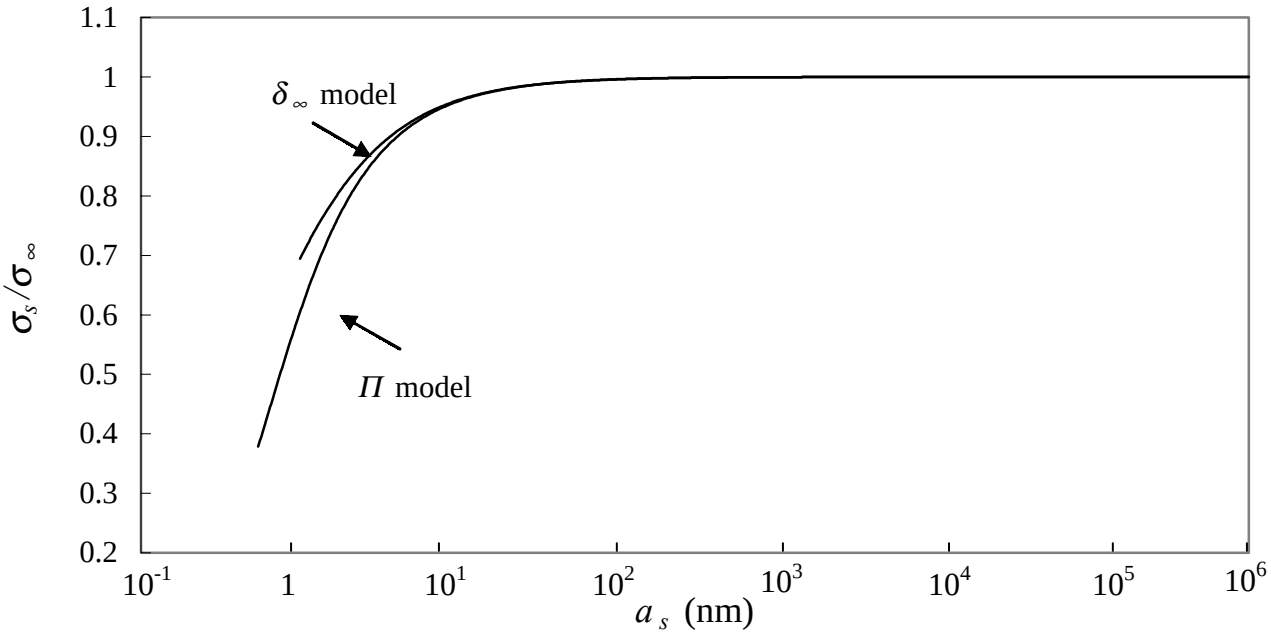

Figure 1 - Curvature dependence of the surface tension for a bubble of n-pentane at 310.9 K from the δ_∞ and the Π models.

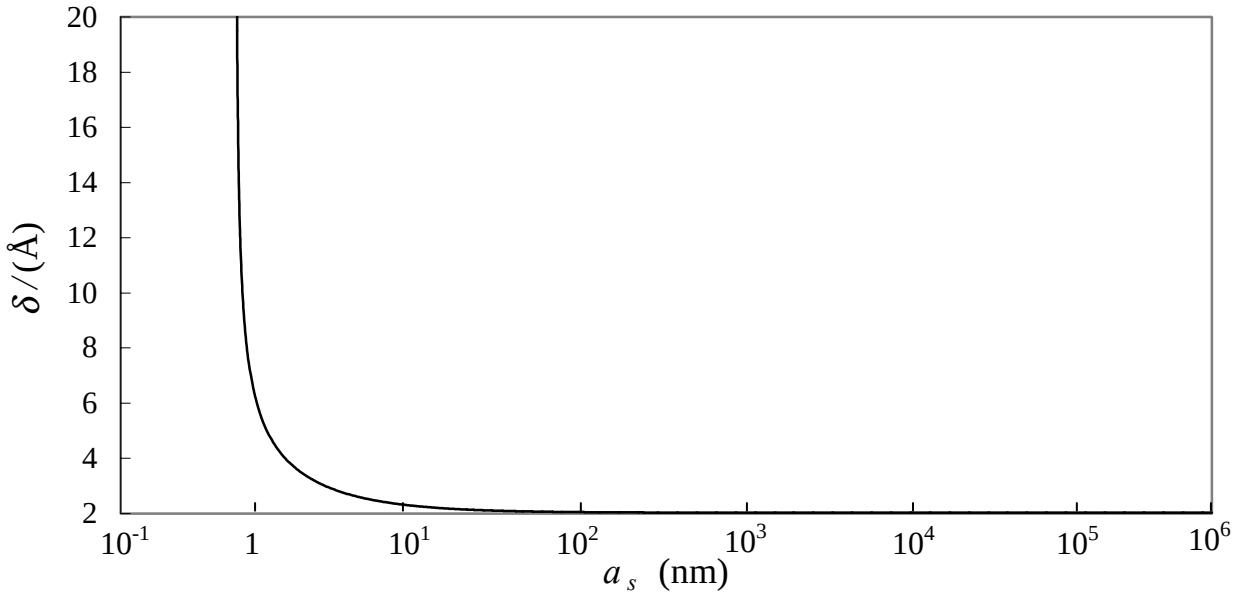

Figure 2 - Curvature dependence of the parameter δ for the Π model in the n-pentane bubble example (T=310.9 K).

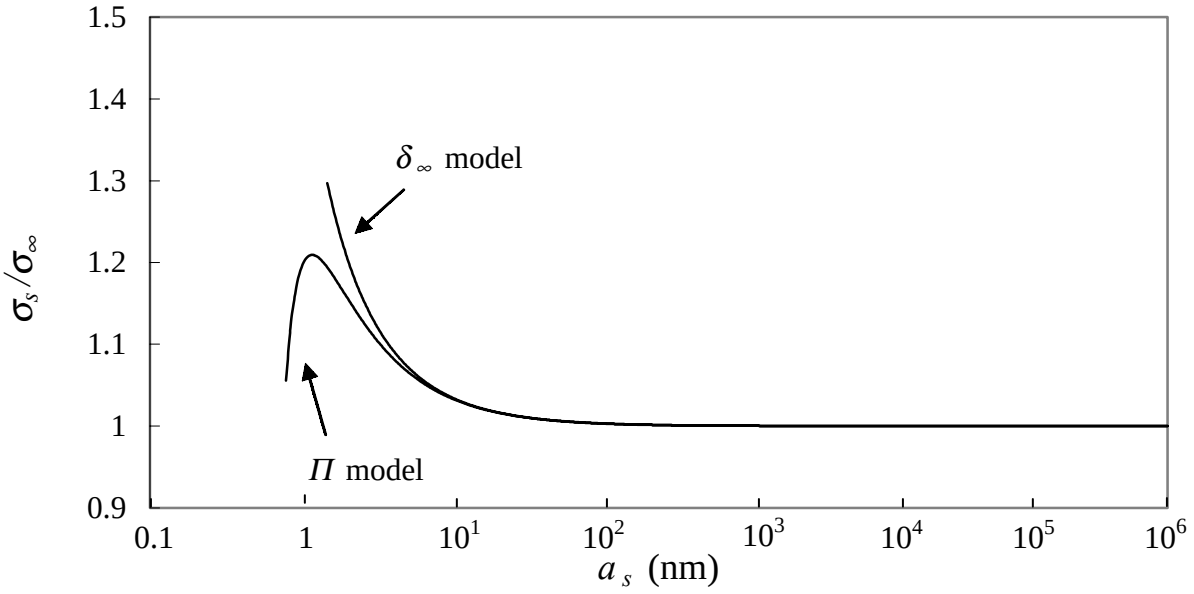

Figure 3 - Curvature dependence of the surface tension for a droplet of n-pentane at 310.9 K from the δ_∞ and the Π models.

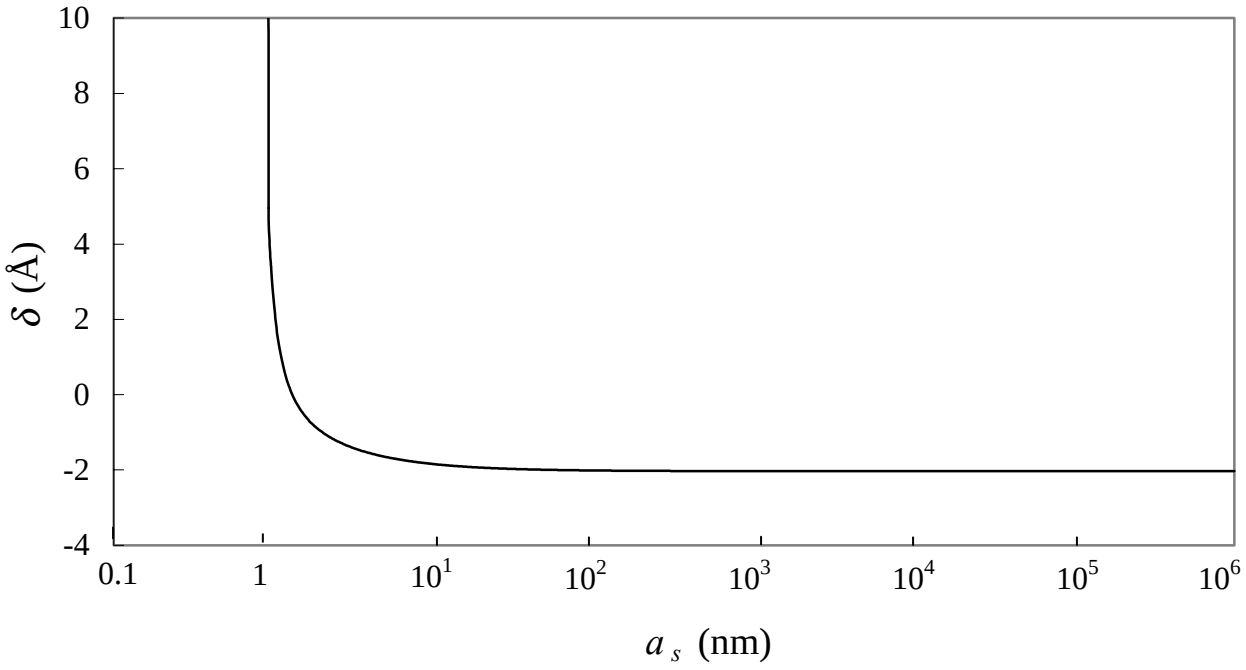

Figure 4 - Curvature dependence of the parameter δ for the Π model in the n-pentane droplet example (T=310.9 K).

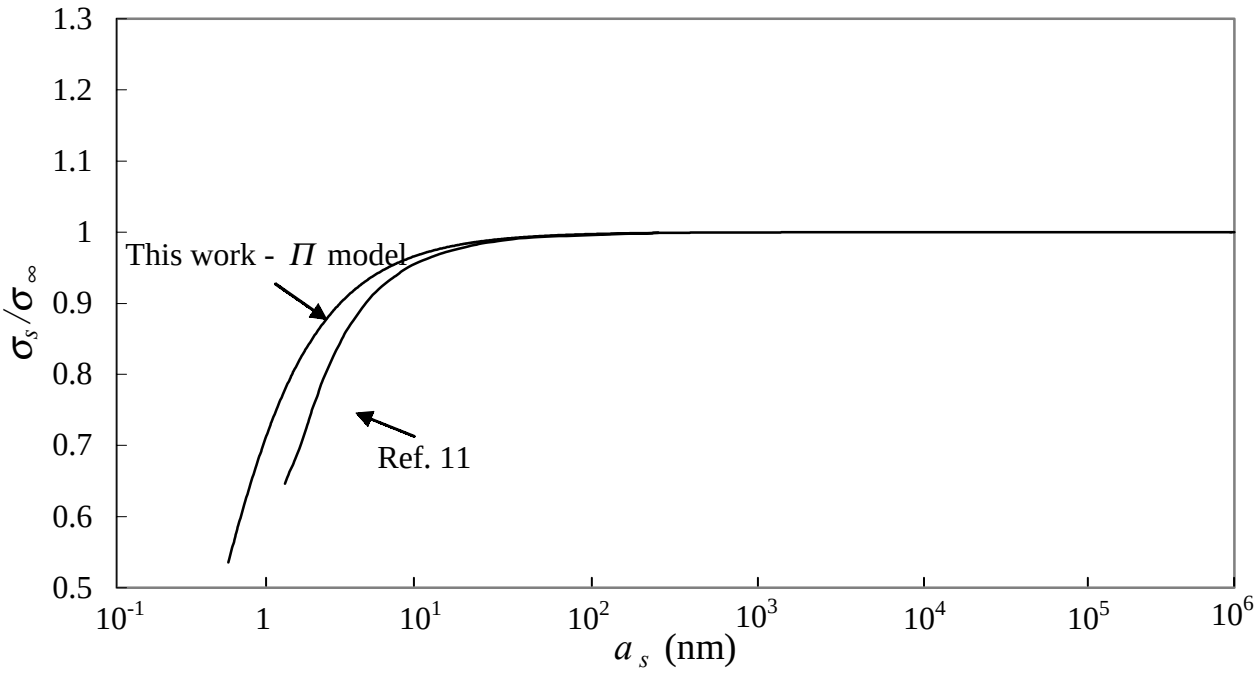

Figure 5 - Curvature dependence of the surface tension predicted by the Π model and the results from Ref. 11 for a nitrogen bubble at 77.3 K .

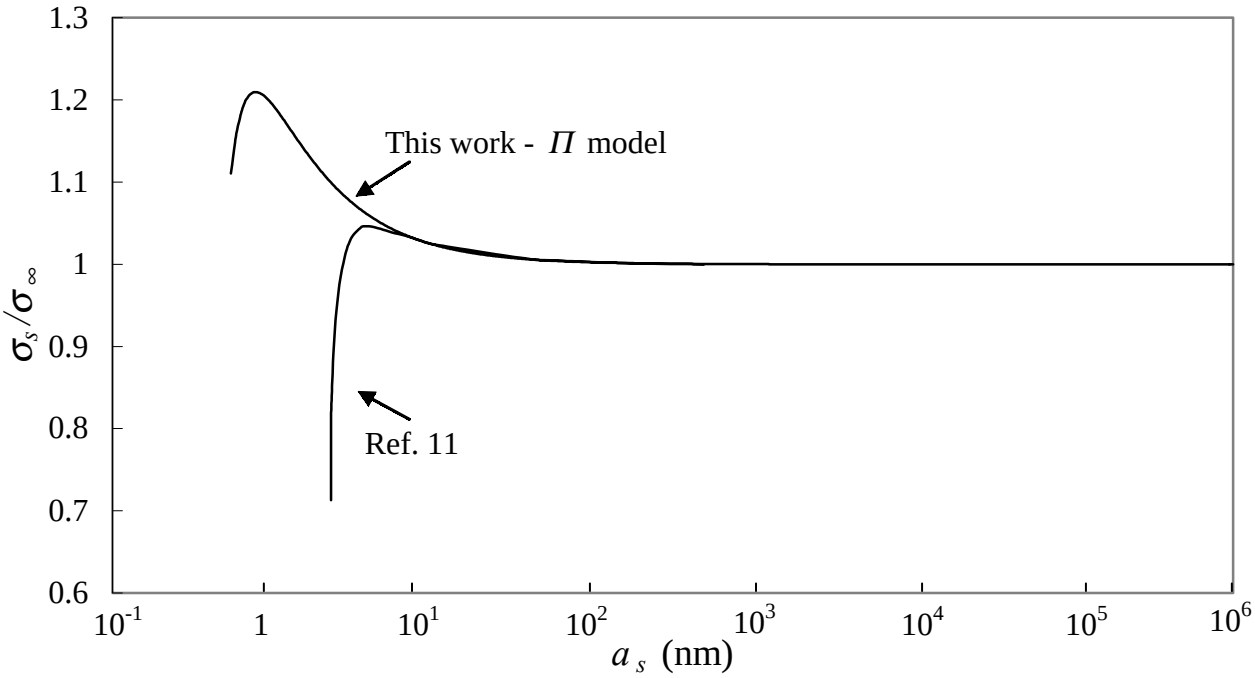

Figure 6 - Comparison between the curvature dependence of the surface tension predicted by the Π model and the results from Ref. 11 for a nitrogen droplet at 77.3 K .

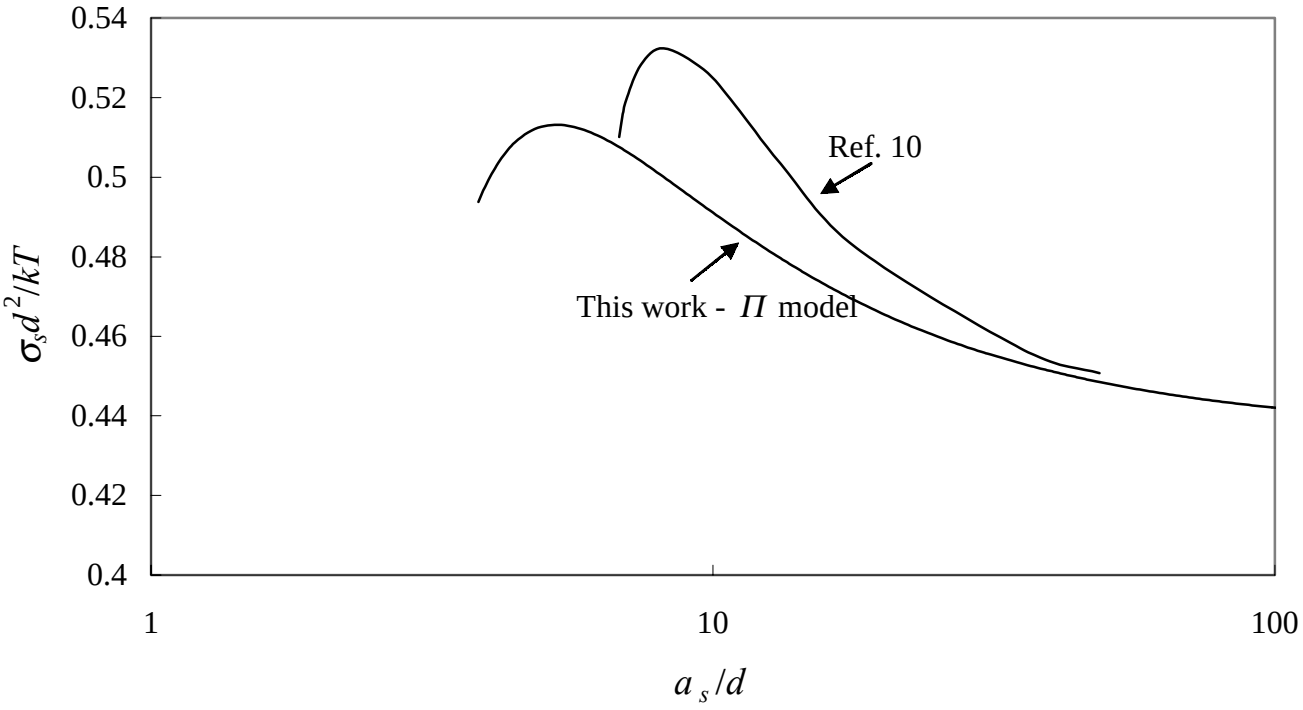

Figure 7 - Curvature dependence of the surface tension predicted by the Π model for Argon at a reduced temperature of 0.8 and the results from Ref. 11. The new variables appearing in the dimensionless groups plotted are *d* (molecular diameter) and *k* (Boltzmann's constant).

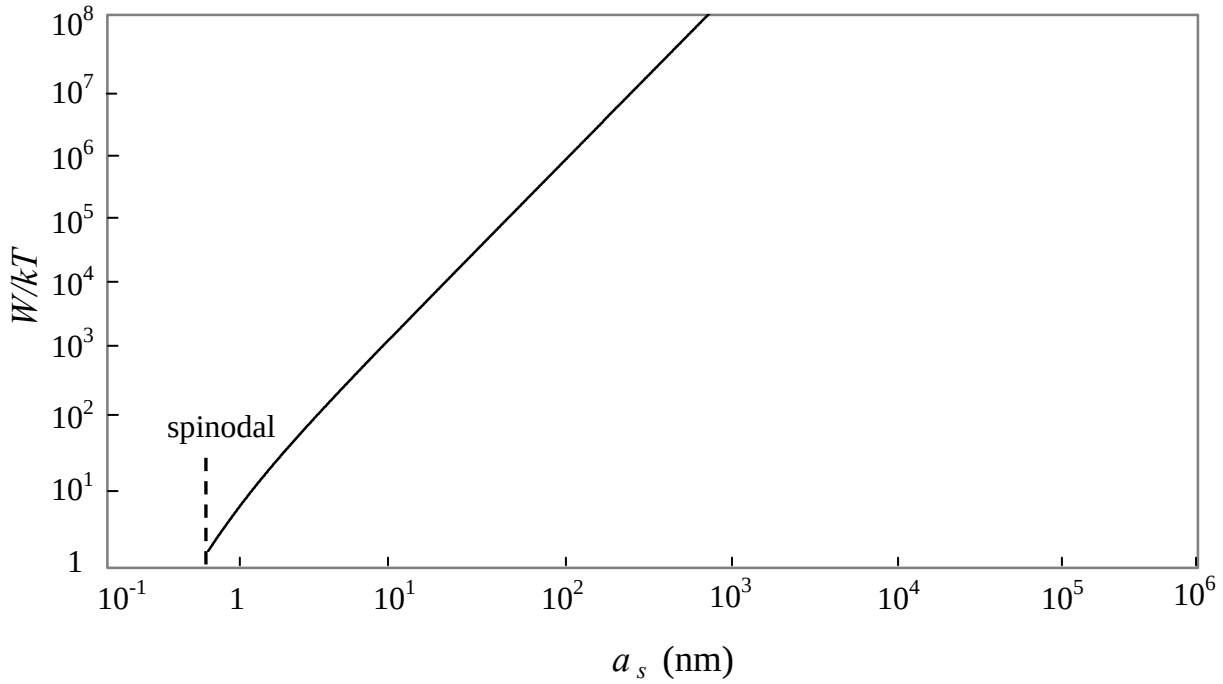

Figure 8 - Work of cluster formation (critical) vs. radius of the surface of tension in the n-pentane bubble at T = 310.9 K.

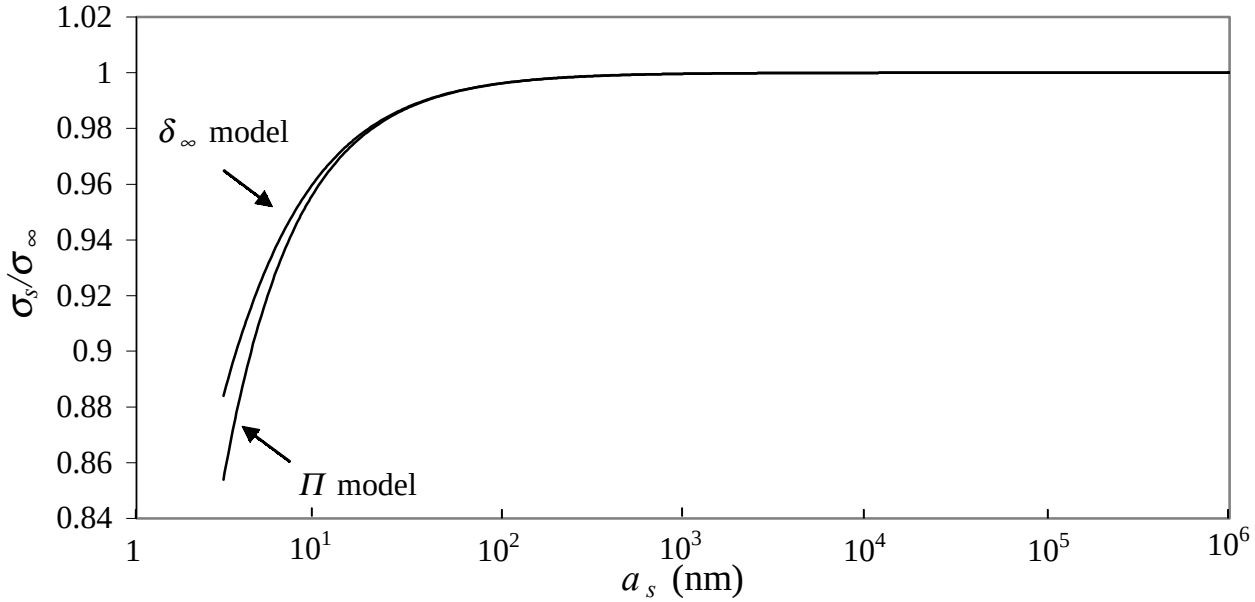

Figure 9 - Curvature dependence of the surface tension for a bubble in an equimolar liquid mixture of propane and n-octane at 300 K from the δ_∞ and the Π models.

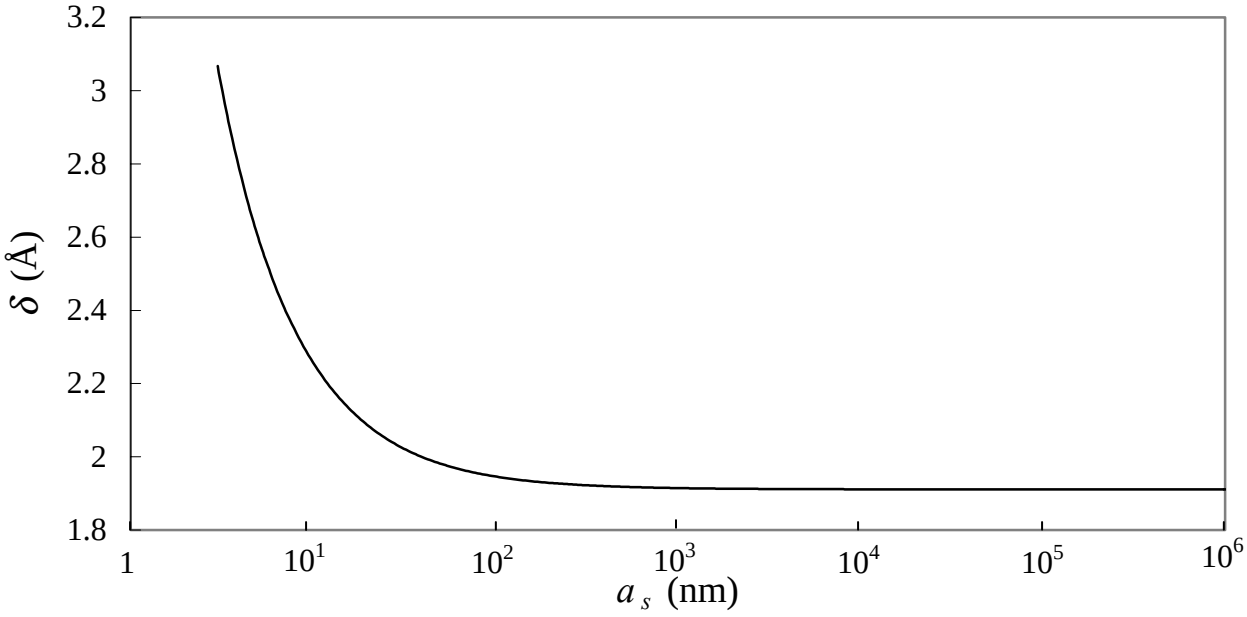

Figure 10 - Curvature dependence of the parameter δ for the Π model in the binary-bubble example (equimolar liquid mixture of propane and n-octane at 300 K).

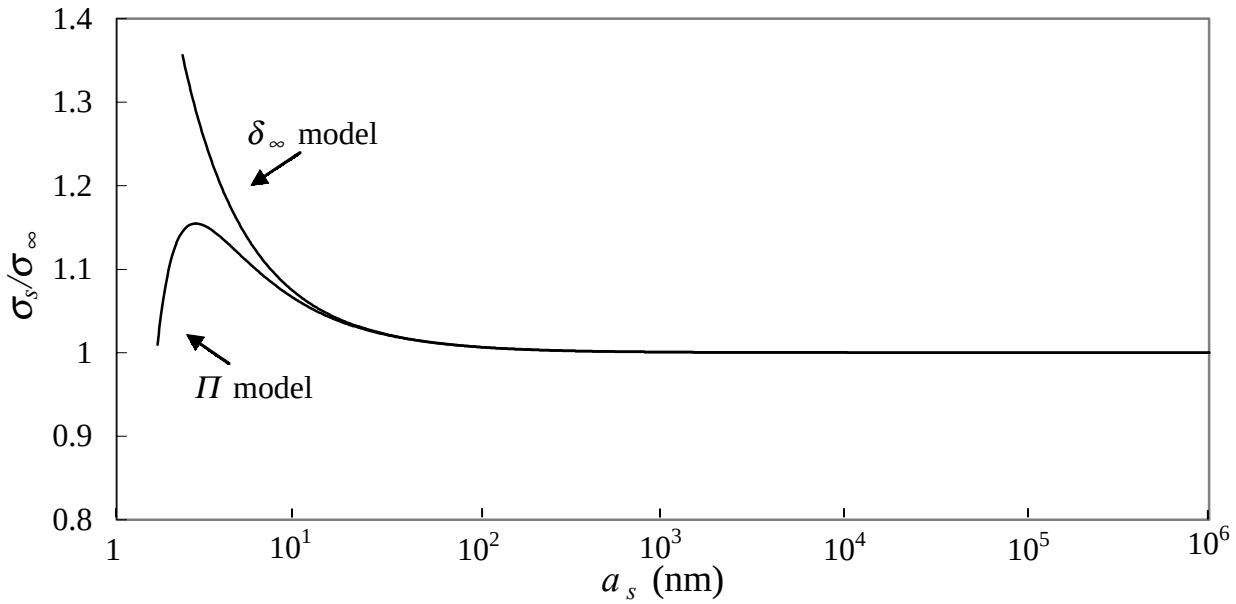

Figure 11 - The parameter δ_∞^b vs. composition for a bubble in a liquid mixture of propane and n-octane at different temperatures.

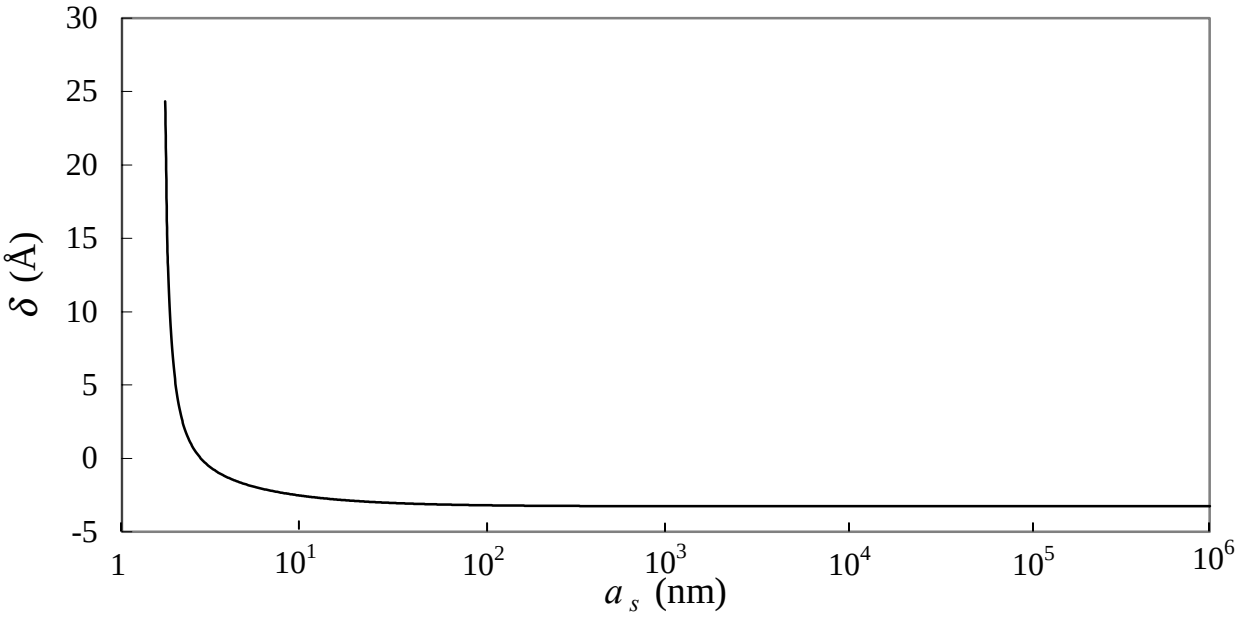

Figure 12 - The parameter δ_{∞}^{b} vs. temperature for a bubble in an equimolar mixture of propane and n-octane.

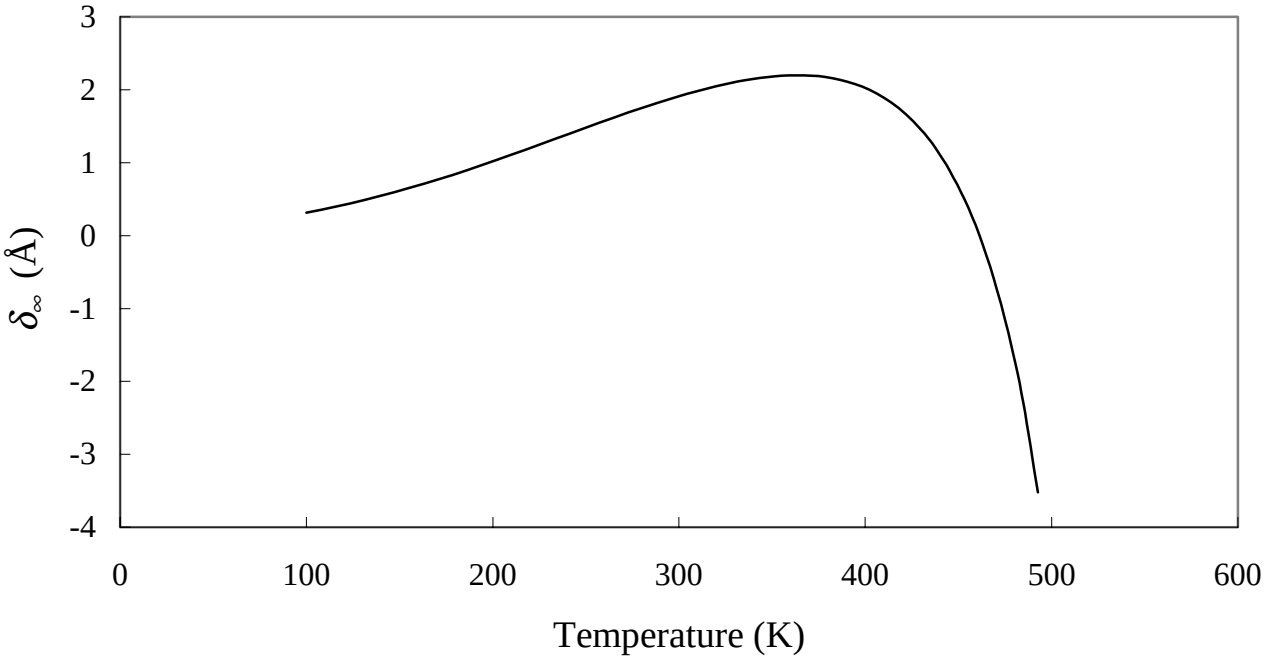

Figure 13 - Curvature dependence of the parameter δ from the Π model in the binary droplet example (equimolar gaseous mixture of propane and n-octane at 400 K).

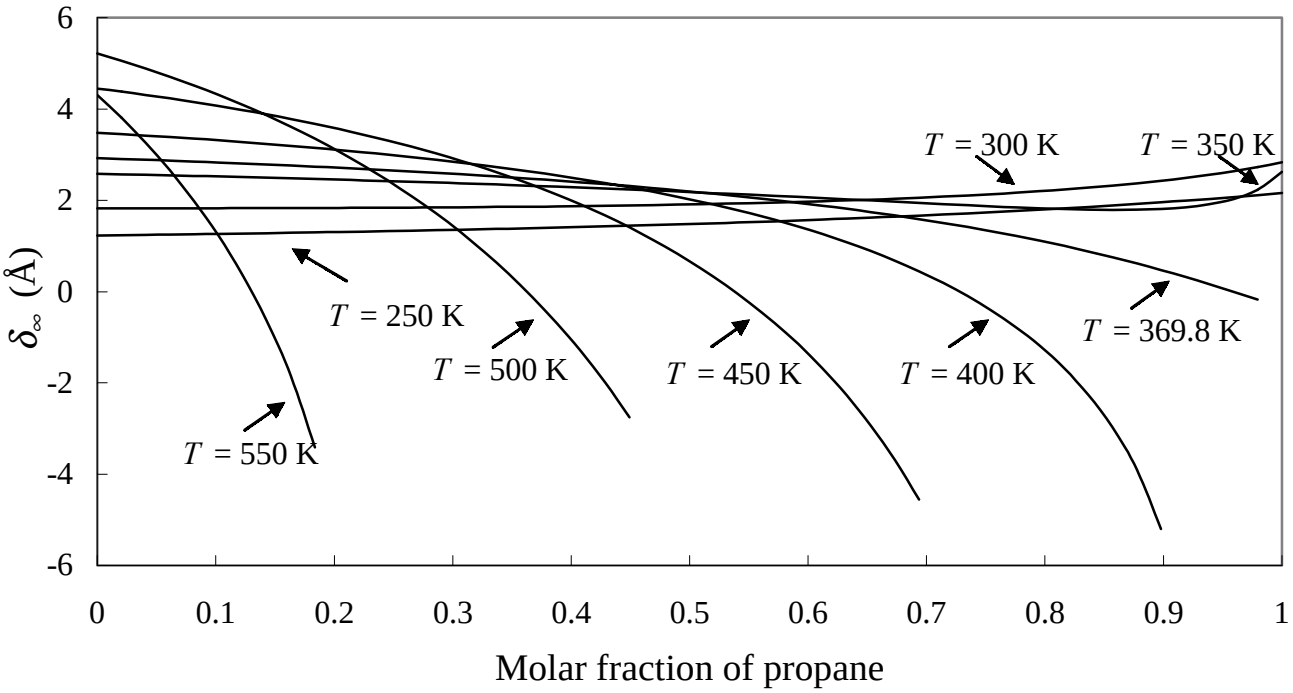

Figure 14 - Curvature dependence of the surface tension for a droplet in an equimolar gaseous mixture of propane and n-octane at 400 K from the δ_∞ and the Π models.

Chapter III - Adsorption, Surface Energy, and Surface Entropy in Multicomponent Systems

Erik Santiso and Abbas Firoozabadi

Summary

In a multicomponent two-phase mixture, the amount of adsorption at the interface (that is, the interface composition) plays a key role. As an example, in a two-phase gas-liquid system, when a surfactant is added to a bulk liquid phase, it mostly moves to the interface between the gas and liquid bulk phases; the result can be a large reduction of the interfacial tension. In a solid-liquid system, there may be a similar process which can result in the change of wettability. In this study, we provide a formulation for the calculation of the amount of the adsorption in the gas-liquid multicomponent systems. As a first step, the fluid mixture is assumed to consist of non-polar species. This would then allow the use of the simple equations of state such as the Peng-Robinson EOS for the description of bulk phase properties.

Introduction

A large number of processes in petroleum reservoirs and production and in other disciplines are affected by the composition and the energy of the interface between the phases. When a component is added to a phase in a gas-liquid system, it is often distributed in the two bulk phases and the interface. Sometimes when a small amount of a component is added to a two-phase system, most of it may end up at the interface between the phases. It is because of high adsorption at the interface that the surface tension can be lowered significantly by a small amount of a surfactant. Another important phenomenon is the surface wetting, which is related to composition and surface energy. In our work on wettability alteration (Tang and Firoozabadi, 2002a and b), it is because of the adsorption of polymers onto the rock substrate that the surface energy is lowered. The result is change in wettability. Our goal is to model the process of adsorption at the interface between gas and liquid, liquid-solid, and gas-solid systems in order to examine the effect of temperature among other factors.

This work is our second report on interfacial thermodynamics which addresses the issues related to interface adsorption and interface energy. The first report was focused on the effect of curvature on interfacial tension (Santiso and Firoozabadi, 2002). In this work, we provide a formulation for the calculation of interface composition (or sufrace composition), as well as surface energy and entropy. The objective is to estimate the amount of adsorption for all the components in the mixture. In our approach, there is no need to assign zero value of adsorption for one of the components. The conventional approach in the literature is to compute the relative adsorption (Defay and Prigogine, 1966).

This report is structured along the following lines. We first provide thermodynamic relations for the calculation of the amount of adsorption at the interface for a gas-liquid system at equilibrium. Several numerical examples provide the amount of adsorption at the interface for a binary mixture and a ternary mixture. We then provide expressions for surface entropy and surface energy.

Thermodynamic relations for the amounts of adsorption at the interface.

The surface tension σ, the amount of adsorption of component i, Γ_i, the chemical potential of component i at the interface μ_i^σ for the spherical interface with radius a are related by

$$d\sigma = -s^\sigma dT - \sum_{i=1}^{c} \Gamma_i d\mu_i^\sigma + \left[\frac{\partial \sigma}{\partial a}\right] da \qquad (1)$$

where s^{σ} is the entropy per unit area of the interface (the superscript σ denotes a surface property), c is the number of components, and $[\partial\sigma/\partial a]$ represents the change in the interfacial tension when the mathematical dividing surface between the two phases is displaced. The above equation was used by Santiso and Firoozabadi (2002) to study the effect of curvature on σ.

We can consider the flat interface just as the limit when the radius goes to infinity. If we choose the surface of tension as our dividing surface, (1) becomes:

$$d\sigma_s = -s_s^{\sigma}\,dT - \sum_{i=1}^{c} \Gamma_{i,s}\,d\mu_{i,s}^{\sigma} \tag{2}$$

The properties referring to the surface of tension are identified with subscript s.Since the system under consideration is in phase equilibrium we can replace the surface chemical potentials in (2) by the chemical potentials of bulk phase α:

$$d\sigma_s = -s_s^{\sigma}\,dT - \sum_{i=1}^{c} \Gamma_{i,s}\,d\mu_i^{\alpha} \tag{3}$$

The chemical potential of bulk phase α can be written in terms of independent variables temperature T, pressure of phase α, P^{α}, and composition of component j in phase α x_j^{α}:

$$d\mu_i^{\alpha} = -\tilde{s}_i^{\alpha}dT + \tilde{v}_i^{\alpha}dP^{\alpha} + \sum_{j=1}^{c-1}\left(\frac{\partial\mu_i^{\alpha}}{\partial x_j^{\alpha}}\right)_{T,P^{\alpha},x_{k\neq j,c}^{\alpha}} dx_j^{\alpha} \tag{4}$$

where $\tilde{s}_i^{\alpha}$ and $\tilde{v}_i^{\alpha}$ are the partial molar entropy and partial molar volume, respectively. Substituting (4) into (3) we obtain

$$d\sigma_s = \left(-s_s^{\sigma} + \sum_{i=1}^{c}\Gamma_{i,s}\tilde{s}_i^{\alpha}\right)dT - \left(\sum_{i=1}^{c}\Gamma_{i,s}\tilde{v}_i^{\alpha}\right)dP^{\alpha} - \sum_{j=1}^{c-1}\left[\sum_{i=1}^{c}\Gamma_{i,s}\left(\frac{\partial\mu_i^{\alpha}}{\partial x_j^{\alpha}}\right)_{T,P^{\alpha},x_{k\neq j,c}^{\alpha}}\right]dx_j^{\alpha} \tag{5}$$

which is equation (17) in Ref. 3 There, we only developed relations involving the second term of the equation. However, the other two terms contain also valuable information. The first will provide an expression for the surface entropy and the third will provide expressions for the surface adsorptions. In particular, (5) implies that:

$$\left(\frac{\partial\sigma_s}{\partial x_j^{\alpha}}\right)_{T,P^{\alpha},x_{k\neq j,c}^{\alpha}} = -\sum_{i=1}^{c}\Gamma_{i,s}\left(\frac{\partial\mu_i^{\alpha}}{\partial x_j^{\alpha}}\right)_{T,P^{\alpha},x_{k\neq j,c}^{\alpha}} \qquad j=1,\cdots,c-1 \tag{6}$$

An expression for the surface tension allows us to calculate the derivatives in the left-hand side of (6) together with an equation of state for the bulk phases (note that (6) would also be valid if we replaced α by β), then (6) is a system of $(c-1)$ equations with c unknowns (the amounts of adsorption). However, we have another equation that also comes from (5):

$$\left(\frac{\partial \sigma_s}{\partial P^{\alpha}}\right)_{T,x_j^{\alpha}} = -\sum_{i=1}^{c} G_{i,s}\tilde{v}_i^{\alpha} \qquad (7)$$

We used this equation in our previous work (Ref. 3) to obtain the size dependence of the surface tension. Equations (6) and (7) complete a system of c equations for the c unknown amounts of adsorption. In the next section, we will proceed with further formulation

Amounts of adsorption for a multicomponent gas-liquid system in equilibrium

In order to solve the system of equations (6)-(7), we need an expression for the surface tension. As we have done in our previous work, we use the Weinaugh-Katz equation (Weinaugh and Katz, 1943) in order to establish the solution procedure.

Let us write the Weinaugh-Katz equation as:

$$\sigma^{1/4} = \sum_{i=1}^{c} P_i \left(c_i^{\beta} - c_i^{\alpha} \right) \tag{8}$$

Here we assign the superscript β to the liquid phase and the superscript α to the vapor phase. We also assume that the equation will be valid for a curved interface; for the flat interface we take the limit as the curvature tends to zero. These are the same assumptions made in our previous work.

The Weinaugh-Katz equation will provide the left-hand side terms in equations (6)-(7). From equation (6)-(7) we have:

$$\sum_{i=1}^{c} G_{i,s} \tilde{\nu}_i^{\alpha} = -4\sigma^{3/4} \sum_{i=1}^{c} P_i \left[c_T^{\alpha} - c_T^{\beta} \sum_{j=1}^{c} c_j^{\beta} \tilde{\nu}_j^{\alpha} - \rho^{\beta} \left(\frac{\partial x_i^{\beta}}{\partial P^{\alpha}} \right)_{T, x_i^{\alpha}} + \rho^{\beta} c_i^{\beta} \right] \tag{9}$$

which is (54) in Santiso and Firoozabadi (2002). The derivatives of the compositions of phase β with respect to the pressure of phase α are obtained by solving the system of equations:

$$\sum_{j=1}^{c-1} \left(\frac{\partial x_j^{\beta}}{\partial P^{\alpha}} \right)_{T, x_j^{\alpha}} \left(\frac{\partial m_i^{\beta}}{\partial x_j^{\beta}} \right)_{T, P^{\beta}, x_{k \neq j,c}^{\beta}} = \tilde{\nu}_i^{\alpha} - \tilde{\nu}_i^{\beta} \sum_{j=1}^{c} c_j^{\beta} \tilde{\nu}_j^{\alpha} \quad i = 1, \cdots, c \tag{10}$$

The above equation is the same as (53) in Santiso and Firoozabadi (2002). Now we need the derivatives of the surface tension with respect to the compositions of phase α from equation (6). The procedure to obtain these derivatives is similar to the one we used for the derivative with respect to the pressure, but it is somewhat more involved. We start by differentiating (8) with respect to the composition of component *j* in phase α and combine the result with (6):

$$\left(\frac{\partial \sigma_s}{\partial x_j^{\alpha}} \right)_{T, P^{\alpha}, x_{k \neq j,c}^{\alpha}} = 4\sigma^{3/4} \sum_{i=1}^{c} P_i \left[\left(\frac{\partial c_i^{\alpha}}{\partial x_j^{\alpha}} \right)_{T, P^{\alpha}, x_{k \neq j,c}^{\alpha}} - \left(\frac{\partial c_i^{\beta}}{\partial x_j^{\alpha}} \right)_{T, P^{\alpha}, x_{k \neq j,c}^{\alpha}} \right] \quad j = 1, \cdots, c-1 \tag{11}$$

The first derivative in the square bracket can be readily obtained from an equation of state:

$$\left(\frac{\partial c_i^{\alpha}}{\partial x_j^{\alpha}} \right)_{T, P^{\alpha}, x_{k \neq j,c}^{\alpha}} = \rho^{\alpha} \left[c_i^{\alpha} \left(\tilde{\nu}_c^{\alpha} - \tilde{\nu}_j^{\alpha} \right) + \delta_{ij} - \delta_{ic} \right] \quad i = 1, \cdots, c \text{ and } j = 1, \cdots, c-1 \tag{12}$$

where δ_{ij} is the Kronecker delta.

The second derivative is, however, more complicated. In order to get an expression for it, we first write the differential of the concentrations in phase β as a function of the properties of both phase α and phase β :

$$dc_i^{\beta} = \left(\frac{\partial c_i^{\beta}}{\partial T}\right)_{P^{\beta},x_j^{\beta}} dT + \left(\frac{\partial c_i^{\beta}}{\partial P^{\beta}}\right)_{T,x_j^{\beta}} dP^{\beta} + \sum_{j=1}^{c-1}\left(\frac{\partial c_i^{\beta}}{\partial x_j^{\beta}}\right)_{T,P^{\beta},x_{k\neq j,c}^{\beta}} dx_j^{\beta} \quad i=1,\cdots,c \tag{13}$$

$$dc_i^{\beta} = \left(\frac{\partial c_i^{\beta}}{\partial T}\right)_{P^{\alpha},x_j^{\alpha}} dT + \left(\frac{\partial c_i^{\beta}}{\partial P^{\alpha}}\right)_{T,x_j^{\alpha}} dP^{\alpha} + \sum_{j=1}^{c-1}\left(\frac{\partial c_i^{\beta}}{\partial x_j^{\alpha}}\right)_{T,P^{\alpha},x_{k\neq j,c}^{\alpha}} dx_j^{\alpha} \quad i=1,\cdots,c \tag{14}$$

Considering now a process where the temperature, the pressure of phase α and the compositions of all components in phase α except for components j and c are held constant and equating (13) and (14) we obtain:

$$\left(\frac{\partial c_i^{\beta}}{\partial x_j^{\alpha}}\right)_{T,P^{\alpha},x_{k\neq j,c}^{\alpha}} = \left(\frac{\partial c_i^{\beta}}{\partial P^{\beta}}\right)_{T,x_j^{\beta}} \left(\frac{\partial P^{\beta}}{\partial x_j^{\alpha}}\right)_{T,P^{\alpha},x_{k\neq j,c}^{\alpha}} + \sum_{k=1}^{c-1}\left(\frac{\partial c_i^{\beta}}{\partial x_k^{\beta}}\right)_{T,P^{\beta},x_{m\neq k,c}^{\beta}} \left(\frac{\partial x_k^{\beta}}{\partial x_j^{\alpha}}\right)_{T,P^{\alpha},x_{m\neq j,c}^{\alpha}} \quad i=1,\cdots,c \text{ and } j=1,\cdots,c-1 \tag{15}$$

There are four types of derivatives in the right-hand side of (15). The first one can be directly obtained from an equation of state:

$$\left(\frac{\partial c_i^{\beta}}{\partial P^{\beta}}\right)_{T,x_j^{\beta}} = c_i^{\beta} C_T^{\beta} \qquad i=1,\cdots,c \tag{16}$$

where C_T is the isothermal compressibility. The third set of derivatives in (15) is similar to the one in (12):

$$\left(\frac{\partial c_i^{\beta}}{\partial x_k^{\beta}}\right)_{T,P^{\beta},x_{m\neq k,c}^{\beta}} = \rho^{\beta}\left[c_i^{\beta}\left(\tilde{v}_c^{\beta} - \tilde{v}_k^{\beta}\right) + \delta_{ik} - \delta_{ic}\right] \quad i=1,\cdots,c,\ k=1,\cdots,c-1 \tag{17}$$

Now we need expressions for the second and the fourth set of derivatives in (15). These can be obtained from the chemical equilibrium condition:

$$\mu_i^{\alpha} = \mu_i^{\beta} \Rightarrow \left(\frac{\partial \mu_i^{\alpha}}{\partial x_j^{\alpha}}\right)_{T,P^{\alpha},x_{k\neq j,c}^{\alpha}} = \left(\frac{\partial \mu_i^{\beta}}{\partial x_j^{\alpha}}\right)_{T,P^{\alpha},x_{k\neq j,c}^{\alpha}} \quad i=1,\cdots,c;\ k=1,\cdots,c-1 \tag{18}$$

The left-hand side in (18) can be directly obtained from an equation of state. In order to calculate the right-hand side, we follow a procedure similar to that of equations (13)-(15) for the chemical potentials of phase β , obtaining:

$$\left(\frac{\partial m_i^{\beta}}{\partial x_j^{\alpha}}\right)_{T,P^{\alpha},x^{\alpha}_{k\neq j,c}} = \left(\frac{\partial m_i^{\beta}}{\partial P^{\beta}}\right)_{T,x_j^{\beta}} \left(\frac{\partial P^{\beta}}{\partial x_j^{\alpha}}\right)_{T,P^{\alpha},x^{\alpha}_{k\neq j,c}} + \sum_{k=1}^{c-1}\left(\frac{\partial m_i^{\beta}}{\partial x_k^{\beta}}\right)_{T,P^{\beta},x^{\beta}_{m\neq k,c}} \left(\frac{\partial x_k^{\beta}}{\partial x_j^{\alpha}}\right)_{T,P^{\alpha},x^{\alpha}_{m\neq j,c}} \qquad (19)$$

$$i=1,\cdots,c \text{ and } j=1,\cdots,c-1$$

The first derivative on the right-hand side of (19) is the partial molar volume of component *i* in phase β. Substituting (19) into (18) we obtain:

$$\left(\frac{\partial m_i^{\alpha}}{\partial x_j^{\alpha}}\right)_{T,P^{\alpha},x^{\alpha}_{k\neq j,c}} = \tilde{v}_i^{\beta}\left(\frac{\partial P^{\beta}}{\partial x_j^{\alpha}}\right)_{T,P^{\alpha},x^{\alpha}_{k\neq j,c}} + \sum_{k=1}^{c-1}\left(\frac{\partial m_i^{\beta}}{\partial x_k^{\beta}}\right)_{T,P^{\beta},x^{\beta}_{m\neq k,c}} \left(\frac{\partial x_k^{\beta}}{\partial x_j^{\alpha}}\right)_{T,P^{\alpha},x^{\alpha}_{m\neq j,c}} \qquad (20)$$

$$i=1,\cdots,c;\ j=1,\cdots,c-1$$

Multiplying (20) by x_i^{β} and summing over $i=1,\cdots,c$ we get:

$$\sum_{i=1}^{c} x_i^{\beta}\left(\frac{\partial m_i^{\alpha}}{\partial x_j^{\alpha}}\right)_{T,P^{\alpha},x^{\alpha}_{k\neq j,c}} = \nu^{\beta}\left(\frac{\partial P^{\beta}}{\partial x_j^{\alpha}}\right)_{T,P^{\alpha},x^{\alpha}_{k\neq j,c}} + \sum_{k=1}^{c-1}\left(\frac{\partial x_k^{\beta}}{\partial x_j^{\alpha}}\right)_{T,P^{\alpha},x^{\alpha}_{m\neq j,c}} \sum_{i=1}^{c} x_i^{\beta}\left(\frac{\partial m_i^{\beta}}{\partial x_k^{\beta}}\right)_{T,P^{\beta},x^{\beta}_{m\neq k,c}}$$

$$j=1,\cdots,c-1 \qquad (21)$$

From the Gibbs-Duhem equation for phase β we have:

$$\sum_{i=1}^{c} x_i^{\beta}\left(\frac{\partial m_i^{\beta}}{\partial x_k^{\beta}}\right)_{T,P^{\beta},x^{\beta}_{m\neq k,c}} = 0 \qquad (22)$$

Substituting (22) into (21) we obtain:

$$\left(\frac{\partial P^{\beta}}{\partial x_j^{\alpha}}\right)_{T,P^{\alpha},x^{\alpha}_{k\neq j,c}} = \rho^{\beta}\sum_{i=1}^{c} x_i^{\beta}\left(\frac{\partial m_i^{\alpha}}{\partial x_j^{\alpha}}\right)_{T,P^{\alpha},x^{\alpha}_{k\neq j,c}} = \sum_{i=1}^{c} c_i^{\beta}\left(\frac{\partial m_i^{\alpha}}{\partial x_j^{\alpha}}\right)_{T,P^{\alpha},x^{\alpha}_{k\neq j,c}} \qquad j=1,\cdots,c-1 \qquad (23)$$

This is the second derivative in the right-hand side of (15). Substituting (23) into (20) we obtain:

$$\sum_{k=1}^{c-1}\left(\frac{\partial m_i^{\beta}}{\partial x_k^{\beta}}\right)_{T,P^{\beta},x^{\beta}_{m\neq k,c}} \left(\frac{\partial x_k^{\beta}}{\partial x_j^{\alpha}}\right)_{T,P^{\alpha},x^{\alpha}_{m\neq j,c}} = \left(\frac{\partial m_i^{\alpha}}{\partial x_j^{\alpha}}\right)_{T,P^{\alpha},x^{\alpha}_{k\neq j,c}} - \tilde{v}_i^{\beta}\sum_{k=1}^{c} c_k^{\beta}\left(\frac{\partial m_k^{\alpha}}{\partial x_j^{\alpha}}\right)_{T,P^{\alpha},x^{\alpha}_{k\neq j,c}}$$

$$i=1,\cdots,c;\ j=1,\cdots,c \qquad (24)$$

Equations (24), for each value of $j=1,\cdots,c-1$, are a system of *c* equations that can be used to obtain the derivatives of the composition of all components in phase β with respect to the composition of component *j* of phase α. Note that one of these *c* equations is dependent because we used their sum to obtain the derivative of the pressure in (23). These systems of equations provide us with the last set of derivatives in (18), thus completing the information needed to calculate the derivatives of the surface tension with respect to the compositions. Substituting (16), (17), (23) into (15) we obtain:

$$\left(\frac{\partial c_i^{\beta}}{\partial x_j^{\alpha}}\right)_{T,P^{\alpha},x^{\alpha}_{k\neq j,c}} = c_i^{\beta} C_T^{\beta} \sum_{k=1}^{c} c_k^{\beta} \left(\frac{\partial m_k^{\alpha}}{\partial x_j^{\alpha}}\right)_{T,P^{\alpha},x^{\alpha}_{m\neq j,c}} + \rho^{\beta}\left(\frac{\partial x_i^{\beta}}{\partial x_j^{\alpha}}\right)_{T,P^{\alpha},x^{\alpha}_{m\neq j,c}}$$
$$+ \sum_{k=1}^{c-1} \rho^{\beta} c_i^{\beta}\left(\tilde{v}_c^{\beta} - \tilde{v}_k^{\beta}\right)\left(\frac{\partial x_k^{\beta}}{\partial x_j^{\alpha}}\right)_{T,P^{\alpha},x^{\alpha}_{m\neq j,c}} \qquad i=1,\cdots,c\,;\ j=1,\cdots,c-1 \qquad (25)$$

It is necessary to use the sum condition of phase β to obtain the equation for $i=c$. Finally, substituting (12) and (25) into (11):

$$\left(\frac{\partial \sigma_s}{\partial x_j^{\alpha}}\right)_{T,P^{\alpha},x^{\alpha}_{k\neq j,c}} = 4\sigma_s^{3/4}\sum_{i=1}^{c} P_i \left\{ c_i^{\beta}\beta^{\beta}\sum_{k=1}^{c} c_k^{\beta}\left(\frac{\partial m_k^{\alpha}}{\partial x_j^{\alpha}}\right)_{T,P^{\alpha},x^{\alpha}_{m\neq j,c}} + \rho^{\beta}\left(\frac{\partial x_i^{\beta}}{\partial x_j^{\alpha}}\right)_{T,P^{\alpha},x^{\alpha}_{m\neq j,c}} \right.$$
$$\left. + \sum_{k=1}^{c-1} \rho^{\beta} c_i^{\beta}\left(\tilde{v}_c^{\beta} - \tilde{v}_k^{\beta}\right)\left(\frac{\partial x_k^{\beta}}{\partial x_j^{\alpha}}\right)_{T,P^{\alpha},x^{\alpha}_{m\neq j,c}} - \rho^{\alpha}\left[c_i^{\alpha}\left(\tilde{v}_c^{\alpha} - \tilde{v}_j^{\alpha}\right) + \delta_{ij} - \delta_{ic}\right]\right\} \quad j=1,\cdots,c-1 \quad (26)$$

Equations (9) and (26) can be combined with (10) and (24) to provide a system of equations for the amounts of adsorption at the interface.

Figures 1 to 8 present the results for the amount of adsorption at the interface for the system propane-normal octane at various temperatures and composition of the liquid phase. These calculations are made for a flat interface. The same type of calculations can be performed for a curved interface.

Figures 1 to 7 reveal that propane (that is, the lighter component) is selectively adsorbed at the interface except at high concentrations of propane in the bulk liquid phase. It is also interesting to note that for the temperatures considered, there is at least one extremum in the amount of adsorption with a secondary extremum when the temperature approaches the critical temperature of propane from below (see Fig. 4). Fig. 8 shows that the temperature variation may not have strong effect on adsorption when the liquid composition is fixed to be equimolar value.

Fig. 9 shows the adsorption at the interface vs. normal fraction of C_1 and C_3 in the ternary mixture of $C_1/C_3/nC_8$ at 250 K. Note that methane adsorption is positive for the whole range of composition. Propane exhibits both positive and negative adsorption, and a clear increasing and decreasing trend. The adsorption of n-octane is negative and its behavior is in the opposite direction to propane.

Surface entropy and surface energy

So far, we considered the consequence of looking closely at the second and third terms of equation (5). Let us look now at the first one. The process will be pretty much the same as we have used for the other two. From equation (5) we can directly infer that:

$$\left(\frac{\partial \sigma_s}{\partial T}\right)_{P^{\alpha},x_i^{\alpha}} = -s_s^{\sigma} + \sum_{i=1}^{c} \Gamma_{i,s}\tilde{s}_i^{\alpha} \qquad (27)$$

This can again be combined with an equation for the surface tension to obtain the surface entropy.

In order to illustrate the use and the results that can be obtained from (27), we use again equation (8). Differentiating (8) with respect to temperature keeping constant the pressure and composition of phase α leads to:

$$\left(\frac{\partial \sigma_s}{\partial T}\right)_{P^a, x_i^a} = 4\sigma_s^{3/4}\sum_{i=1}^{c}\Gamma_i\left[\left(\frac{\partial c_i^{\beta}}{\partial T}\right)_{P^a, x_j^a} - \left(\frac{\partial c_i^{\alpha}}{\partial T}\right)_{P^a, x_j^a}\right] \tag{28}$$

The second derivative term in the brackets can be readily obtained from an equation of state:

$$\left(\frac{\partial c_i^{\alpha}}{\partial T}\right)_{P^a, x_j^a} = x_i^{\alpha}\left(\frac{\partial \rho^{\alpha}}{\partial T}\right)_{P^a, x_j^a} = -\rho^{\alpha} x_i^{\alpha}\kappa^{\alpha} = -c_i^{\alpha}\kappa^{\alpha} \quad i = 1, \cdots, c \tag{29}$$

where κ is the isobaric expansion coefficient. To obtain the first derivative in (28) we need to use equation (13) to obtain:

$$\left(\frac{\partial c_i^{\beta}}{\partial T}\right)_{P^a, x_j^a} = \left(\frac{\partial c_i^{\beta}}{\partial T}\right)_{P^b, x_j^b} + \left(\frac{\partial c_i^{\beta}}{\partial P^{\beta}}\right)_{T, x_j^b}\left(\frac{\partial P^{\beta}}{\partial T}\right)_{P^a, x_j^a} + \sum_{j=1}^{c-1}\left(\frac{\partial x_j^{\beta}}{\partial T}\right)_{P^a, x_k^a}\left(\frac{\partial c_i^{\beta}}{\partial x_j^{\beta}}\right)_{T, P^b, x_{k\neq j,c}^b} \quad i = 1, \cdots, c \tag{30}$$

The first derivative on the right-hand side of (30) is similar to the one in (29):

$$\left(\frac{\partial c_i^{\beta}}{\partial T}\right)_{P^b, x_j^b} = -c_i^{\beta}\kappa^{\beta} \quad i = 1, \cdots, c \tag{31}$$

The derivatives of the concentration with respect to pressure in phase β can be obtained from (16), and the derivatives of the concentration with respect to mole fractions can be obtained from (17).

We need an expression for the two remaining derivatives; we differentiate the chemical equilibrium condition with respect to the temperature:

$$\mu_i^{\alpha} = \mu_i^{\beta} \Rightarrow \left(\frac{\partial \mu_i^{\alpha}}{\partial T}\right)_{P^a, x_j^a} = \left(\frac{\partial \mu_i^{\beta}}{\partial T}\right)_{P^a, x_j^a} \quad i = 1, \cdots, c \tag{32}$$

The left-hand side is the partial molar entropy of component i in phase α; $(\partial \mu_i^{\alpha} / \partial T)_{p^a, x_j^a} = \tilde{s}_i^{\alpha}$. For the right-hand side we repeat the procedure used for the concentrations in equation (30) to get:

$$\left(\frac{\partial \mu_i^{\beta}}{\partial T}\right)_{P^a, x_j^a} = \left(\frac{\partial \mu_i^{\beta}}{\partial T}\right)_{P^b, x_j^b} + \left(\frac{\partial \mu_i^{\beta}}{\partial P^{\beta}}\right)_{T, x_j^b}\left(\frac{\partial P^{\beta}}{\partial T}\right)_{P^a, x_j^a} + \sum_{j=1}^{c-1}\left(\frac{\partial x_j^{\beta}}{\partial T}\right)_{P^a, x_k^a}\left(\frac{\partial \mu_i^{\beta}}{\partial x_j^{\beta}}\right)_{T, P^b, x_{k\neq j,c}^b} \quad i = 1, \cdots, c \tag{33}$$

Substituting (33) into (32) and recognizing the partial molar entropies and volumes we get:

$$\tilde{s}_i^{\alpha} = \tilde{s}_i^{\beta} + \tilde{v}_i^{\beta}\left(\frac{\partial P^{\beta}}{\partial T}\right)_{P^{\alpha},x_j^{\alpha}} + \sum_{j=1}^{c-1}\left(\frac{\partial x_j^{\beta}}{\partial T}\right)_{P^{\alpha},x_k^{\alpha}}\left(\frac{\partial m_i^{\beta}}{\partial x_j^{\beta}}\right)_{T,P^{\beta},x_{k\neq j,c}^{\beta}} \qquad i=1,\cdots,c \tag{34}$$

Multiplying (34) by x_i^{β} and summing over $i=1,\cdots,c$:

$$\sum_{i=1}^{c} x_i^{\beta}\tilde{s}_i^{\alpha} = s^{\beta} + v^{\beta}\left(\frac{\partial P^{\beta}}{\partial T}\right)_{P^{\alpha},x_j^{\alpha}} + \sum_{j=1}^{c-1}\left(\frac{\partial x_j^{\beta}}{\partial T}\right)_{P^{\alpha},x_k^{\alpha}}\sum_{i=1}^{c} x_i^{\beta}\left(\frac{\partial m_i^{\beta}}{\partial x_j^{\beta}}\right)_{T,P^{\beta},x_{k\neq j,c}^{\beta}} \tag{35}$$

The last term vanishes due to the Gibbs-Duhem equation for phase β. Thus, we obtain:

$$\left(\frac{\partial P^{\beta}}{\partial T}\right)_{P^{\alpha},x_j^{\alpha}} = \rho^{\beta}\left(-s^{\beta} + \sum_{i=1}^{c} x_i^{\beta}\tilde{s}_i^{\alpha}\right) \tag{36}$$

Substituting (36) into (34) and rearranging leads to:

$$\sum_{j=1}^{c-1}\left(\frac{\partial x_j^{\beta}}{\partial T}\right)_{P^{\alpha},x_k^{\alpha}}\left(\frac{\partial m_i^{\beta}}{\partial x_j^{\beta}}\right)_{T,P^{\beta},x_{k\neq j,c}^{\beta}} = \tilde{s}_i^{\alpha} - \tilde{s}_i^{\beta} - \tilde{v}_i^{\beta}\rho^{\beta}\left(-s^{\beta} + \sum_{i=1}^{c} x_i^{\beta}\tilde{s}_i^{\alpha}\right) \quad i=1,\cdots,c \tag{37}$$

Equations (37) form a system of c equations (one of which is dependent) that can be solved to obtain the $(c-1)$ derivatives of the composition of phase β with respect to temperature. The last one can be obtained from the sum condition. Substituting (16), (17), (31), (36) into (30) leads to:

$$\left(\frac{\partial c_i^{\beta}}{\partial T}\right)_{P^{\alpha},x_j^{\alpha}} = -c_i^{\beta}\kappa^{\beta} + c_i^{\beta}\rho^{\beta}\beta^{\beta}\left(-s^{\beta} + \sum_{i=1}^{c} x_i^{\beta}\tilde{s}_i^{\alpha}\right) + \rho^{\beta}\left(\frac{\partial x_i^{\beta}}{\partial T}\right)_{P^{\alpha},x_k^{\alpha}} + \sum_{j=1}^{c-1}\rho^{\beta}c_i^{\beta}\left(\tilde{v}_c^{\beta} - \tilde{v}_j^{\beta}\right)\left(\frac{\partial x_j^{\beta}}{\partial T}\right)_{P^{\alpha},x_k^{\alpha}} \qquad i=1,\cdots,c \tag{38}$$

And finally, substituting (29) and (37) into (28):

$$\left(\frac{\partial \sigma_s}{\partial T}\right)_{P^{\alpha},x_i^{\alpha}} = 4\sigma_s^{3/4}\sum_{i=1}^{c}\Gamma_i\left\{-c_i^{\beta}\kappa^{\beta} + c_i^{\beta}\rho^{\beta}\beta^{\beta}\left(-s^{\beta} + \sum_{i=1}^{c} x_i^{\beta}\tilde{s}_i^{\alpha}\right) + \rho^{\beta}\left(\frac{\partial x_i^{\beta}}{\partial T}\right)_{P^{\alpha},x_k^{\alpha}} + \sum_{j=1}^{c-1}\rho^{\beta}c_i^{\beta}\left(\tilde{v}_c^{\beta} - \tilde{v}_j^{\beta}\right)\left(\frac{\partial x_j^{\beta}}{\partial T}\right)_{P^{\alpha},x_k^{\alpha}} + c_i^{\alpha}\kappa^{\alpha}\right\} \tag{39}$$

Equation (39), combined with (27), can be used to obtain the surface entropy. The surface energy can then be readily obtained from:

$$u_s^s = \sigma_s + Ts_s^s + \sum_{i=1}^{c} \Gamma_i \mu_i^s \qquad (40)$$

Conclusions

We have derived the expression for the calculation of adsorption at the gas-liquid interface in multicomponent systems. The expressions for the interface entropy and energy are also derived for gas-liquid systems for multicomponents.

Numerical results show that the adsorption of one of the components in a binary mixture can increase and then decrease when the concentration of the same component increases. Numerical results for the same binary mixtures reveal that these may be two extremums of adsorption when the concentration of the same component is varied.

References

1. Tang, T. and Firoozabadi, A.: "Relative Permeability Modification in Gas-Liquid Systems through Wettability Alteration to Intermediate Gas-Wetting," SPE Reservoir and Engineering (Dec. 2002), also SPE 62934.
2. Tang, T. and Firoozabadi, A.: "Wettability Alteration to Intermediate Gas-Wetting in Porous Media at Elevated Temperature," Transport in Porous Media (Nov. 2002).
3. Santiso, E. and Firoozabadi, A.: "Curvature Dependency of Surface Tension in Multicomponent 02.
4. Defay, R. and Prigogine, J.: "Surface Tension and Adsorption," Longman (1966) London.
5. Weinaugh, C.F. and Katz, D.G.: "Surface Tension of Methane-Propane Mixtures," Industrial & Eng. Chem. 35, 239 (Feb. 1943).

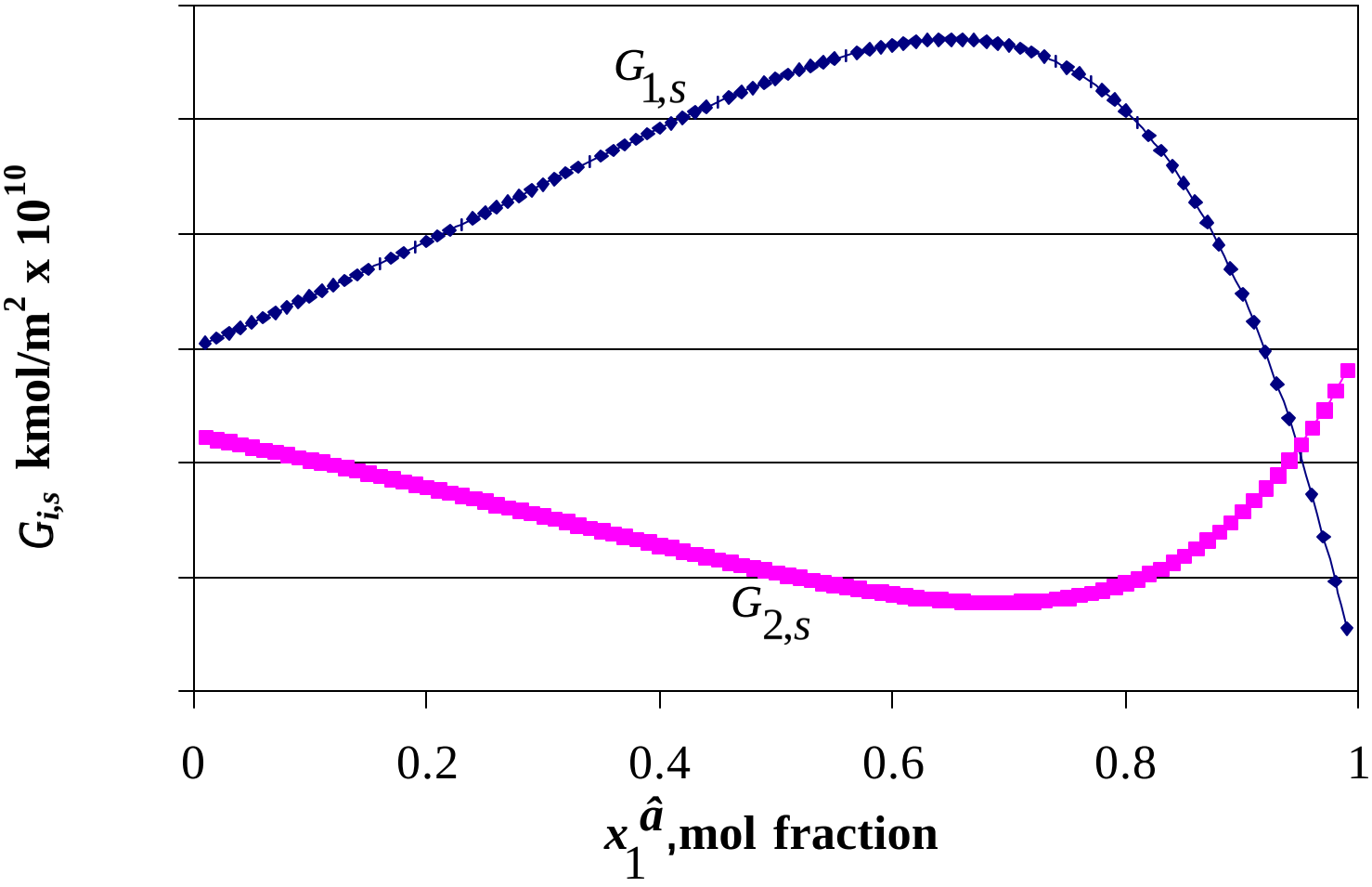

Fig. 1 – Adsorption at the Gas-Liquid Interface for Propane (1) and Normal Octane (2) Mixture vs. Mol Fraction of Propane in Liquid Phase: T = 250 K.

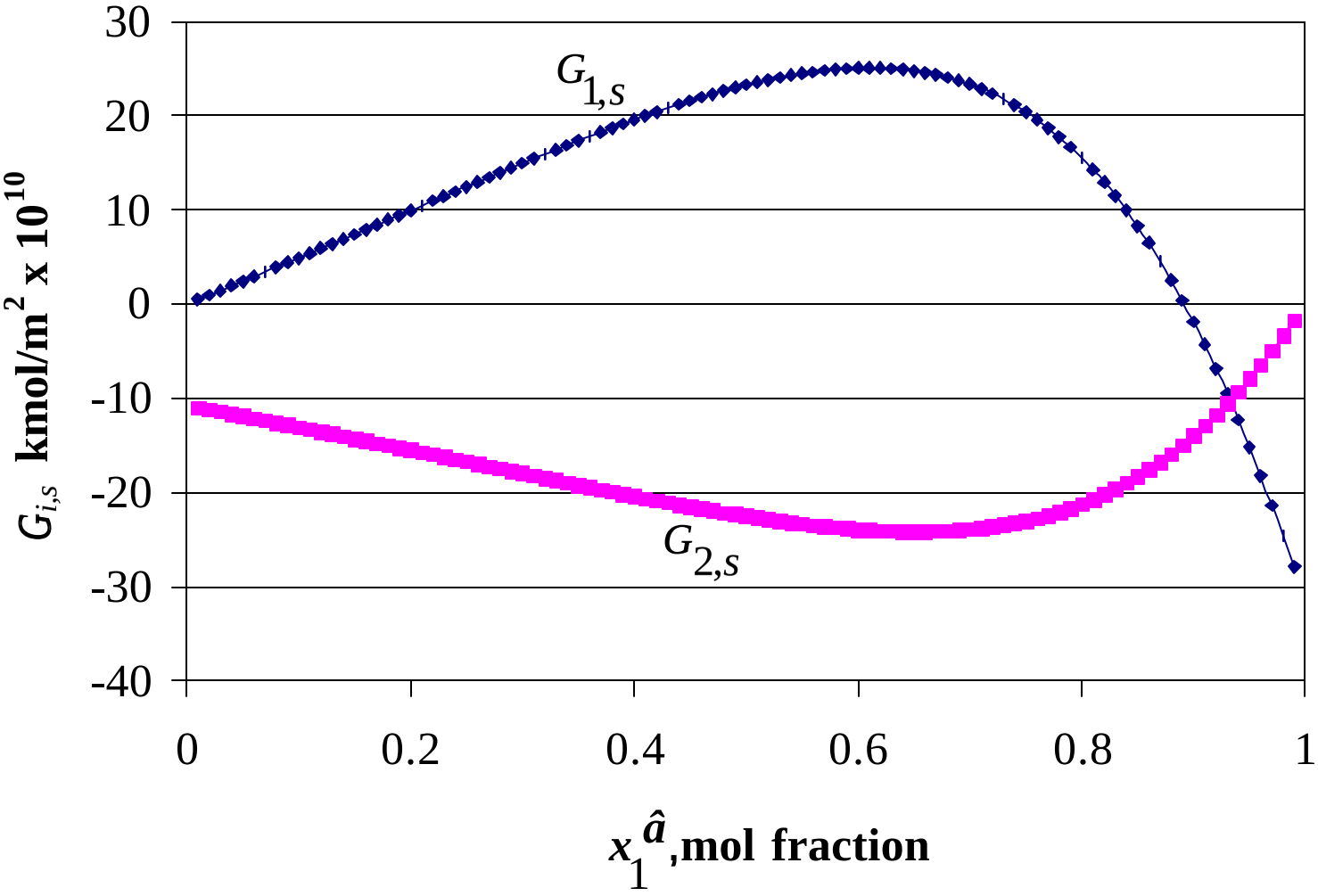

Fig. 2 – Adsorption at the Gas-Liquid Interface for Propane (1) and Normal Octane (2) Mixture vs. Mol Fraction of Propane in Liquid Phase: T = 300 K.

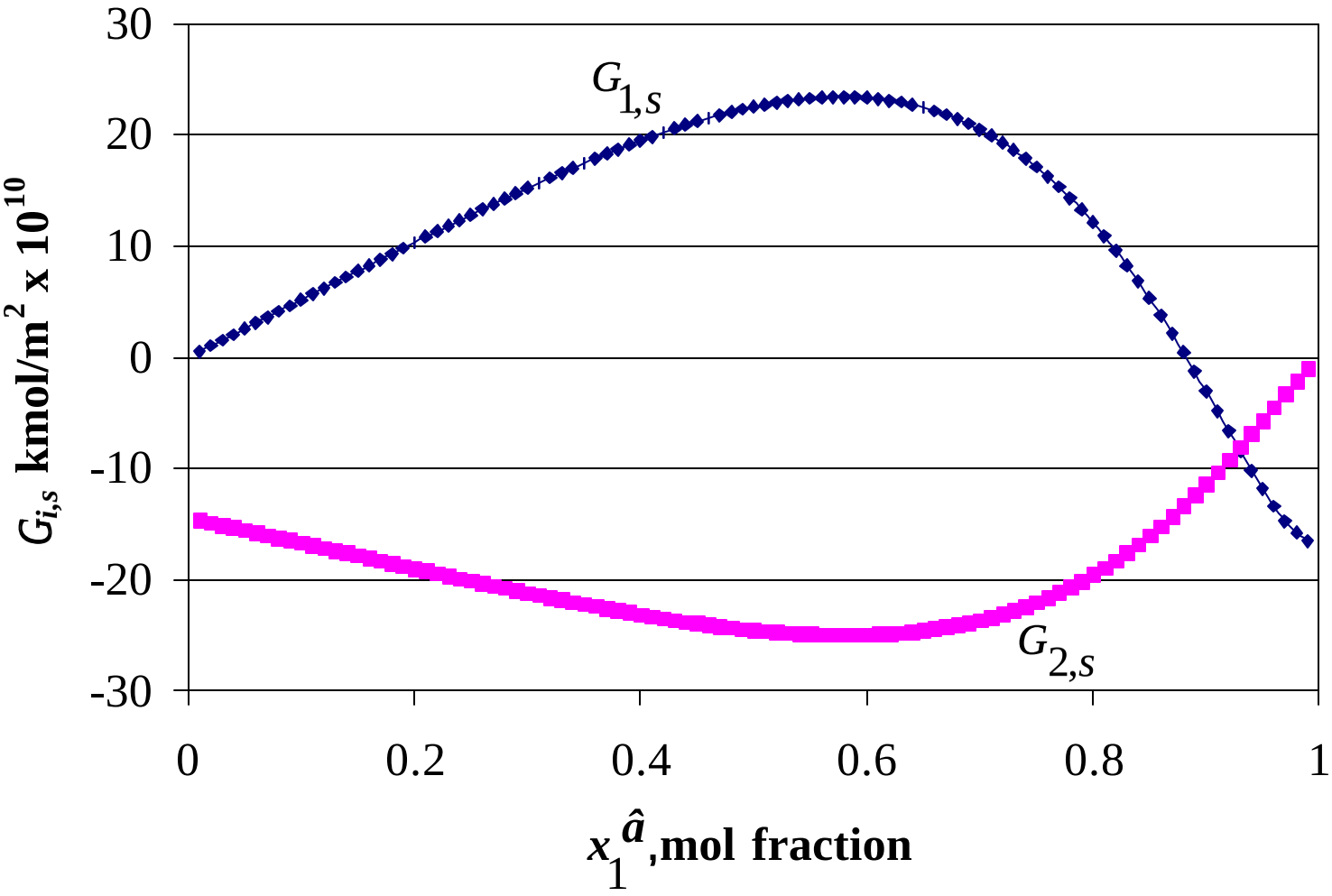

Fig. 3 – Adsorption at the Gas-Liquid Interface for Propane (1) and Normal Octane (2) Mixture vs. Mol Fraction of Propane in Liquid Phase: T = 350 K.

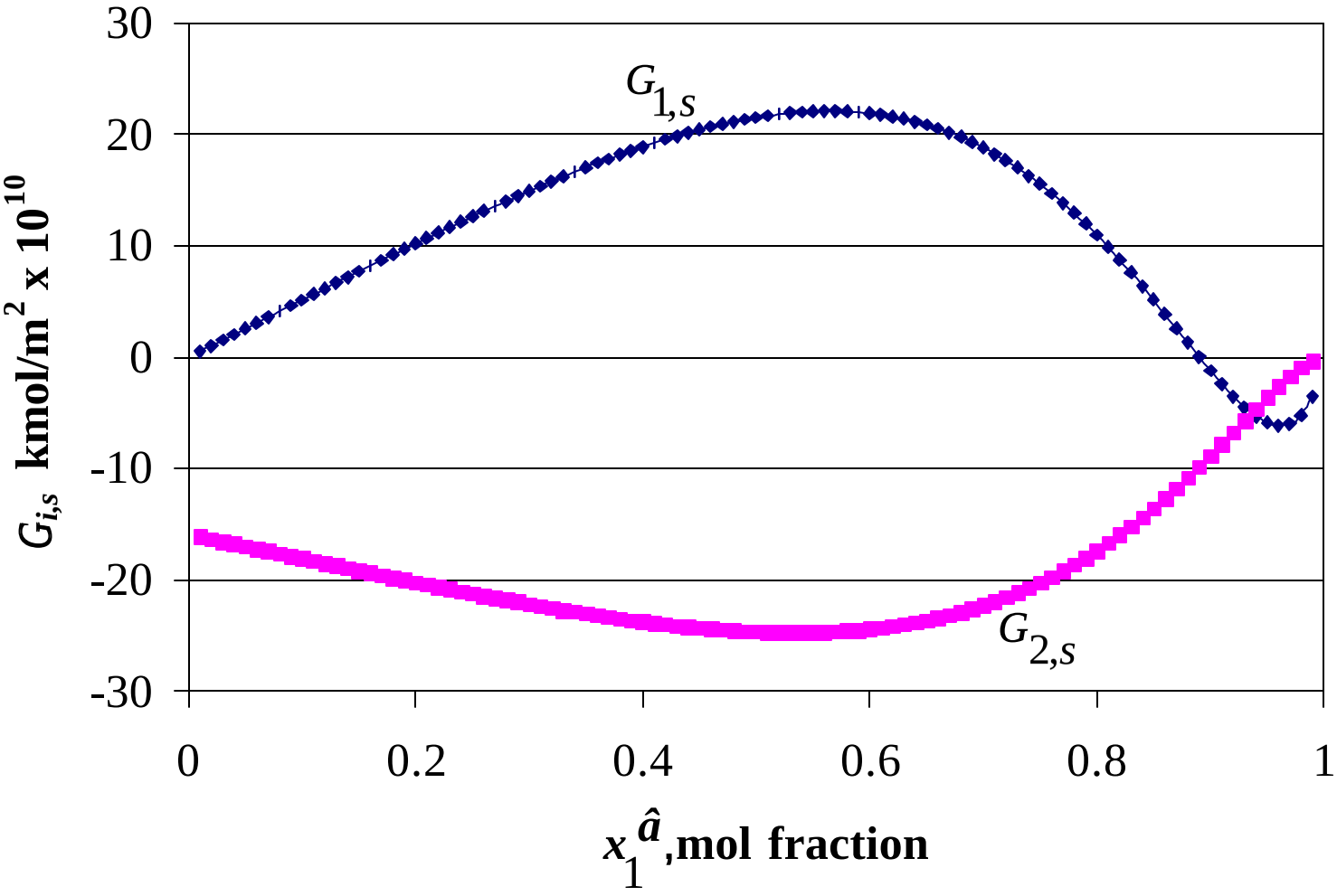

Fig. 4 – Adsorption at the Gas-Liquid Interface for Propane (1) and Normal Octane (2) Mixture vs. Mol Fraction of Propane in Liquid Phase: T = 369.8 K.

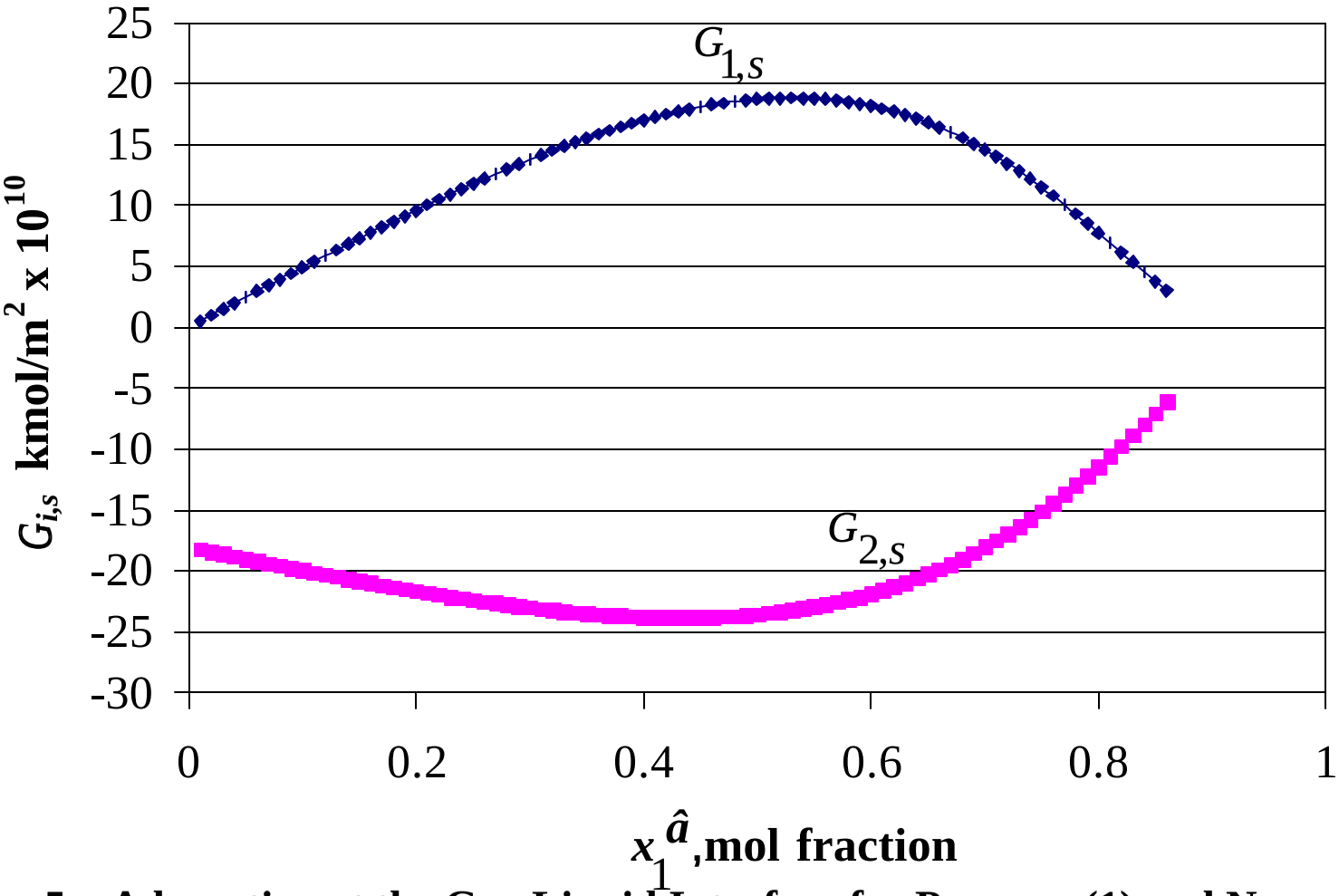

Fig. 5 – Adsorption at the Gas-Liquid Interface for Propane (1) and Normal Octane (2) Mixture vs. Mol Fraction of Propane in Liquid Phase: T = 400 K.

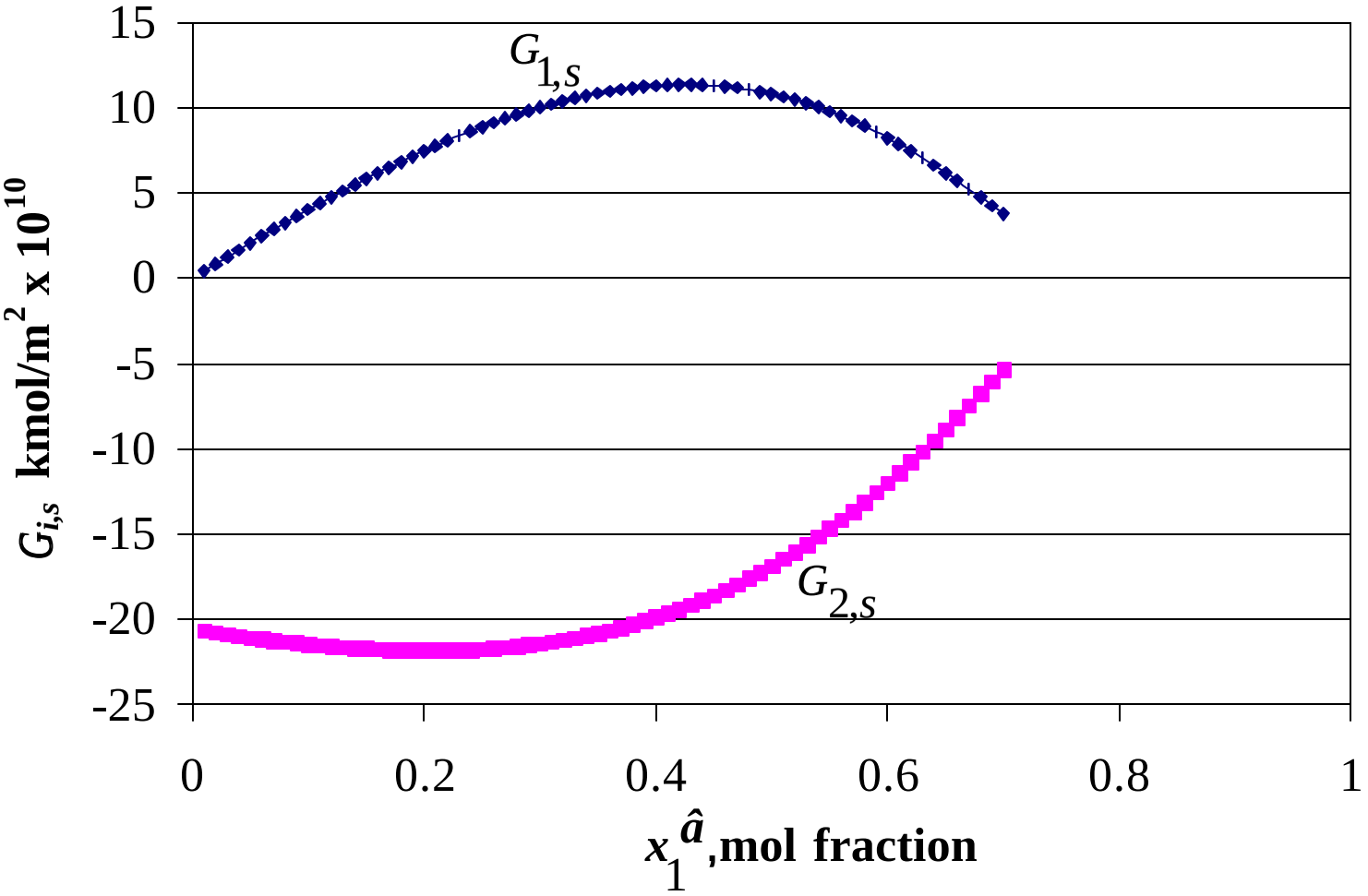

Fig. 6 – Adsorption at the Gas-Liquid Interface for Propane (1) and Normal Octane (2) Mixture vs. Mol Fraction of Propane in Liquid Phase: T = 450 K.

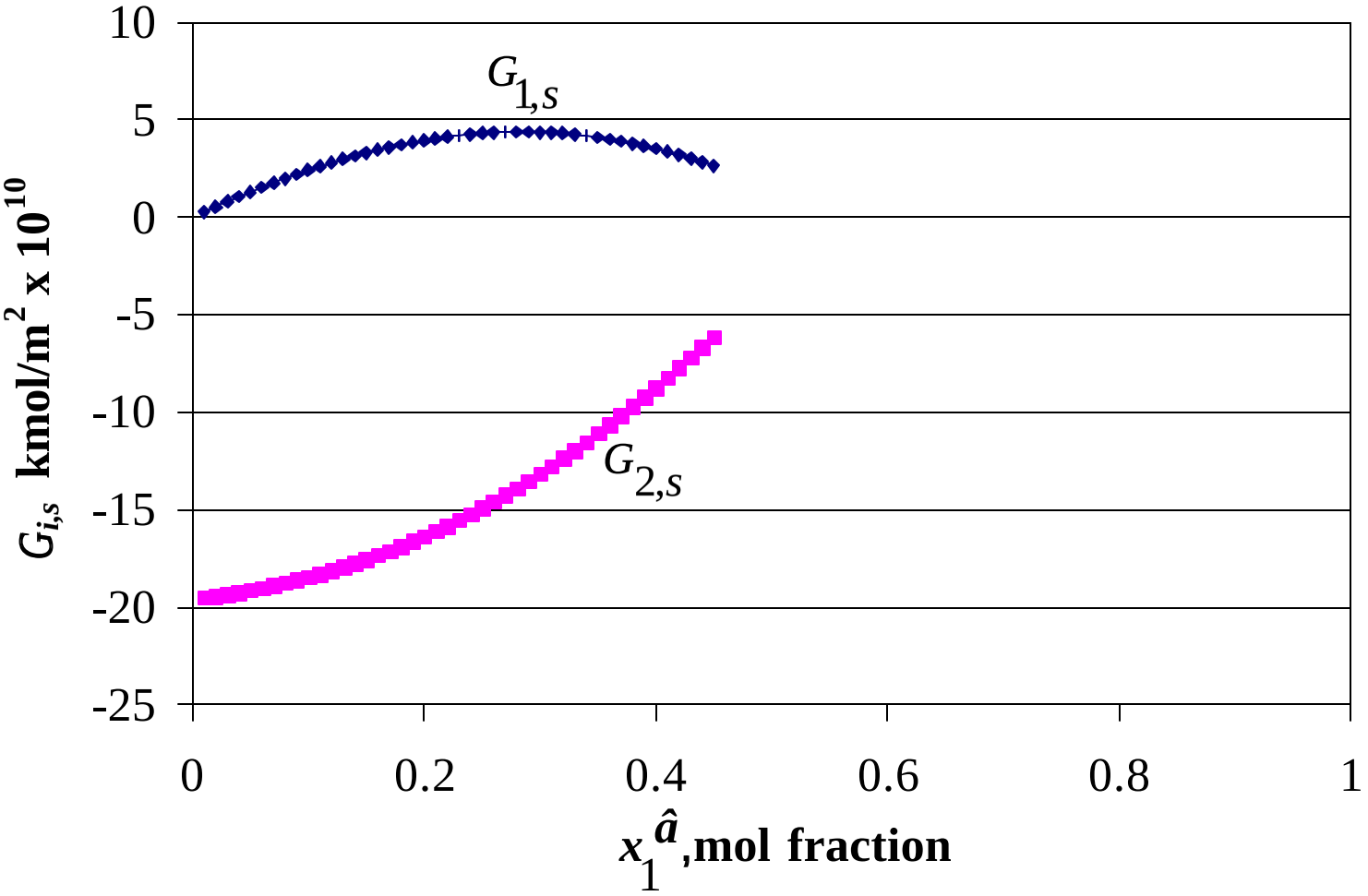

Fig. 7 – Adsorption at the Gas-Liquid Interface for Propane (1) and Normal Octane (2) Mixture vs. Mol Fraction of Propane in Liquid Phase: T = 500 K.

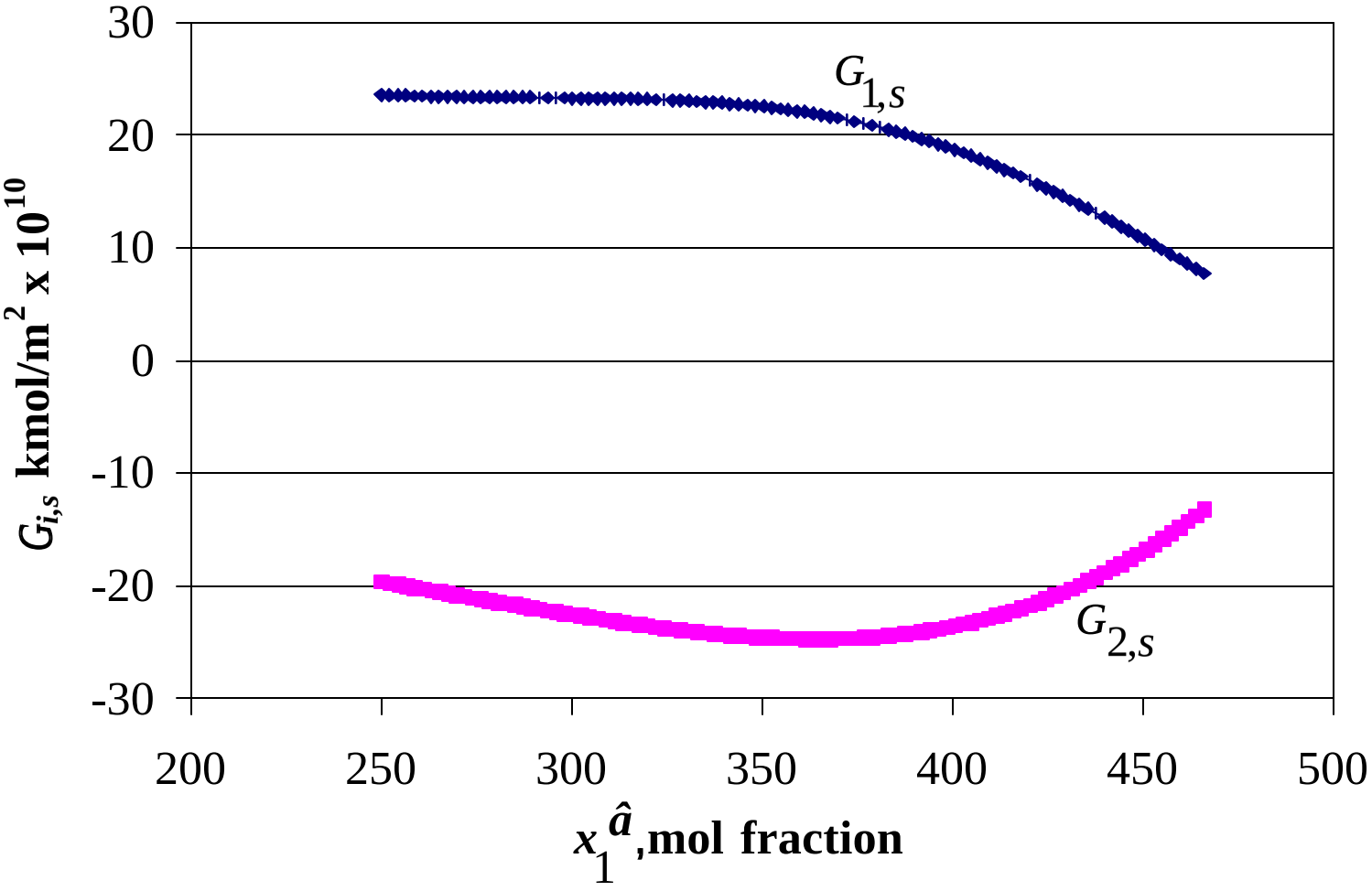

Fig. 8 – Adsorption at the Gas-Liquid Interface for Propane (1) and Normal Octane (2) Mixture vs. Temperature for the Liquid Equimolar Mixture.

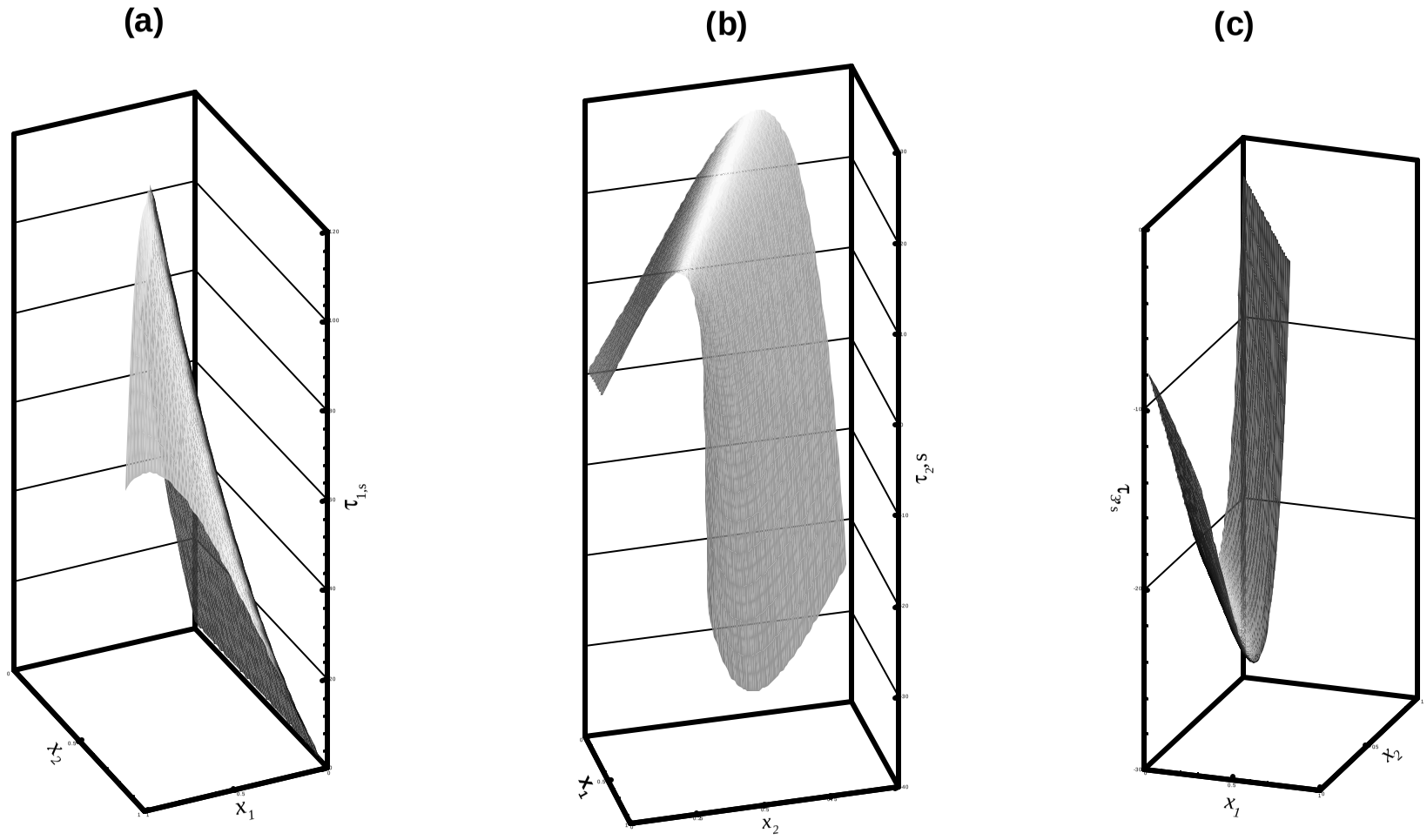

Fig. 9- Adsorption at the gas-liquid interface for the methane(1)/ propane(2)/ n- octane (3) ternary mixture: T=250K (The unit for adsorption τ is 10^{-10} kmole/m^2)